A Study of a Novel Design for Efficient Hydrolysis Reactor for the Cu-Cl Thermochemical Hydrogen Production Cycle

by

Leonard I. Finney

A thesis submitted to the
School of Graduate and Postdoctoral Studies in partial
fulfillment of the requirements for the degree of

Master of Applied Science in Mechanical Engineering

The Faculty of Engineering and Applied Science

University of Ontario Institute of Technology (Ontario Tech University)

Oshawa, Ontario, Canada

June 2021

THESIS EXAMINATION INFORMATION

Submitted by: **Leonard Indiana Finney**

Master of Science in **Mechanical Engineering**

Thesis title: A Study of a Novel Design for Efficient Hydrolysis Reactor for the Cu-Cl Thermochemical Hydrogen Production Cycle

An oral defense of this thesis took place on May 7th, 2021 in front of the following examining committee:

Examining Committee:

Chair of Examining Committee	Martin Agelin-Chaab
Research Supervisor	Kamiel Gabriel
Research Co-supervisor	Kevin Pope
Examining Committee Member	Bale Reddy
Thesis Examiner	Liliana Trevani

The above committee determined that the thesis is acceptable in form and content and that a satisfactory knowledge of the field covered by the thesis was demonstrated by the candidate during an oral examination. A signed copy of the Certificate of Approval is available from the School of Graduate and Postdoctoral Studies.

ABSTRACT

In this thesis, methods to optimize the Hydrolysis reactor for the Cu-Cl thermochemical Hydrogen production cycle were investigated. A simplified Hydrolysis reactor using simple off-the-shelf components was tested and found to suffer from corrosion due to the materials selected for the atomizing nozzle. Because of this corrosion issue, the decision was made to focus on gas-solid Hydrolysis reactors, such as the fluidized bed. This led to the investigation of a novel design for a Hydrolysis reactor, referred to as the Recirculating Steam Fluidized Bed (RSFB) reactor. By recirculating un-used steam through the Hydrolysis reaction directly, the RSFB reactor lowers the steam-to-copper ratio significantly while maintaining favorable reaction kinetics. This design was found to result in a more concentrated HCl acid product, simplifying integration between Hydrolysis and Electrolysis. This novel design represents an opportunity for advancing the Cu-Cl cycle and paves the way to large-scale deployment.

Keywords: hydrogen; energy; Cu-Cl; thermochemical; environment

AUTHOR'S DECLARATION

I hereby declare that this thesis consists of original work of which I have authored. This is a true copy of the thesis, including any required final revisions, as accepted by my examiners.

I authorize the University of Ontario Institute of Technology (Ontario Tech University) to lend this thesis to other institutions or individuals for the purpose of scholarly research. I further authorize University of Ontario Institute of Technology (Ontario Tech University) to reproduce this thesis by photocopying or by other means, in total or in part, at the request of other institutions or individuals for the purpose of scholarly research. I understand that my thesis will be made electronically available to the public.

Leonard Indiana Finney

STATEMENT OF CONTRIBUTIONS

The work presented in Chapter 3 is derived from a journal article published as: K. Gabriel, L. Finney and P. Dolloso, "Preliminary Results of the Integrated Hydrolysis Reactor in the Cu-Cl Hydrogen Production Cycle," International Journal of Hydrogen Energy, vol. 44, pp. 9743-9752, 2019. I performed the majority of the design, experimental process, and analysis, as well as writing the first draft of the manuscript.

ACKNOWLEDGEMENTS

I would like to express my deepest appreciation to Dr. Kamiel Gabriel for his guidance and patience in the preparation of this thesis. I would also like to thank Dr. Kevin Pope for his advice on the technical aspects of this work.

Additionally, I am grateful to my friends and family for their support and encouragement during this process. I thank my mom, dad, and brother for their support and inspiration which made this work possible.

Finally, I thank my current and former colleagues at Ontario Tech U's Clean Energy Research Laboratory for lending a hand in experimentation and analysis.

Funding for this research was provided by NSERC and Canadian Nuclear Laboratories.

TABLE OF CONTENTS

LIST OF TABLES

LIST OF FIGURES

LIST OF ABBREVIATIONS AND SYMBOLS

°C	Degrees Celsius
CERL	Clean Energy Research Laboratory
CNL	Canadian Nuclear Labs
COVID-19	Coronavirus Disease - 2019
EES	Engineering Equation Solver
GHSV	Gas Hourly Space Velocity
GLS	Gas-Liquid Separator
H_2O	Water
HCl	Hydrogen Chloride
L	Liter
N_2	Nitrogen
NIST	National Institute of Standards and Technology
NIST REFPROP	NIST Reference Fluid Thermodynamic and Transport Properties Database
OTU	Ontario Tech University
P	Pressure
PID	Proportional - Integral - Derivative control
PSD	Pressure Swing Distillation
PTFE	Polytetrafluoroethylene
RSFB	Recirculating Steam Fluidized Bed
SCM	Shrinking Core Model
SCR	Steam-to-copper ratio
SMR	Steam-methane reforming
TG-MS	Thermo-gravimetric mass spectrometer
UBM	Un-ball-milled
BM3	Ball-milled for 3 hours
BM6	Ball-milled for 6 hours
BM12	Ball-milled for 12 hours
UOIT	University of Ontario Institute of Technology
W	Watts
XRD	X-Ray Diffraction

Chapter 1 Introduction

1.1 Introduction to the Cu-Cl cycle

Hydrogen energy is quickly becoming a major factor in developing a worldwide clean energy economy. Domestically, this can be seen by the release of the Hydrogen Strategy for Canada, which identifies many major Hydrogen uses in Canadian industry and predicts that Canada alone may need to increase production capacity to 4 million tons per year by 2030 [1]. Many major manufacturers of automobiles, ships, trains, and utility vehicles are investing significantly in Hydrogen-based transportation [2] [3]. Hydrogen is also heavily used in petrochemical plants and refineries, fertilizer production, food processing, and other industries. Due to the environmental impact of existing fossil fuel-based methods of Hydrogen production, such as Steam Methane Reforming (SMR), there is a need to develop sustainable routes for large-scale Hydrogen production.

Thermochemical water splitting cycles are one of the most promising clean alternatives to traditional Hydrogen production methods, as they use water as a feedstock, with no external emissions to the environment [4] [5] [6] [7]. Thermal energy and water are the main inputs, with electricity sometimes used to a lesser extent. Over 200 thermochemical cycles have been identified to produce Hydrogen [4]. Lewis and Taylor [5] reported from a survey of open literature that the Cu-Cl cycle is one of the leading methods for sustainable Hydrogen production. A future commercial Cu-Cl plant would utilize thermal energy from sources such as nuclear, solar, or other industrial heat sources. This includes heat recovery from the emissions of power plants, or industrial petrochemical plants, steel recycling, or cement production.

The Cu-Cl cycle is a system of chemical reactors which allow for waste heat to be used as the primary energy input in producing Hydrogen. This contrasts against Electrolysis, which uses only electricity. To do this, the Cu-Cl cycle employs a copper and chlorine salt, which changes form throughout the process. This Cu-Cl salt starts as $CuCl_2$, which reacts with high-temperature steam at 400°C and forms Cu_2OCl_2 and HCl. The products of this reaction carry Hydrogen and Oxygen separately, with Cu_2OCl_2 carrying Oxygen, and HCl carrying Hydrogen. The Cu_2OCl_2 is heated to its melting point at 500°C, releasing Oxygen gas and forming CuCl as a product. The CuCl and HCl are reacted in an electrochemical cell, forcing Hydrogen gas to release from the HCl and liberating Chlorine (Cl) which binds with CuCl, forming CuCl2. The CuCl2 is then introduced back into the Hydrolysis step, beginning another cycle to be repeated. A Schematic of the Cu-Cl cycle is presented in Figure 1-1. The chemical reactions involved in the Cu-Cl cycle are Hydrolysis (Equation 1-1), Electrolysis (Equation 1-2), and Electrolysis (Equation 1-3).

$$2CuCl_{2(s)} + H_2O_{(g)} \rightarrow Cu_2OCl_{2(s)} + 2HCl_{(g)} \quad (1\text{-}1)$$

$$2Cu_2OCl_{2(s)} \rightarrow 4CuCl_{(l)} + O_{2(g)} \quad (1\text{-}2)$$

$$2CuCl_{(aq)} + 2HCl_{(aq)} \rightarrow H_{2(g)} + 2CuCl_{2(aq)} \quad (1\text{-}3)$$

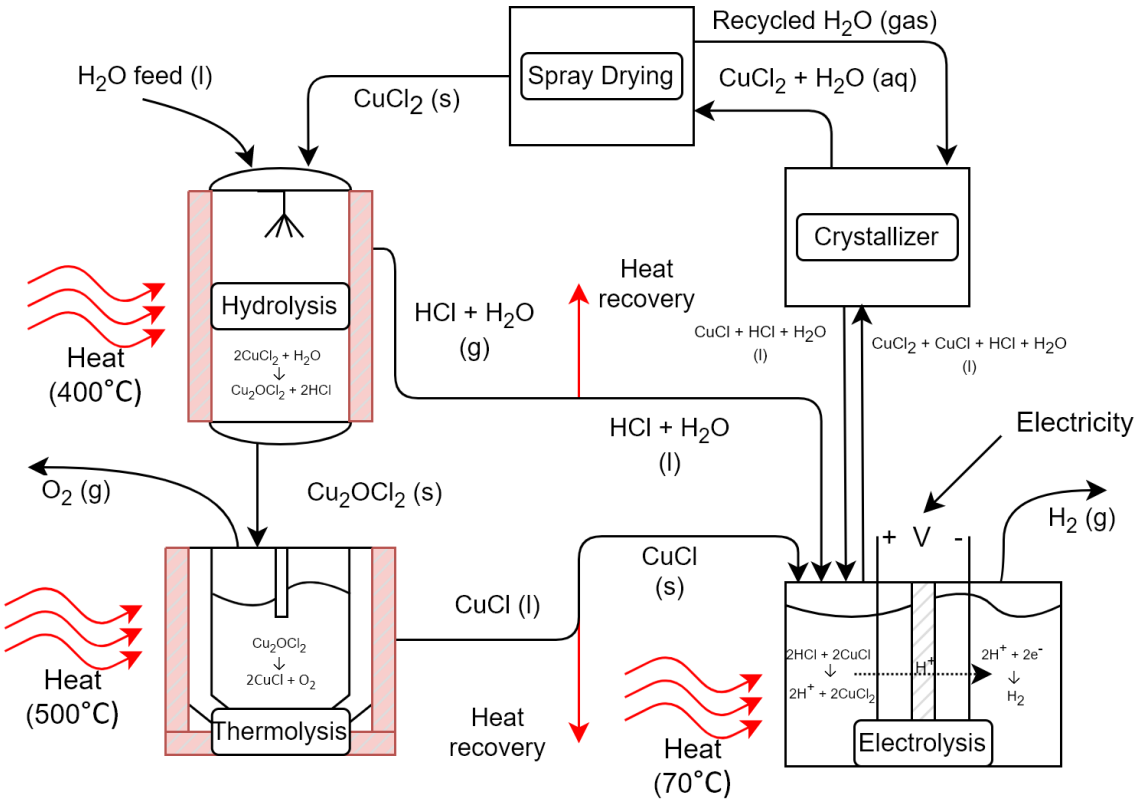

Figure 1-1: Schematic of processes in the Cu-Cl cycle

Hydrolysis is the first stage of water dissociation in thermochemical cycles. It exists in various types of thermochemical water splitting cycles, whereby water decomposes and associates with reactant substances to form intermediate compounds for subsequent splitting into Hydrogen and Oxygen. This thesis focuses on improving the Hydrolysis step and effectively integrating it into the Cu-Cl cycle. This is a crucial step towards achieving optimal integration, thermodynamic efficiency, and economic viability of the Cu-Cl cycle.

Over the past decade and a half, significant progress was made in designing and testing unit operations of the Electrolysis, Hydrolysis, and Electrolysis steps. Researchers at Ontario Tech University (formerly UOIT) led an international team of researchers in the design and testing of unit operations [8]. Researchers at the Argonne National Laboratory, Pennsylvania State University, and Canadian Nuclear Laboratories (CNL) focused on

CuCl / HCl Electrolysis [9] [10]. CNL has demonstrated continuous Hydrogen production, with a CuCl / HCl electrolytic cell over several weeks at its Chalk River Laboratories in Ontario, Canada [11].

At this stage, the focus is on the optimization of the individual components and addressing technical issues with integration. The Hydrolysis reactor needs to be optimized to achieve higher yield and provide for better process integration. Further, the Hydrolysis reactor requires a large excess of steam to drive the reaction which presents yet another integration challenge.

1.2 Thesis Objectives

The objective of this thesis is to examine novel designs for the Hydrolysis reactor in the Cu-Cl cycle. The long-term goal of such effort is to develop a Hydrolysis reactor that is suitable for large-scale industrial deployment. A Hydrolysis reactor using a simplified design and off-the-shelf components was designed and operated at the Clean Energy Research Laboratory at Ontario Tech University. This design and testing served as preliminary work for the following investigation, providing important experience with Hydrolysis and the specific considerations that a scaled-up Hydrolysis reactor requires. This reactor design was developed to support at least 100 g/day of Hydrogen production in the Cu-Cl cycle. A novel design for a reactor dubbed the Recirculating Steam Fluidized Bed (RSFB) was developed to address the challenges that the simplified Hydrolysis reactor faced.

The simplified Hydrolysis reactor was designed to be constructed from commonly available and inexpensive stainless steel pipes and fittings. The heat was provided by an

external clamshell furnace which heated the surface of the reactor, while chemical reactants were provided by a liquid solution of $CuCl_2$ in water. An atomizing nozzle was located in the center of the reactor to atomize the liquid solution into a fine mist, increasing contact with the steam cloud in the reaction chamber. Gaseous products were condensed and recovered to determine the conversion of $CuCl_2$ to Cu_2OCl_2.

The simplified Hydrolysis reactor provided important information regarding the practicalities of operating a Hydrolysis reactor on a large scale. The atomizing nozzle, constructed from 316 stainless steel, deteriorated quickly due to corrosion caused by the liquid $CuCl_2$ solution. This corrosion leads to poor conversion of $CuCl_2$ by forming large droplets of $CuCl_2$ solution, which could not sufficiently be heated and reacted by the time they reached the bottom of the reactor. This information led to the decision to separate spray drying and Hydrolysis, and shift focus to gas-solid reactors such as fluidized beds.

Scale-up and industrial deployment of the Cu-Cl cycle will require a Hydrolysis reactor which can be integrated with other cycle processes while allowing for effective heat transfer and high conversion. Separating spray drying from Hydrolysis allows for fluidized-bed type reactors to be used, which have been shown to meet these criteria. The steam flow of the fluidized bed further provided an opportunity for increasing the efficiency of Hydrolysis by recirculating unused steam, reducing the thermal energy requirements, and increasing the efficiency of the overall cycle. The proposed "Recirculating Steam Fluidized Bed" reactor was evaluated thermodynamically using EES and Aspen Plus simulation packages. EES was used to evaluate the system in detail using mass transfer, fluid dynamics, and heat transfer equations. Aspen Plus was used to verify the mass transfer and thermal data found by EES. Results showed that the new design was

able to reduce the steam-to-copper ratio of the system while maintaining an effective steam-to-copper ratio in the reactor chamber of 18. As a result of this lower steam-to-copper ratio, the RSFB reactor consumed less thermal energy and produced a stronger HCl acid solution for the downstream reaction in the electrolyzer unit.

1.3 Outline of Thesis

Chapter 2 of this thesis is a literature review of the body of research conducted on the Cu-Cl cycle with a focus on the Hydrolysis step and its integration within the system.

Chapter 3 follows the design, experimental setup, and results from the simplified Hydrolysis reactor. Hydrolysis

Chapter 4 investigates a novel design for a Hydrolysis reactor based on the principle of recirculating unused steam. This design, dubbed as the Recirculating Steam Fluidized Bed, was evaluated theoretically.

Chapter 5 summarizes the conclusions of the results of both the simplified Hydrolysis reactor, presented in Chapter 3, and the Recirculating Steam Fluidized Bed, presented in Chapter 4. Chapter 5 ends with a discussion of the lessons learned from these investigations and provides an outline of considerations for future work.

Chapter 2 Literature Review

2.1 Introduction to The Cu-Cl Thermochemical Hydrogen Production Cycle

The Copper-Chlorine cycle is a thermochemical Hydrogen production process that uses heat as its main energy source, along with a small amount of electrical energy. This makes the Copper-Chlorine cycle a promising option for the recovery and use of industrial waste heat as well as for large-scale nuclear-thermal Hydrogen production [12] [13]. This is accomplished by linking three main chemical reactions together; two of which use heat as the primary energy input.

Starting with Hydrolysis, high-temperature steam is split by the salt Copper (II) Chloride ($CuCl_2$) into the resulting chemicals of Hydrogen Chloride (HCl) gas and Copper-Oxy-Chloride (Cu_2OCl_2) solids. The products from the Hydrolysis step carry the Hydrogen and Oxygen, to be released by downstream processes. The Copper-Oxy-Chloride is decomposed in a molten salt Electrolysis reactor, releasing Oxygen gas and forming Copper (I) Chloride (CuCl). The CuCl from Electrolysis is combined with HCl in an Electrolysis reactor, releasing Hydrogen gas and forming an aqueous solution of $CuCl_2$. The $CuCl_2$ is recycled back as a feed chemical for the Hydrolysis step, and the reaction begins again. The fact that no additional chemicals are consumed in the process means that the Cu-Cl cycle causes no pollution. The Cu-Cl cycle requires a maximum temperature of 500°C to operate the Electrolysis reaction, which is the highest temperature reaction of the cycle. The hydrolysis step requires between 390°C and 400°C, with much of the required energy used to generate the high-temperature steam.

2.2 The Hydrolysis reactor

The Hydrolysis reactor is a critical component of the Cu-Cl cycle. By splitting water into Hydrogen-carrying and Oxygen-carrying compounds, the Hydrolysis reactor acts as the first step of the Cu-Cl cycle. This reaction occurs between superheated steam and solid particles of $CuCl_2$, meaning that the Hydrolysis reaction requires the handling of at least two phases of matter as inputs and outputs. This reaction has thus far proved difficult to optimize, as many parameters influence its overall kinetic performance and must be tuned to achieve high conversion of $CuCl_2$ [14]. Complete conversion of $CuCl_2$ in the Hydrolysis reactor is critical since unreacted $CuCl_2$ will result in Cl_2 emission downstream in the Electrolysis reactor, causing a chemical imbalance in the cycle [14] [15]. An imbalance of Cl_2 could slow or halt the reaction and would require makeup $CuCl_2$ to be introduced over time. It is therefore critical that $CuCl_2$ is completely converted into Cu_2OCl_2 before passing downstream to the Electrolysis reactor.

As a chemical reaction, Hydrolysis requires one mole of H_2O to react with two moles of $CuCl_2$. This stoichiometric balance can be also expressed as a ratio of steam-to-copper, with 0.5 moles of H_2O per mole of $CuCl_2$. In the literature, this is abbreviated as “S-Cu ratio”, or as the “steam-to-copper molar ratio” (H_2O/Cu). In this thesis, the term “steam-to-copper ratio” or “SCR” will be used. The steam-to-copper ratio is a factor that must be examined closely since experimental and theoretical studies have determined that large amounts of steam are required for better conversion. Such large amounts of excess steam result in decreased energy and exergy efficiencies of the cycle, as the water consumed is only 2.7% of the total water present [16]. Pope *et al*. [17] and [18] investigated a means of reducing steam flow requirements by introducing a flow of inert nitrogen carrier gas. Their

investigations provided compelling evidence of the ability to lower the steam-to-copper ratio to between 3 and 0.5. This lower steam requirement is not yet ready for widespread adoption, but it suggests that options exist to lower the steam-to-copper ratio of the system, resulting in lower steam demands and a higher concentration of HCl acid from the condensers.

2.2.1 Gas-Solid reactions

The reaction kinetics of the Hydrolysis reactor are significantly more complicated than other chemical reactions due to the phases involved. In a two-phase gas-solid reaction, such as that which takes place in the Hydrolysis step, physical properties need to be considered in addition to the flow rate and temperature of reactants. The reacting $CuCl_2$ is in a solid phase and is typically a small porous particle. In gas-solid reactions, the rate of reaction is modeled with consideration of the contact between the reactants. As shown in Figure 2-1, such models include the shrinking core model, pore models, grain models, and nucleation models [19]. In the Cu-Cl cycle, a uniform conversion model is used if gaseous diffusion progresses faster than the Hydrolysis reaction. If gaseous diffusion progresses slower than Hydrolysis, the shrinking core model is used [20].

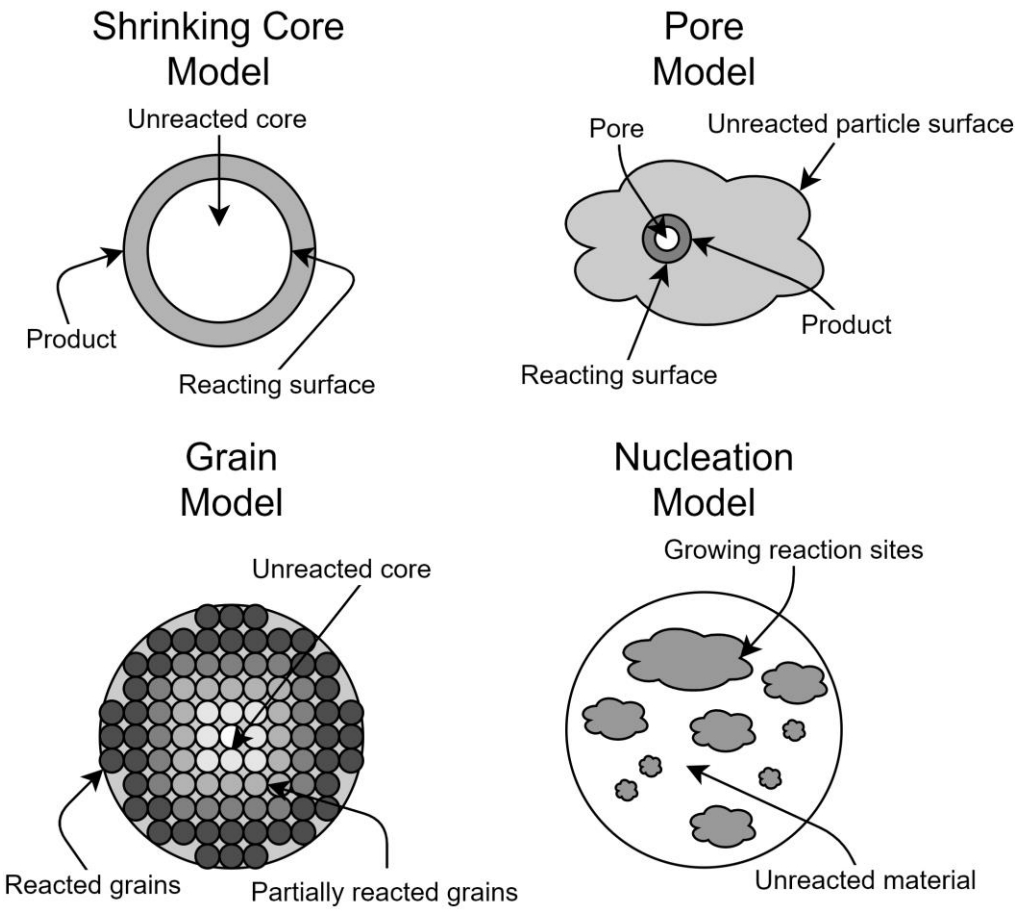

Figure 2-1: Solid gas reaction models

The shrinking core model (SCM) treats the particle as non-porous, with the diffusion of gases contributing to the reaction rate. SCM describes two main reaction rate controls: diffusion control, and reaction kinetics control. $CuCl_2$ conversion to Cu_2OCl_2 results in the particle shrinking to 66% of its original size [21]. This contraction may result in cracks or pores opening in the Cu_2OCl_2 shell around the core, changing the rate of steam and HCl diffusion through the particle. The shrinking core model has a larger effect as time goes on, as discussed by Pope *et al.* [22]. Using horizontal and vertical packed bed reactors, Pope *et al.* [22] investigated the production of HCl and Cu_2OCl_2 over time, finding that the reaction rate of $CuCl_2$ dropped by 75% as the reaction progresses. Their results suggest that this may be due to Cu_2OCl_2 forming on the exterior of the $CuCl_2$ particle, presenting

a barrier that inhibits steam diffusion into - and HCl diffusion out of - the particle. Further evidence of this physical resistance can be found in the earlier work by Pope *et al.* [23] which showed a 40% drop in reaction rate, and a steady-state condition that would take upwards of 13 hours to completely convert the bed of $CuCl_2$.

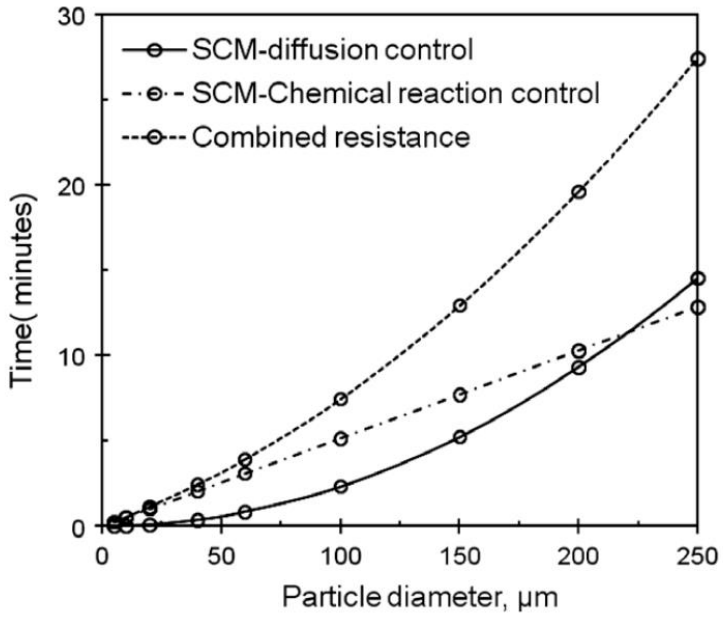

Figure 2-2: Variation of the cupric chloride conversion time with particle diameter. (Source: Daggupati et al. [24] reproduced with permission)

Daggupati *et al.* [24] investigated the Hydrolysis reaction using both reaction kinetics control and diffusion control and presented a combined control model which describes the reaction time required for maximum conversion given a range of particle sizes. For particles 200 µm in size, the reaction times given by both control models nearly match, and when combined, they predict complete conversion in 20 minutes [24]. For particles smaller than 40 µm, diffusion is the least dominant of the control models, predicting just 22 seconds, while reaction control predicts 60 seconds [24]. Daggupati concluded that particles larger than 40 µm should be reacted using fluidized beds instead of spray reactors

since fluidized beds can provide effective mass transfer and facilitate the required longer reaction time.

2.2.2 Hydrolysis reaction equilibrium

Beyond the reaction rate, the equilibrium of gasses must also be considered with partial pressures of the gaseous components having a major effect on the yield of the reaction. The equilibrium and thermodynamics of the reaction can also provide information about the limit of HCl in the steam flow, and allow for the conditions in a reactor to be evaluated against the equilibrium condition. Depending on how the Hydrolysis reactor is integrated with Electrolysis, the electrolyte solution can be directly pumped into Hydrolysis reactor sprayer heads after having CuCl removed. If this is the case, a considerable amount of HCl would be present in the input stream, causing a concentration of HCl product to build up in the reactants. Chemical equilibrium would then be shifted in the reverse direction, potentially reducing effective Hydrolysis yield. Daggupati *et al.* [24] performed an analysis of the fluidized bed reactor using diffusion modeling and reaction equilibrium. The equilibrium conversion X was found to be highly sensitive to the ratio of the moles of HCl ($N3$) to the moles of input steam ($N1$) [24].

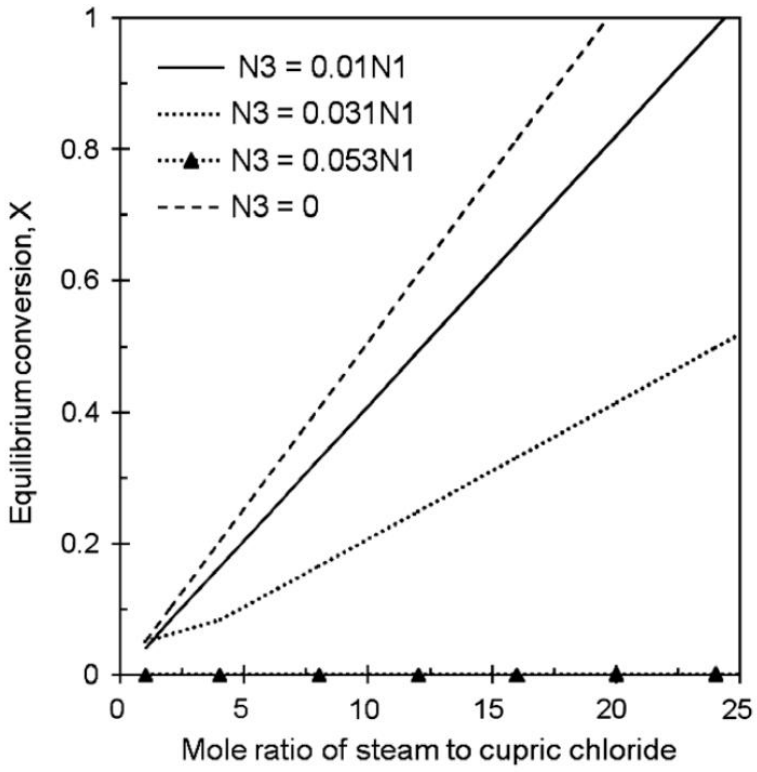

Figure 2-3: Equilibrium conversion of cupric chloride solid with hydrochloric acid concentrations in the feed steam. (Source, Daggupati et al. [24] reproduced with permission)

As seen in Figure 2-3, for 0% HCl in the steam input, the reaction is expected to reach full conversion at a steam-to-copper ratio (SCR) of 18. Increasing the mole ratio to 1%, the SCR required to reach full conversion is 24, with 3.1% HCl requiring an SCR of 48. At 5.3% HCl, the equilibrium conversion is 0, essentially stopping the reaction altogether. This presents an issue for reactors integrating with Electrolysis using liquid transport in that $CuCl_2$ should be free of any HCl before being dissolved in pure H_2O and transported to the Hydrolysis reactor.

As briefly discussed earlier, Pope *et al*. [18] demonstrated a mechanism to lower the excess steam required by the Hydrolysis reactor by increasing the amount of nitrogen carrier gas. This can be explained by Le Chatellier's principle, which states that a system will respond

to a disturbance to regain equilibrium. Thus, a chemical reaction can be evaluated by comparing the reaction quotient Q_R and the equilibrium constant K_e. The reaction quotient describes the balance of products and reactants present at any given time. The equilibrium constant describes the balance of products and reactions at equilibrium. When the reaction quotient of a reaction is below the equilibrium constant, the reaction will progress in the forward direction until the two values reach unity [18]. To find the equilibrium constant K_e, the sum of the Gibbs free energies of the products and the reactants is used.

$$K_e = \mathrm{e}^{\left(-\frac{\Delta G_R^\circ}{RT}\right)} \tag{2-1}$$

The reaction quotient Q_R is a ratio of the fugacity of the involved gases (or activity of solids), raised to the power of their stoichiometric constants.

$$Q_R = \left[\frac{a_{Cu_2OCl_2} f_{HCl}^2}{a_{CuCl_2}^2 f_{H_2O}}\right] \tag{2-2}$$

The solid compounds involved are not volatile at the given temperatures and pressures, and thus have an activity of 1. The reaction quotient can be further simplified by assuming the gasses will behave ideally due to the low-pressure environment, making the fugacity and partial pressure nearly identical ($f \approx p$) [18].

$$Q_R = \frac{p_{HCl}^2}{p_{H_2O}} \tag{2-3}$$

The resulting ratio of partial pressures can be restated in terms of mole ratios and the total gas pressure. By Dalton's law, it can be assumed that the presence of inert gas will reduce the partial pressures of the other gasses present. If inert gas is present, the term N_i is used to represent the number of moles of the inert gas present. Since the inert gas is not involved

in the reaction itself, N_i is only relevant to the total number of moles used to calculate the partial pressure of the reacting compounds. This inert gas term allows for the reaction quotient to be lowered below equilibrium, shifting the reaction further in the forward direction, and potentially reducing the amount of excess steam required to achieve high conversion [18].

$$Q_R = \frac{N_{HCl}^2}{N_{H_2O}} \left(\frac{p_T}{N_{HCl} + N_{H_2O} + N_i} \right) \tag{2-4}$$

Since the reaction quotient is proportional to the square of the moles of HCl present, while only inversely proportional to the moles of H_2O, an increased presence of inert nitrogen gas reduces the partial pressure of the chemically active components, lowering the reaction quotient further below the equilibrium constant. Excess steam has a similar effect on the reaction quotient but requires a large amount of energy to generate due to the phase transition from water to steam. Because of this, utilizing large amounts of inert gas can result in considerable energy savings. A lower steam-to-copper ratio also has the added benefit of producing a stronger acid in the condenser, removing the reliance of the system on pressure swing distillation to produce HCl acid strong enough for Electrolysis.

In 2012, Pope *et al.* [17] also demonstrated an equation to determine the limit of HCl presence in the gas stream based on the equilibrium constant. The fraction of HCl in the gas stream is represented by X_{HCl} and is given by Equation 2-5.

$$X_{HCl} = \frac{\dot{N}_{HCl}}{\dot{N}_{H2O} + \dot{N}_{HCl}} \tag{2-5}$$

At equilibrium, $K_e = Q_R$, therefore the reaction quotient can be substituted by the equilibrium constant in Equation 2-3 and restated as:

$$K_e = \left[\frac{\left(X_{HCl}\frac{p_T}{p_0}\right)^2}{\left((1-X_{HCl})\frac{p_T}{p_0}\right)}\right] \quad (2\text{-}6)$$

Finally, the amount of HCl in the reaction at equilibrium can be found by rearranging Equations 2-1, 2-5, and 2-6 to yield:

$$X_{HCl} = \sqrt{\left(\frac{e^{-\left(\frac{\Delta G_R^\circ}{RT}\right)}}{2\left(\frac{p_T}{P_0}\right)}\right)^2 + \frac{e^{-\left(\frac{\Delta G_R^\circ}{RT}\right)}}{\left(\frac{p_T}{P_0}\right)}} - \frac{e^{-\left(\frac{\Delta G_R^\circ}{RT}\right)}}{2\left(\frac{p_T}{P_0}\right)} \quad (2\text{-}7)$$

Equation 2-7 provides a method to determine the limit of HCl within a reaction given the concentration of H_2O, pressure, and temperature of the reactor [17]. If a reaction is found to have more HCl than is predicted by X_{HCl} , then it can be assumed that the reaction will be beyond equilibrium and will proceed in the reverse direction. This can further be evaluated by comparing Q_R from Equation 2-4, and K_e from Equation 2-1 using the following conditions:

$Q_R = K_e$ The reaction is in equilibrium

$Q_R < K_e$ The reaction is below equilibrium and will progress in the forward direction.

$Q_R > K_e$ The reaction is above equilibrium and will progress in the reverse direction.

2.2.3 Kinetic data of Hydrolysis and side reactions

In addition to the desirable Hydrolysis reaction, decomposition reactions can occur in the Hydrolysis reactor. These side reactions are undesirable as they consume both reactants and products before they can be chemically utilized. While the yield of the Hydrolysis reactor increases with temperature, so does the undesirable decomposition of $CuCl_2$ to Chlorine gas and CuCl [20] [25].

Ferrandon *et al.* [26] demonstrated that hydrolysis of $CuCl_2$ and production of Cu_2OCl_2 was possible even at low steam-to-copper ratios given a high amount of inert gas. This may be due to a high velocity of inert gas quickly removing HCl from the reaction bed, promoting the reaction kinetics in the forward direction. Their results suggest that the superficial velocity of gas through the hydrolysis reactor may be a factor to promote hydrolysis conversion. This observed effect of inert gas promoting conversion also supports the conclusions of Pope *et al.* [18] [17]. Further, Ferrandon *et al*. found that the formation of CuO side-products was independent of the chemical make-up of the reactor's atmosphere occurring under both a steam and inert gas atmosphere [26]. The presence of these CuO impurities in Cu_2OCl_2 is not eliminated even when the Cu_2OCl_2 is generated using alternate means such as the oxidation of CuCl, as noted by Nixon *et al.* [27].

Recent investigations at the Bhabha Atomic Research Center in Mumbai India have yielded valuable kinetic information for Hydrolysis and undesirable side reactions. Thomas *et al.* [28] used a fluidized bed to investigate the conversion-time relation of the reactions present in the Hydrolysis reactor. The fluidized bed used fine glass beads of diameter 350 μm coated with a thin layer of $CuCl_2$ on the surface. It was found that good conversion of $CuCl_2$ to Cu_2OCl_2 could be achieved with low temperatures given a sufficient concentration of steam [28]. It was found that to achieve high conversion while minimizing the progress of undesirable side reactions, the reaction should operate at a low temperature of 300-325°C, with a steam mole fraction of at least 0.5, and a residence of 20-40 minutes [28]. The side reactions occurring in the Hydrolysis reactor are:

$$2CuCl_2(s) \rightarrow CuCl(s) + 0.5Cl_2(g) \quad (2\text{-}8)$$

$$Cu_2OCl_2(s) \rightarrow 2CuCl(s) + 0.5O_2(g) \quad (2\text{-}9)$$

$$Cu_2OCl_2 \rightarrow CuCl_2(s) + CuO(s) \quad (2\text{-}10)$$

Longer reaction times were required to achieve high conversion of $CuCl_2$ at low temperatures with the benefit of minimizing the decomposition reactions. By reducing the temperature of the reaction, undesirable reactions were significantly minimized while $CuCl_2$ conversion to Cu_2OCl_2 was high, suggesting that Hydrolysis can be performed at low temperatures (given a sufficiently long residence time). The temperature dependence of the $CuCl_2$ decomposition is confirmed by some of the results reported by Pope *et al.* [18]. Experimental results showed that Cl_2 production was low until the reactor bed reached 400°C [18]. The concentration of chlorine gas in the reactor outlet can be linked to the decomposition of $CuCl_2$ into CuCl and Cl_2, which tends to occur at temperatures at or above 400°C.

At a particle size of 350 μm, the activation energy was found to be 44.8 kJ/mol, while Singh *et al.* [29] found much higher activation energies (106 kJ/mol) using whole particles of a similar thickness to the thin film of $CuCl_2$ used by Thomas *et al.* [28].

BM3	$CuCl_2$ Ball-milled for 3 hours.
BM12	$CuCl_2$ Ball-milled for 12 hours.
BM6	$CuCl_2$ Ball-milled for 6 hours.
UBM	Un-ball milled $CuCl_2$.

Table 2-1: Legend of ball-milled sample abbreviations. (Source: Singh et al. [29])

Singh *et al.* [29] investigated the Hydrolysis reaction using fine powders of $CuCl_2$ categorized by the time it takes to ball mill the original material (Un-ball-milled, UBM) to the desired particle size. The yield of this reactor was determined using an acid-base titration of the condensate liquid and confirmed by the amount of O_2, which was emitted by the solid Cu_2OCl_2 as it underwent electrolysis in a thermogravimetric-mass-spectrometer (TG-MS). The steam-to-copper ratio was controlled by adjusting the flow rate of gasses (GHSV) and the residence time. It was observed that CuO became a dominant product for the reactions exceeding 60 min at 400°C and a GHSV or 17,630 h^{-1} (Experiments 9-12) [29]. Reaction 6, which ran for only 45 minutes with the same specifications for temperature, particle size, and GHSV, resulted in 97% conversion with the major product being Cu_2OCl_2 [29]. This suggests that reaction time and steam-to-copper ratio are linked to the decomposition of Cu_2OCl_2 into CuO, Cl_2, and CuCl. It is therefore critical that reaction time is minimized to avoid the decomposition side reactions, while lower temperatures can also have a similar effect. The conversion-time relationship of 4 experiments with varying sizes of particles is shown in Figure 2-4, with the total run time of 45 minutes, temperature 400ºC, GHSV of 17630 h^{-1}, and a Steam-to-copper ratio of 33. It was observed that conversion was positively affected by smaller particle sizes, except for the case of BM12. Singh *et al.* [29] identified the low conversion observed with BM12 as the result of fine packing in the fixed bed, causing the gas flow to clog and therefore hindering conversion. In an industrial implementation of a hydrolysis reactor, particle size should be controlled by adjusting the spray-drying nozzle to provide the desired outcomes.

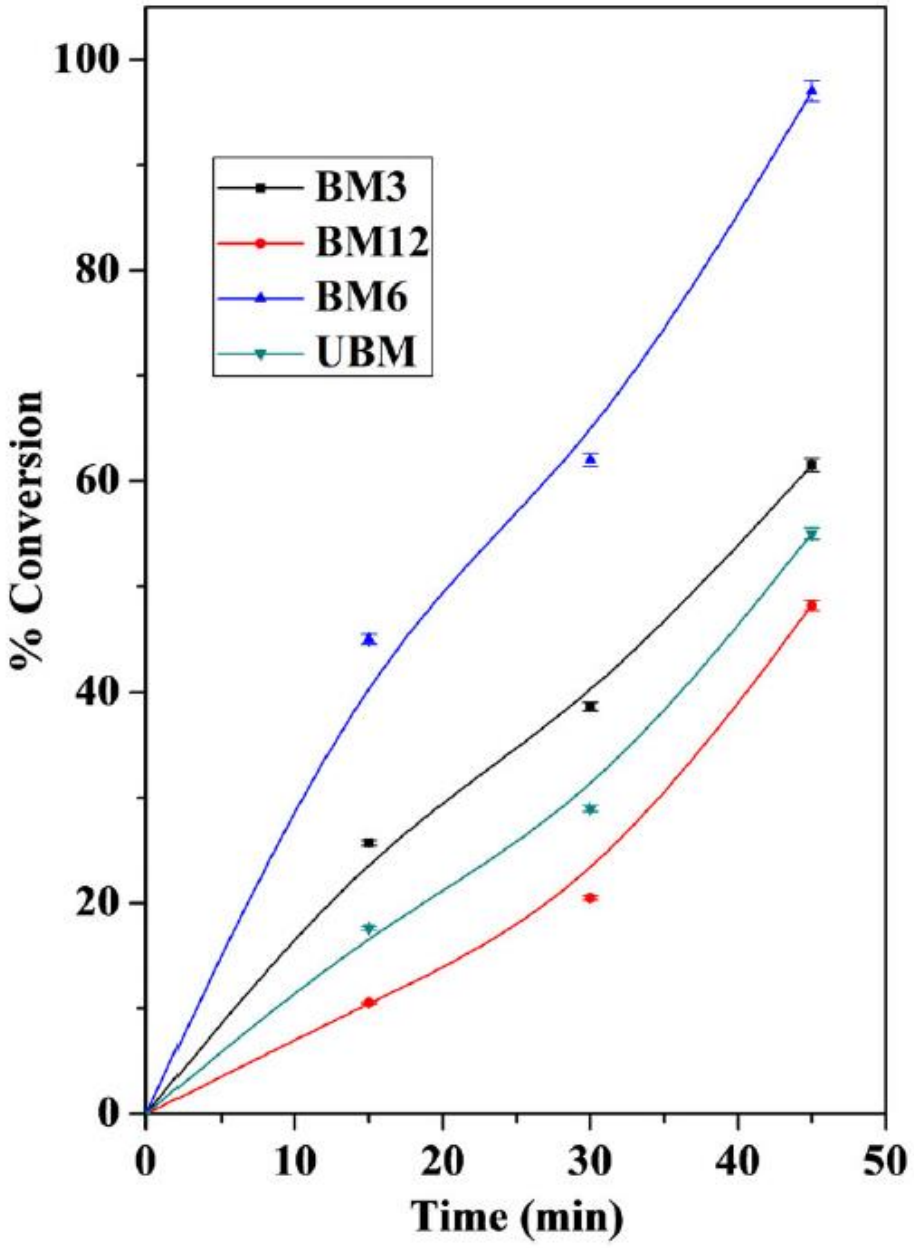

Figure 2-4: Comparison of product yields (% conversion) over different reactants with varying particle sizes. (Source: Singh et al. [29] reproduced with permission)

2.3 Integration

As a thermochemical Hydrogen production cycle, the reactors of the Cu-Cl cycle must be integrated to make the cycle work together in a continuous or semi-continuous mode. Each reactor system will have an energy demand and yield and would require optimization to link them together into a continuous cycle. Farsi *et al.* [16] investigated an integrated lab-scale Cu-Cl Hydrogen production cycle using Aspen Plus and EES simulation packages. Without using heat recovery systems, the system was found to be 11.6% energy efficient and 34.9% exergy efficient. The Hydrolysis reactor was found to be among the most thermal energy-intensive reactors. Integration processes were found to require considerably more thermal energy per unit of Hydrogen, specifically the CuCl2 concentrator and Quench Cell. This is due to the vaporization of water in these two units. It is suggested that the energy efficiency of the system overall can be increased by incorporating heat recovery into the system. Further increases in energy and exergy efficiency can be made by increasing the Electrolysis temperature and decreasing the Electrolysis temperature. Heat recovery within the Cu-Cl cycle was demonstrated by Wang *et al.* [30]. The comparison of these two cycles showed that the Cu-Cl cycle was able to drive many processes on low-grade heat, and found that the energy required by these low-grade heat processes could be sourced partially from within the Cu-Cl cycle itself [30]. Given sufficient heat recovery, the cooling of products from the high-temperature processes can be used to drive some of the low-temperature processes such as spray drying and steam generation [30].

The Electrolysis reactor requires HCl at a concentration of 11 M to operate [7] [31]. The introduction of Nitrogen carrier gas was found to enable a lower steam-to-copper ratio by Pope *et al.* [18], while Ferrandon *et al.* [32] and Farsi *et al.* [33] found that lowering the pressure of the reactor chamber led to a similar reduction of the required steam-to-copper ratio. However, both of these methods have been unable to bring the steam-to-copper ratio low enough to provide a strong enough acid for Electrolysis. An intermediate system is required to link the Hydrolysis reactor to Electrolysis and raise the concentration of HCl in water. The result of this system would be a stream of pure water that can be re-used in the Cu-Cl cycle, and a stream of concentrated HCl in water at the concentration which is required to perform Electrolysis. Such a system is available in the form of pressure-swing distillation. Pressure swing distillation uses a low-pressure distillation column to raise the concentration of HCl to the azeotrope, and a high-pressure column to allow for the azeotrope to be shifted higher and further distilled. Lescisin *et al*. [34] investigated a single-column distillation system to raise the concentration of HCl for use in the Copper-Chlorine cycle. Their experimental setup was limited by safety requirements for a high-pressure pressure swing system, but the theoretical model of the system predicted a maximum concentration of $HCl_{(aq)}$ to the azeotrope of 0.11 mol/mol [34]. The experimental setup was limited due to the buildup of corrosion products in the bottoms extract, but the resulting $HCl_{(aq)}$ concentration was calculated to be 0.1068 mol/mol, near the azeotrope. This demonstrates the initial feasibility of distillation for use in the Cu-Cl cycle, but more work is needed to experimentally demonstrate a multi-column HCl pressure swing distillation system.

Farsi *et al.* [35] developed a theoretical model to predict the operation and performance of a multi-column pressure swing distillation system to raise the concentration of $HCl_{(aq)}$ past the azeotrope. By first distilling $HCl_{(aq)}$ to the azeotrope, then pressurizing and heating once again, the system was able to produce $HCl_{(aq)}$ at high concentrations beyond the azeotrope, a process required to recycle water within the copper-chlorine cycle [35]. This system also conditions the HCl solution for use in the Electrolysis reactor, which requires high concentrations of HCl to operate. This system was done using HCl produced by an integrated Hydrolysis reactor, and the PSD system was investigated as part of an integrated loop [35].

2.4 Summary

In this literature review, key considerations for the Hydrolysis reactor were outlined. To achieve a high yield of Cu_2OCl_2, the particle size, steam-to-copper ratio, and presence of inert carrier gasses must be considered. While early investigations identified the steam-to-copper ratio as critical, recent experiments conducted by Singh *et al.* [29] and Thomas *et al.* [28] show that the concentration of steam in an inert carrier gas can have a greater effect than the steam-to-copper ratio alone. This is supported by the chemical equilibrium which can be shifted by changing the partial pressure of HCl, H_2O, and inert gasses. [18] [22]. By introducing an inert carrier gas, the partial pressure of HCl and H_2O is lowered. The same can be achieved by lowering the total pressure of the reactor. However, since the equilibrium is more sensitive to the concentration of HCl than it is to the concentration of H_2O, lowering the partial pressure of the gases together results in a net increase in forward reactions.

Particle size remains an important parameter in achieving complete conversion since the size of the particle determines whether gaseous diffusion control or chemical reaction control will dominate the reaction time. Particles 400 μm in size are expected to take up to 20 minutes to react, while particles 40 μm and below taking less than two minutes to fully react [24]. The size of the particle formed by the atomizing nozzle in either a spray reactor or spray dryer will determine which reactor type to use, as fluidized beds are capable of achieving longer residence times than spray reactors [24].

Integration of the Hydrolysis reactor depends on the concentration of HCl in the outlet stream. Most Hydrolysis reactors generate HCl condensate with a concentration too low to perform Electrolysis. To remedy this, pressure-swing distillation is required. High pressures are used to shift the azeotrope of the HCl, allowing for HCl to be distilled beyond the azeotrope at standard conditions. While some investigations have yielded results that suggest lower steam-to-copper ratios are possible given inert carrier gases, these methods do not bring the concentration of HCl high enough to perform Electrolysis without some additional distillation step.

Chapter 3 Examination of a Hydrolysis spray reactor

While the Copper-Chlorine cycle has been proven at a lab-scale using purpose-built equipment such as ultrasonic atomizing nozzles and humidified superheated nitrogen flows, these technologies prove difficult to operate at a larger scale. A simplified Hydrolysis reactor will likely be required to operate reliably at a large scale. To achieve this, a simplified Hydrolysis reactor was constructed to determine if the Hydrolysis reactor could achieve a considerable amount of $CuCl_2$ conversion using off-the-shelf components. This reactor consisted of a peristaltic pump that would transport a steady stream of $CuCl_2$ solution into the top of a stainless steel reactor vessel. The reactor vessel was constructed of 316 Stainless Steel, with a pumping and liquid handling apparatus consisting of 316 Stainless Steel fittings.

3.1 Experimental apparatus and Procedure

The simplified Hydrolysis reactor constructed at Ontario Tech University (formerly UOIT) consists of a reaction vessel and interface made of 316 Stainless Steel, which despite its poor corrosion resistance against HCl and $CuCl_2$, contributes to lowering the cost associated with replacing reactor components as they corrode and need replacement. The vessel is constructed from a 44 inch long, nominal pipe size 6, schedule 80, 316 stainless steel pipe, with low-pressure class 150 flanges at both ends. The flanges allow for modified blind caps to be connected using a corrosion-resistant graphite gasket. These modified blind caps contain ¼ inch swage-type stainless fittings to allow for material input, output, and instrument pass-through. A vortex atomizing nozzle, made of 316 stainless steel, is located at the center of the blind cap to atomize the input $CuCl_2$ solution. Thermocouples

pass through the caps to record temperatures at the top, middle, and bottom of the vessel. To input $CuCl_2$ solution, a peristaltic pump is used. On the gaseous outlet of the reactor vessel's top blind cap, a condenser and gas-liquid separator are used to condense the gaseous products. Any gas which is not condensed is passed to a Sodium Hydroxide bubble column to remove HCl fumes before being exhausted to the atmosphere. The reactor vessel is heated by a 13.6 kW Thermcraft Lab-Temp clamshell furnace which maintains a temperature of 390-400°C. Heat tape is wrapped around the portion of the vessel which is not heated by the clamshell furnace at the bottom, controlled by a PID Temperature controller. Mineral wool insulation is used to minimize heat losses. To remove solid products, the reactor vessel is disassembled after being left to cool overnight.

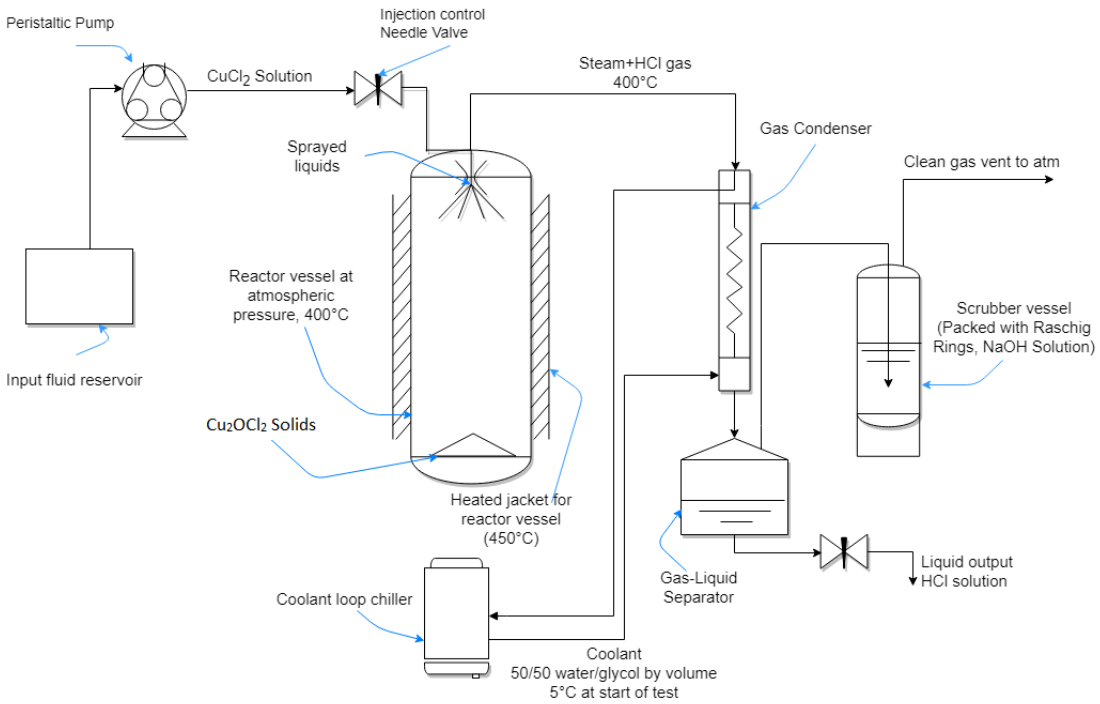

Figure 3-1: Simplified Hydrolysis Experimental Setup

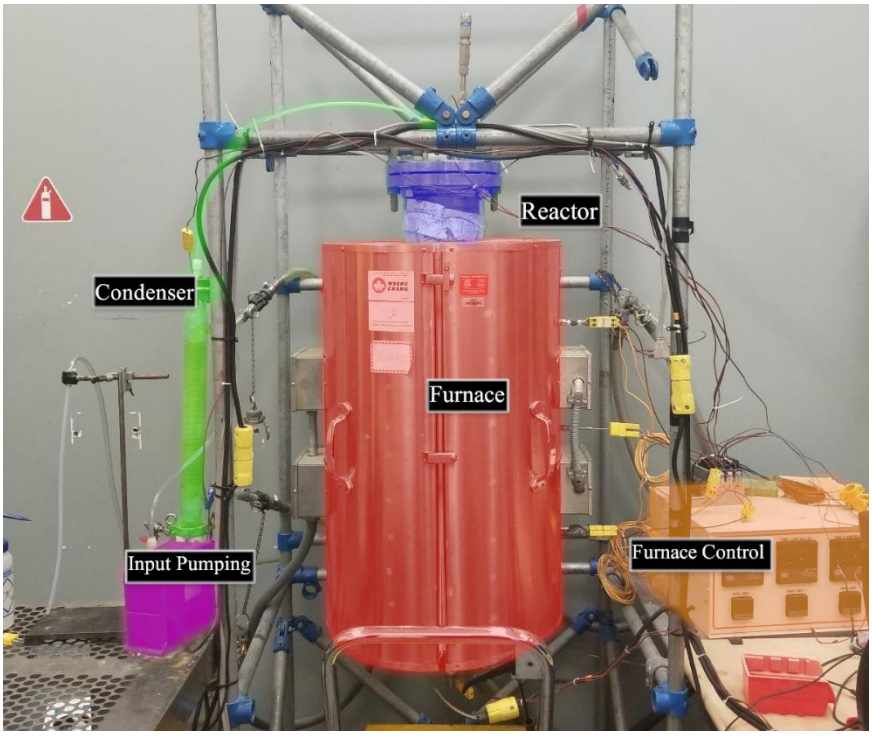

Figure 3-2: Assembled CERL Hydrolysis Reactor Showing Major Components.

The inputs and outputs of the Hydrolysis reactor are listed below.

Inputs:

- 500-550 g of $CuCl_2$ in 900-1000 g of H_2O, pumped via a peristaltic pump.
- Nitrogen (N_2) gas is used to replace air with inert gas before and after each experiment.
- Thermal energy is provided by a 13.6 kW Thermcraft Lab-Temp Split Tube Furnace to keep the temperature of the reactor's centerline at 400°C during the entire reaction.

Outputs:

- Liquid HCl acid solution
- Cu_2OCl_2 solid products

3.1.1 Operating Procedure

The experiments were performed using the following procedure:

1. Start heating up to 400°C

2. Observe temperature in the centerline of reactor until a steady-state condition is reached
3. Pump 350 ml of de-ionized H_2O to create steam conditions in the reactor
4. Once the H_2O pumping is complete, pumping of the $CuCl_2$ solution starts
5. Observe rise in condenser inlet temperature as steam transport begins
6. Once the $CuCl_2$ solution is exhausted, pump another 350 ml of H_2O to flush the inlet lines.
7. Shut off pump
8. Shut down the furnace and allow the reactor to cool.

After each experiment, solids and liquids were collected from the reactor's vessel. The liquids were stored in small vials for analysis, while solids were collected in glass and plastic containers for XRD analysis. Samples that were collected at the end of each experimental run are shown in Section 3.3.2.

3.1.2 Details of individual experiments

Table 3-1 lists the test conditions for four experimental runs.

	Experiment 1	**Experiment 2**	**Experiment 3**	**Experiment 4**
Pre-Flush	1 L	650 mL	350 mL	350 mL
Input Solution	900 mL	900 mL	900 mL	900 mL
Post-Flush	650 mL	650 mL	350 mL	350 mL
Mass of $CuCl_2$	554.4 g	554.5 g	523 g	500 g
Pump flow rate setting	10%	10%	10%	10%
Chiller setting	5°C	5°C	5°C	5°C
Zone 1 temp setting	410°C	410°C	410°C	410°C
Zone 2 temp setting	410°C	410°C	410°C	410°C
Zone 3 temp setting	400°C	430°C	410°C	410°C
Flange heater	N/A	150°C	150°C	150°C

Table 3-1: Experimental Conditions

3.1.3 Sample Collection Method

To collect solid samples at the end of the experiment, the reactor was disassembled by removing the bottom flange, thus exposing the solid products for recovery. The solids were then removed and photographed and later stored in sealed glass vials. Two solid samples were removed from the reactor after each experiment once the furnace has cooled down; one was dried for 24 hr on a watch glass in a desiccator oven at 100°C and is marked "Anhydrous". The other sample was marked "Hydrate". The hydrated sample was removed from the vial and spread onto a watch glass and allowed to dry in the open air for 24 hr, removing excess liquids that would impede XRD analysis but leaving the hydrates intact. The solid samples were ground into a powder by mortar and pestle and were later analyzed using X-Ray diffraction. Liquid samples were withdrawn from the gas-liquid separator throughout the reaction as well as the next day after the reactor had cooled down. These liquid samples were stored in glass vials and analyzed for pH to indicate the presence of HCl throughout the reaction.

3.1.4 Sample Analysis Methods

The conversion rate of $CuCl_2$ to Cu_2OCl_2 and HCl must be measured to determine the effectiveness of the simplified design. To do this, the pH of the recovered liquids was compared to theoretical values. To determine the presence of Cu_2OCl_2 in the solid products of the reaction, powder X-Ray Diffraction was performed on a Rigaku Ultima 4 powder X-Ray Diffraction system from 10° to 50° with a step size of 0.1°. By comparing peak locations and intensities, we can determine the presence of Cu_2OCl_2 in the solid samples. However, due to the limitations of powder X-Ray Diffraction, the exact proportions of compounds in the solid samples were not known. For this reason, the concentration of HCl

in the recovered liquid samples was used as the main performance metric. For a given set of experimental conditions, we can determine the expected concentration of recovered Hydrochloric Acid. We can then determine the molarity of H^+ and Cl^- ions. This can be then compared to the products of the reaction to determine how much of the $CuCl_2$ reacted and produced liquid HCl.

3.2 Theory and Calculations

3.2.1 Flow Rate Calculations

To determine the flow rates and energy requirements of the reactor, we first consider the production goals of the system and find the number of moles of the reactants required to meet these goals. This can be done through the stoichiometric balances of the reactions in the cycle. To determine the flow rates and energy required for the reactor, the production goals of the Hydrolysis reactor must be considered. The flow rates will be derived from Equations 1-1 through 1-3, repeated here for convenience.

$Hydrolysis$

$$2\ CuCl_2 + H_2O \rightarrow CuOCuCl_2 + 2\ HCl$$

$Thermolysis$

$$CuOCuCl_2 \rightarrow \frac{1}{2} O_2 + 2\ CuCl$$

$Electrolysis$

$$2\ CuCl + 2HCl \rightarrow 2\ CuCl_2 + H_2$$

Given the molar balance in Equation 1-1 and the goal to support 100 g of H_2 production per day, we find that the reaction requires 100 mols of $CuCl_2$ and 50 mols of H_2O per day of operation. Assuming 24hr operation, we can find the hourly consumption rate of $CuCl_2$ to be 4.167 mol/hr. Using the solubility of $CuCl_2$ in water at ambient temperature, we can find the amount of water that must be used to transport $CuCl_2$ into the reactor. This transport solution contains many times more water than the amount of water that is consumed in the reaction.

$$4.167\,\frac{mols}{hr}\,CuCl_2 \cdot \frac{134.452\ g}{mol} \cdot \frac{100\ mL\ H_2O}{75.7\ g\ CuCl_2} = \frac{740.1\ mL\ H_2O}{hr} \tag{3-1}$$

$$\frac{740.1\ ml\ H_2O}{hr} \cdot \frac{0.9982\ g}{ml} \cdot \frac{mol}{18.01488\ g} = \frac{41\ mol\ H_2O}{hr} \tag{3-2}$$

Using the consumed water and the transport water, we can calculate the ratio of H_2O to Copper.

$$\frac{41\ mol\ H_2O}{4.167\ mol\ CuCl_2} = 9.839 \tag{3-3}$$

According to the experimental results of Ferrandon *et al.* [32], at 1.0 bar the steam-to-copper ratio required to achieve maximum yield is 18. Given the flow rate used in these experiments, it would require 1.34 L of H_2O for 555 g of $CuCl_2$. Due to the steam already introduced into the system during the pre-flush phase, the steam-to-copper ratio of input fluids will be 12.

3.2.2 Energy Calculations

The goal of this reactor is to achieve vaporization of the liquid inputs to produce solid $CuCl_2$ and water vapor. The $CuCl_2$ solids and water vapor are heated to 400°C to facilitate the Hydrolysis step. Thus, there are five major energy-consuming operations. These five operations are listed in the below table and include: 1) heating water from 20°C to 100°C, 2) vaporizing water, 3) superheating steam from 100°C to 400°C, 4) heating $CuCl_2$ from 20°C to 400°C, and 5) reaction of $CuCl_2$ and steam. The energy requirement for every step is calculated and can be seen in Table 3-2 below.

Energy to heat water from 20°C to 400°C	245.2 kJ/hr
Energy to vaporize water	1653.8 kJ/hr
Energy to heat steam from 100°C to 400°C	457.4 kJ/hr
Energy to heat $CuCl_2$ from 20°C to 400°C	111.5 kJ/hr
Energy to react $CuCl_2$ and Steam at 400°C	485.9 kJ/hr
Total Energy	2842.2 kJ/hr

Table 3-2: Tabulated energy requirements

3.3 Results and Discussion

3.3.1 Tabulated Experimental Results

Experiment Configuration	**Experiment 1**	**Experiment 2**	**Experiment 3**	**Experiment 4**
Pre-Flush water	1 L	650 mL	350 mL	350 mL
Transport water	900 mL	900 mL	900 mL	700 mL
Post-Flush water	650 mL	650 mL	350 mL	350 mL
Total water	1400 mL	1400 mL	1400 mL	1400 mL
Total CuCl2	554.4 g	554.5 g	523 g	500 g
Steam-to-copper ratio during pumping	12.1	12.1	12.8	10.4
Theoretical pH of HCl product	-0.21	-0.28	-0.42	-0.48
Experimental pH of HCl product	0.93	0.69	0.66	0.67
Conversion Rate	7.65%	10.68%	8.28%	7.23%

Table 3-3 summarizes the experimental results for the four experimental runs. Also listed are the theoretical values calculated using the equations in the previous section.

Experiment Configuration	Experiment 1	Experiment 2	Experiment 3	Experiment 4
Pre-Flush water	1 L	650 mL	350 mL	350 mL
Transport water	900 mL	900 mL	900 mL	700 mL
Post-Flush water	650 mL	650 mL	350 mL	350 mL
Total water	1400 mL	1400 mL	1400 mL	1400 mL
Total CuCl2	554.4 g	554.5 g	523 g	500 g
Steam-to-copper ratio during pumping	12.1	12.1	12.8	10.4
Theoretical pH of HCl product	-0.21	-0.28	-0.42	-0.48
Experimental pH of HCl product	0.93	0.69	0.66	0.67
Conversion Rate	7.65%	10.68%	8.28%	7.23%

Table 3-3: Tabulated experimental results

3.3.2 Solid and Liquid Samples

The results presented here are taken from the four experiments listed above. From each experiment, two solid samples and multiple liquid samples were analyzed.

Figure 3-3: Large Solid products (Experiment 1)

Figure 3-3 shows two views of a solid sample from the first experiment. The crystalline structure of the solid products can be seen. This structure suggests that the solid products,

at one point in the experiment, were in a liquid phase and crystalized during the drying period.

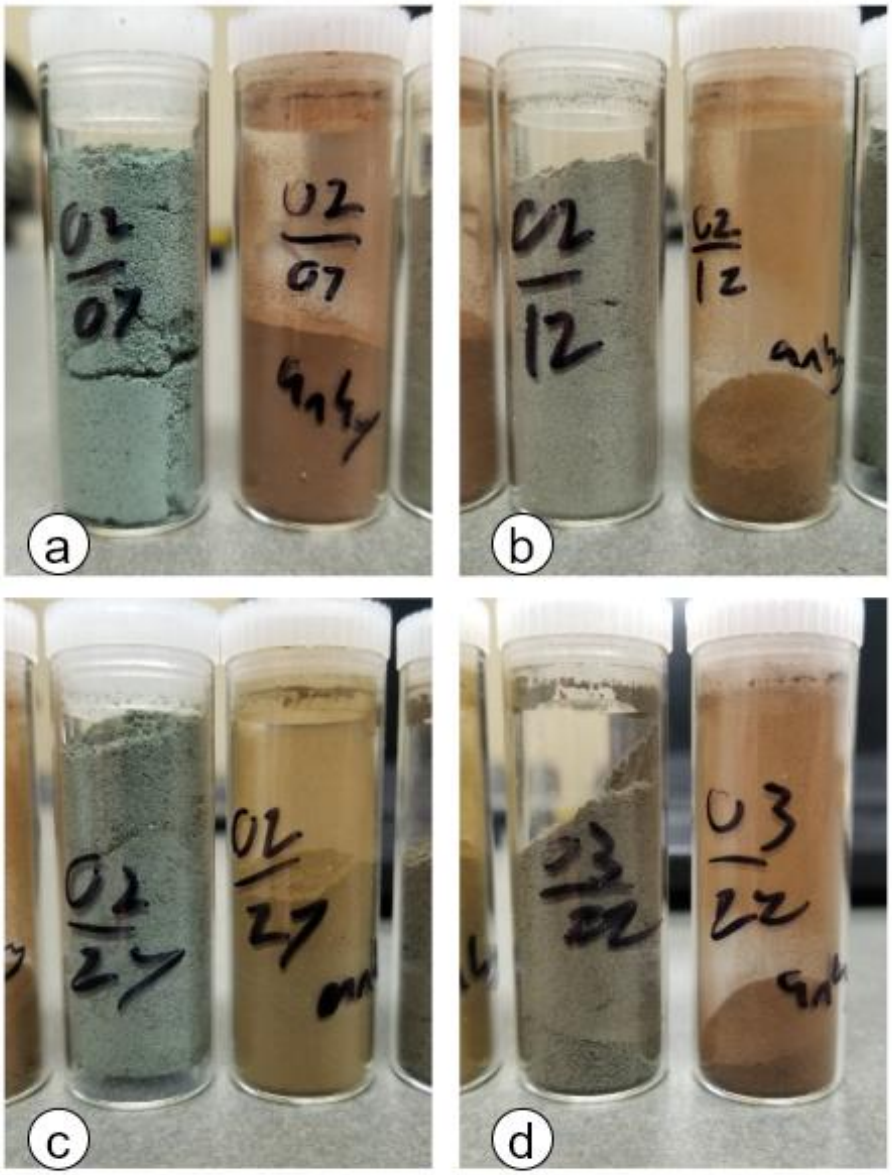

Figure 3-4: Hydrate (left) and Anhydrous (right) samples for a) Experiment 1; b) Experiment 2; c) Experiment 3; d) Experiment 4 (Colours: CuO – Black; Cu_2OCl_2 – Greenish-black, black; $CuCl_2$ anhydrous – black, hydrous – blue/green

Observing the solid samples in Figure 3-4, a trend in the color of products can be seen. In a hydrated state, the solid products are mainly green in color (between teal and olive). Anhydrous products are mostly brown, similar to the color of anhydrous $CuCl_2$.

The liquid samples were recovered from a spigot at the bottom of the gas-liquid-separator (GLS) every 30 min after the $CuCl_2$ pumping operation was completed. A minimum of four samples was drawn to allow the tracking of the pH of the output liquid over time. At the end of each experiment, all remaining liquids in the GLS were removed and stored. When available, a sample was drawn from the GLS the following morning. In this paper, pH was recorded using a PHH-103B portable pH meter by Omega Scientific, with an accuracy of 0.02 pH. It should be noted that at the time of the latest sample taken of the day, most of the liquids were removed. The pH listed for the final sample is the pH of the accumulation of all the liquids recovered, while small samples (~5 ml) were recovered from the GLS the next morning after the reactor had cooled overnight, at 22 hrs past experiment start. The pH of liquid samples are shown in Figures 3-5 through 3-8.

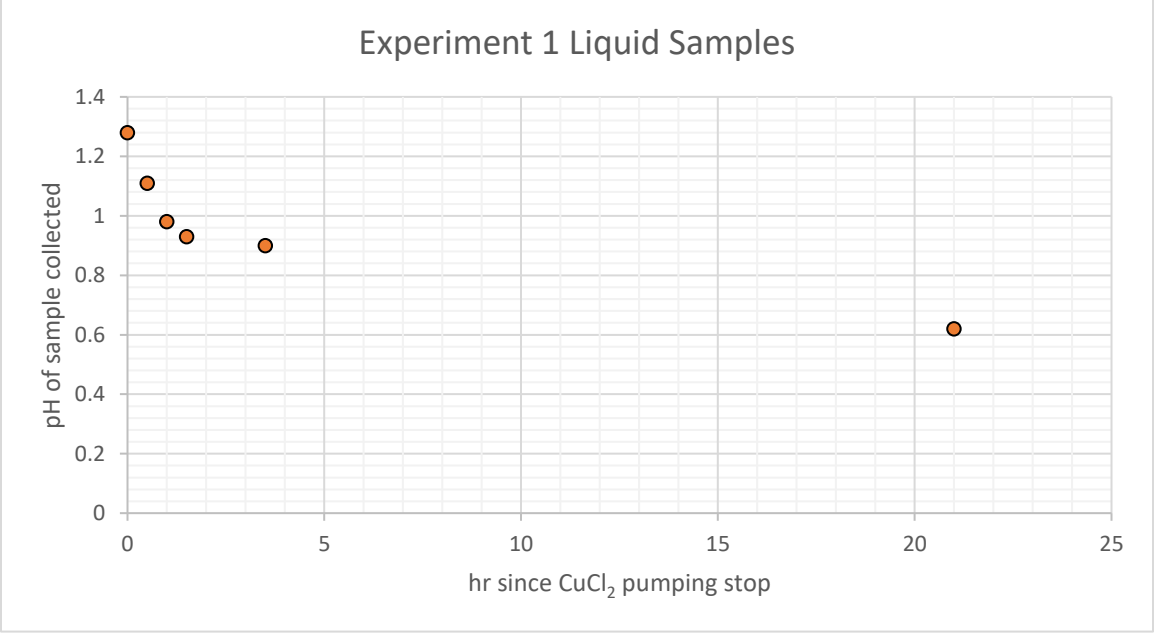

Figure 3-5: pH plot against time for Experiment 1

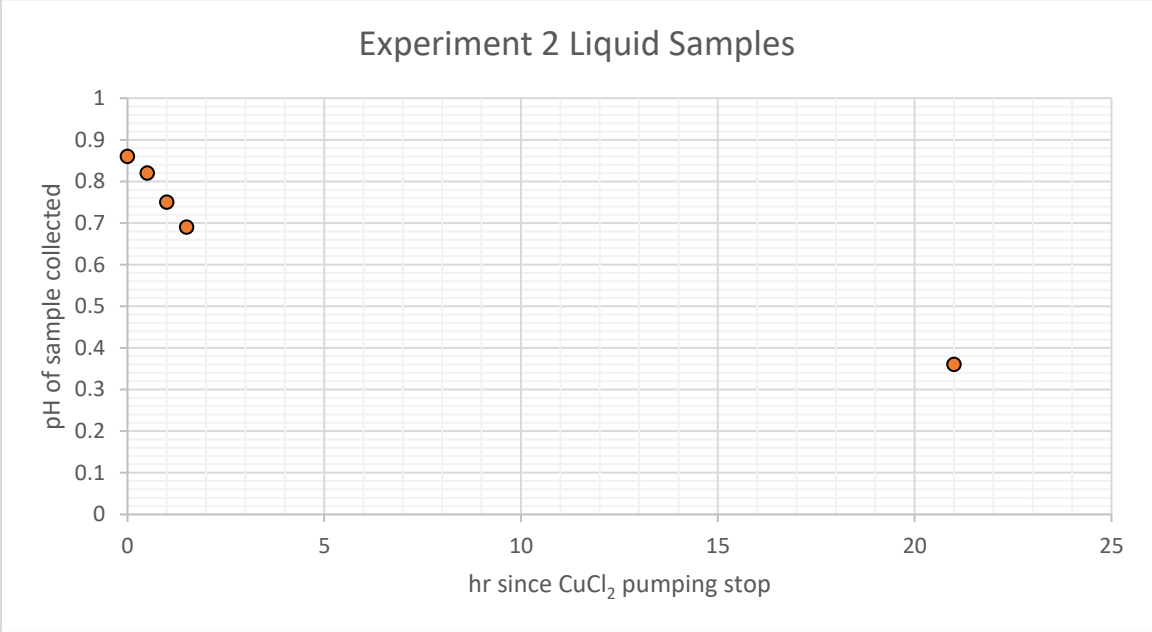

Figure 3-6: pH plot against time for Experiment 2

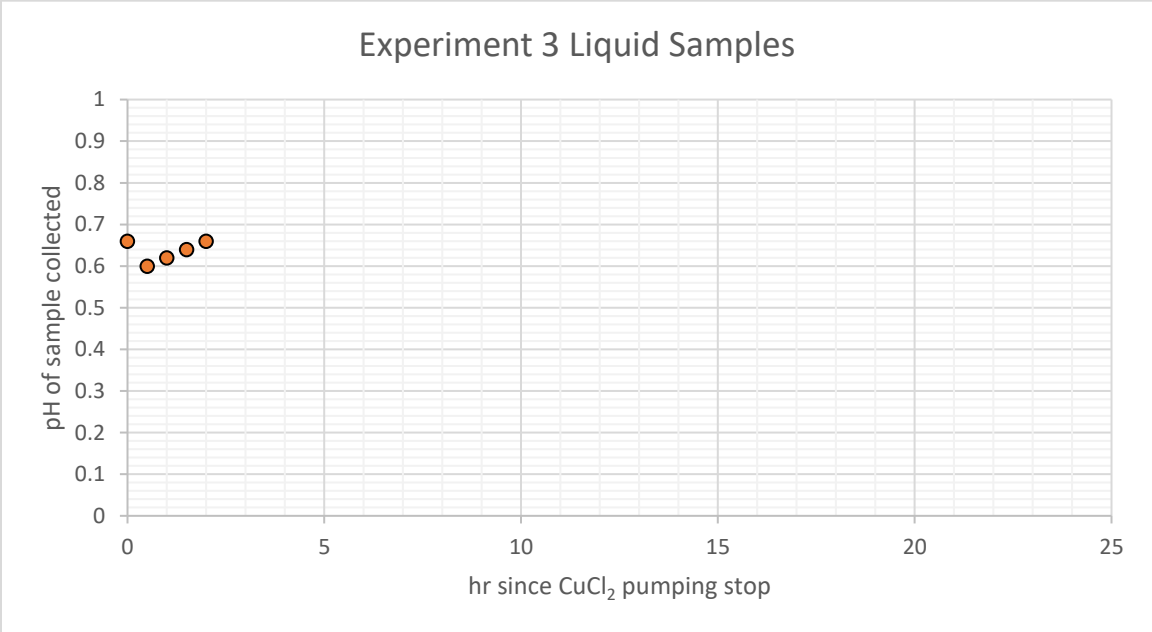

Figure 3-7: pH plot against time for Experiment 3

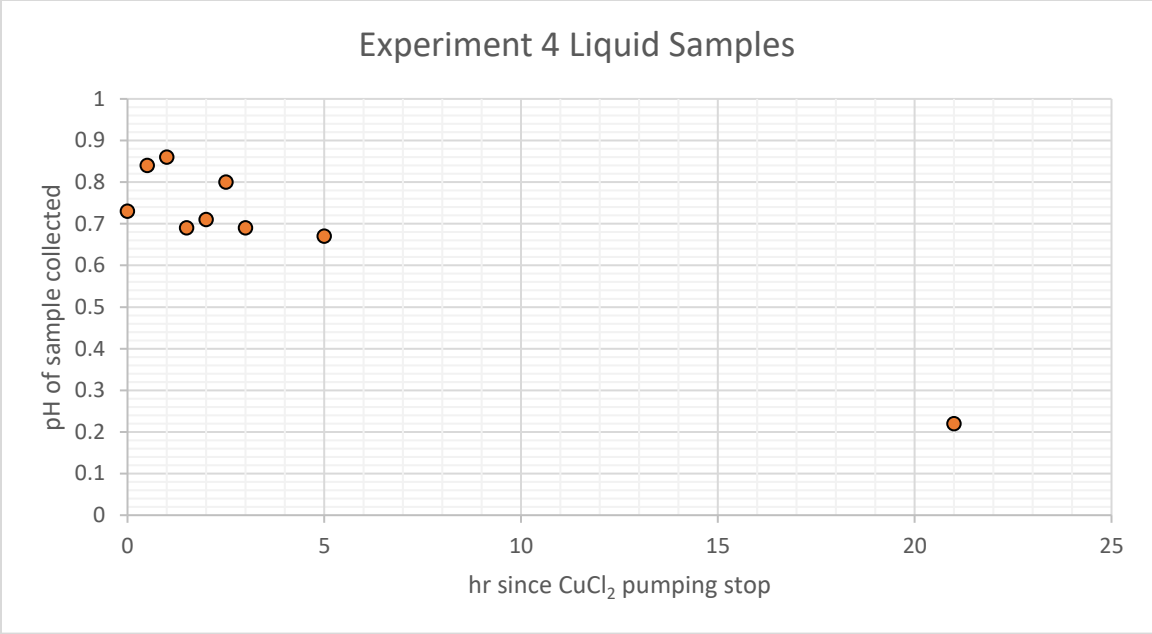

Figure 3-8: pH plot against time for Experiment 4

Figures 3-5 through 3-8 are plots of pH concentration versus time for the four experiments. Examining the trends depicted in these figures, we can see a general downward trend in pH values after the $CuCl_2$ solution pumping was completed. This could be explained as the result of HCl still present in the reactor chamber which is displaced by the post-flush water injection. This downward trend can also be the result of continuing reactions that were not completed at the end of the pumping phase. By converting the pH to the concentration of H^+ ions, we can determine the concentration of HCl in the sample. We find the conversion rate of $CuCl_2$ to Cu_2OCl_2 and HCl to be between 7% and 10% with the current design and operation of the reactor.

3.3.3 Hydrolysis Reference Profiles, High and Low Conversion

The XRD profiles obtained from the solid samples were compared to a pair of reference XRD profiles obtained from experiments conducted at the Argonne National Laboratory. In Figure 3-9, in the lower part of the profile at P = 1 atm, it was noted that the distinct

peaks labeled with a square (■) notation at 17.5, 30.5, 32, 36, 42, and 49 correspond to the presence of Cu_2OCl_2.

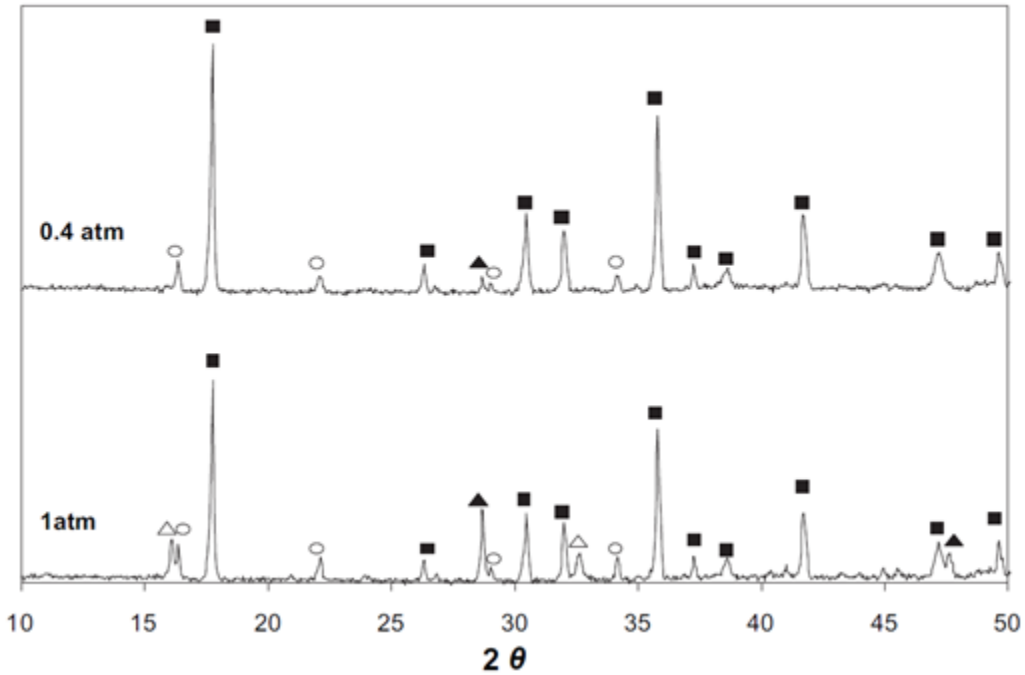

Cu_2OCl_2 (■), $CuCl_2 \cdot 2H_2O$ (○), $CuCl_2$ (●), CuCl (▲) and Cu(OH)Cl (△). Conditions: $CuCl_2$ solution 4.02 m

Figure 3-9: XRD pattern of solid products at 1:15 Cu/H2O molar ratios (source: Ferrandon et al. [32] reproduced with permission)

The second reference profile comes from an earlier experiment at the Argonne National laboratory which demonstrated low $CuCl_2$ to Cu_2OCl_2 conversion. This profile clearly shows prominent $CuCl_2$ peaks at 16, 22, 27, 29, and 34 positions. *Ferrandon et al.* [25] identified the cause of the low conversion in Figure 3-10 as being the result of low Argon gas flow rates, which can shift the equilibrium of the reaction and contribute to poor heat transfer.

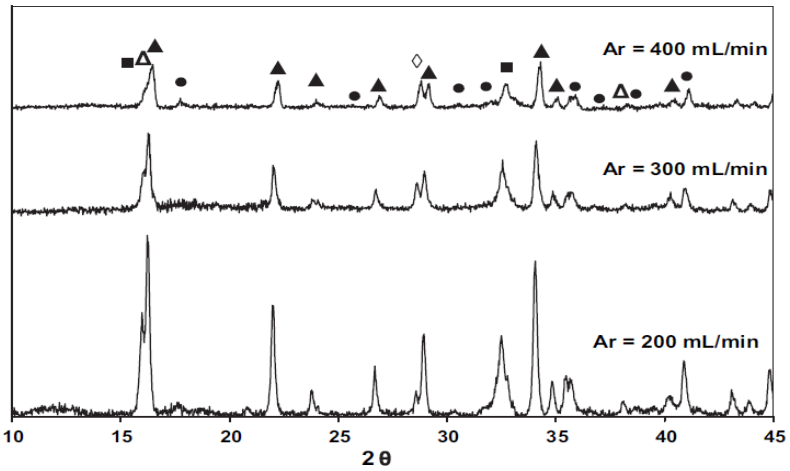

Cu_2OCl_2 (●), $CuCl_2 \cdot 2H_2O$ (▲), $CuCl_2$ (△), CuCl (◊) and Cu(OH)Cl (■). Furnace Temperature = 370°C

Figure 3-10: XRD pattern of solid products at 1:21 Cu/H2O molar ratios (source: Ferrandon et al. [25] reproduced with permission)

3.3.4 XRD Results and Discussion

The XRD profiles for the solid samples are shown below, with Hydrate and Anhydrous profiles superimposed. From these profiles, the prominent peak positions can be identified.

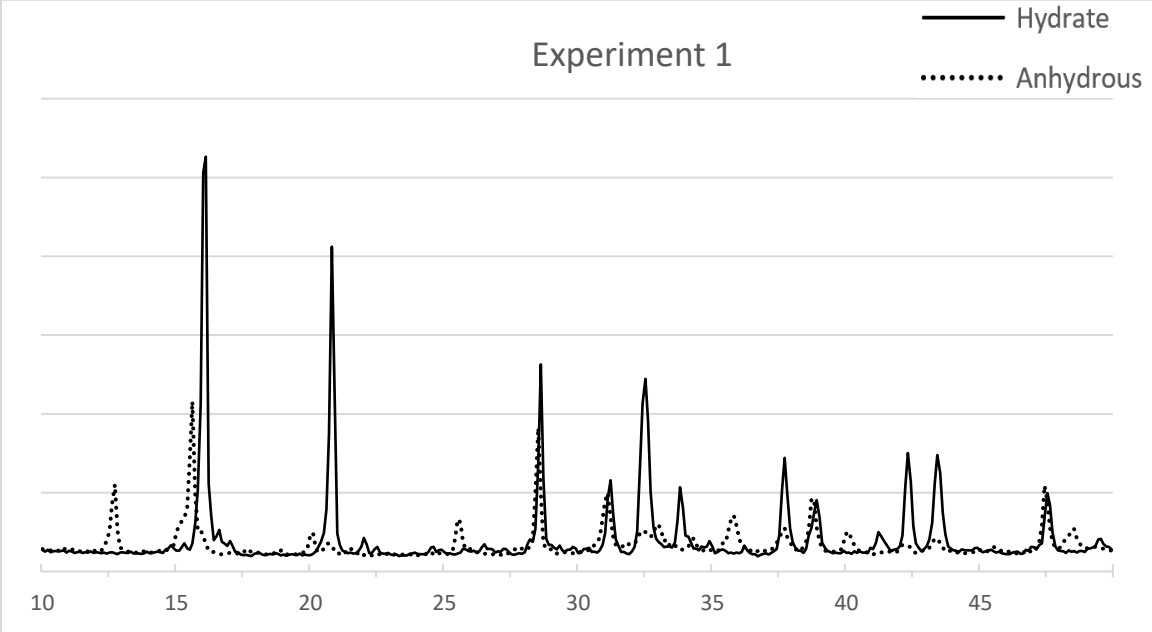

Figure 3-11: XRD results for Experiment 1 Samples

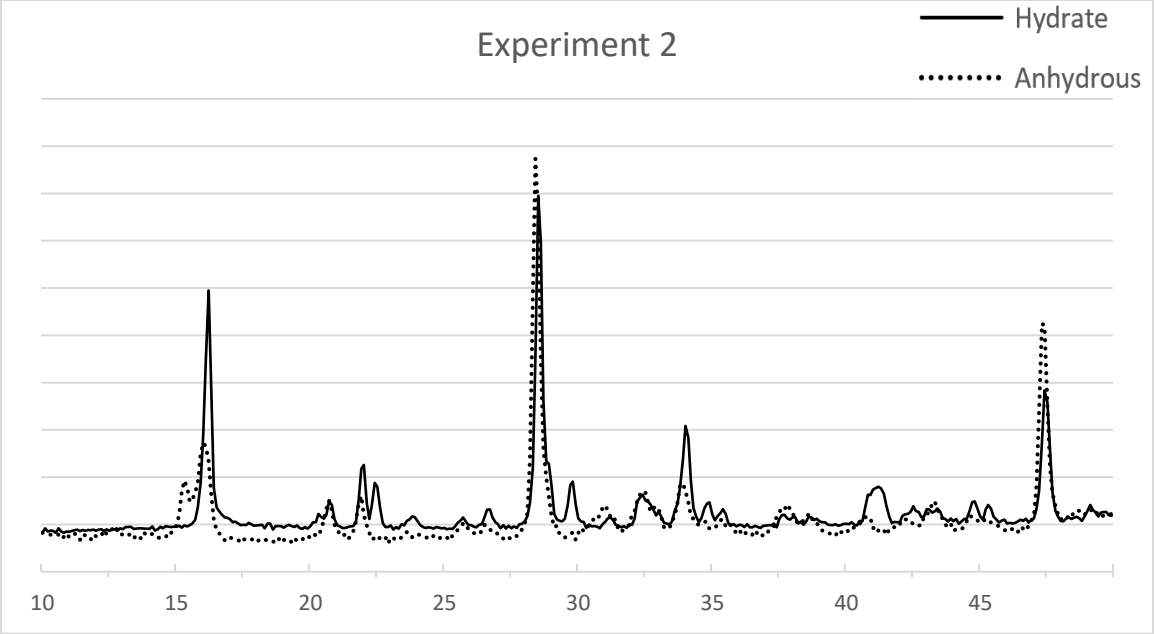

Figure 3-12: XRD results for Experiment 2 Samples

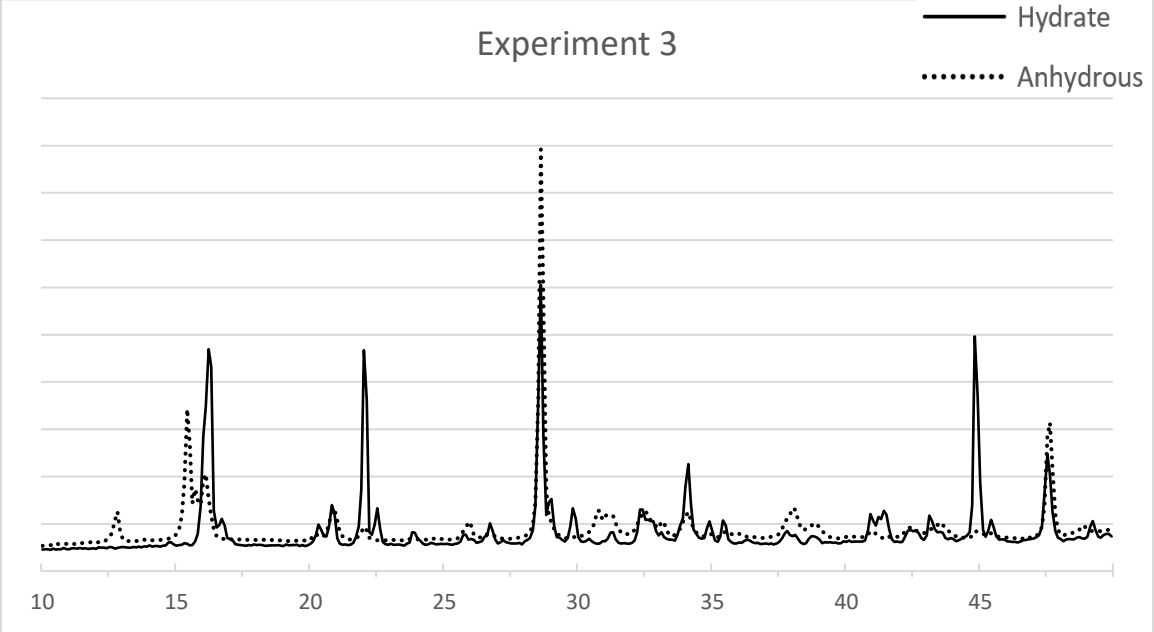

Figure 3-13: XRD results for Experiment 3 Samples

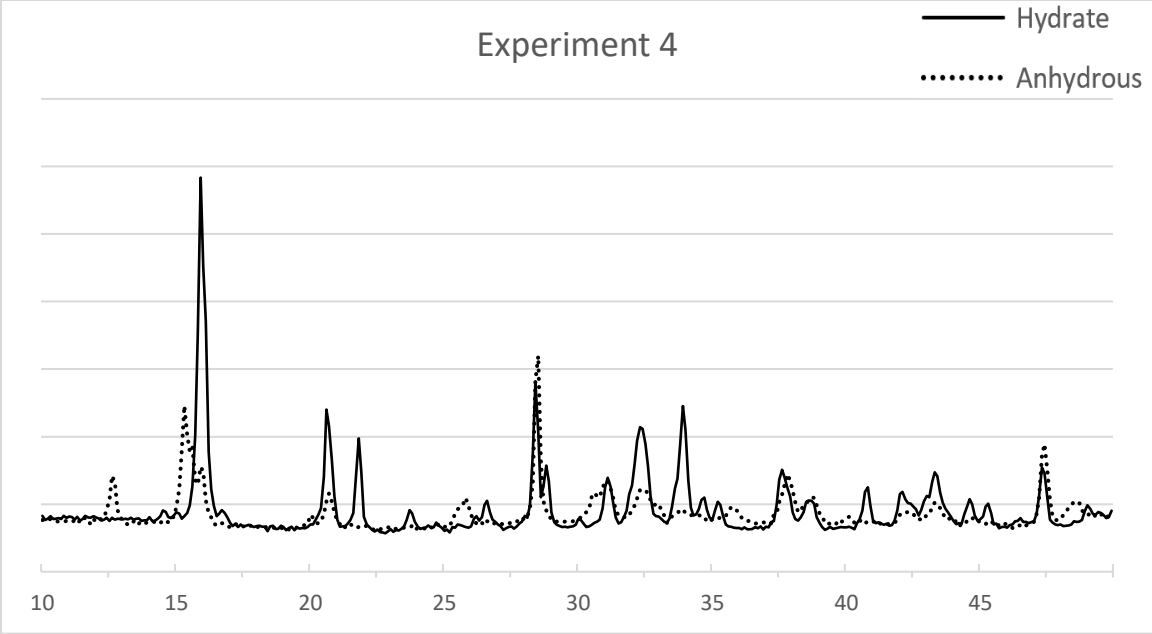

Figure 3-14: XRD results for Experiment 4 Samples

From the locations of prominent peaks in the XRD profiles (Figures 3-11 through 3-14), we can see the peaks line up most prominently with the peaks present in Figure 3-10. These peaks occur mainly at the angles 16º, 22º, 28.5º, and 34º (d-spacing 5.6, 4.02, 3.13, and 2.64) It can be seen that the hydrate peaks line up with peaks indicating the presence of $CuCl_2$ dihydrate, as demonstrated by Ferrandon et al. [32]. Anhydrous profiles demonstrate slightly different peak positions suggesting anhydrous $CuCl_2$. Searching the online mineral database MinDat for these peak angles we can identify these peaks as matching the profiles of Eriochalcite, which is composed of $CuCl_2 \cdot 2H_2O$ [36]. The presence of CuO is not suggested by the XRD results presented in figures 3-11 through 3-14, as these profiles do not show characteristic peaks at 35º and 38º

The presence of large quantities of $CuCl_2$ dihydrate and the absence of Cu_2OCl_2 demonstrated in Figures 3-11 through 3-14 supports the observations made in section 3.3.2,

specifically that little conversion of $CuCl_2$ to Cu_2OCl_2 occurred as evidenced by pH levels in the liquid outputs between 0.6 and 0.8. Comparing this to previous work by Argonne National Laboratory, we can conclude that the low conversion rate was likely caused by the droplets of $CuCl_2$ solution not reacting with the hot steam atmosphere before reaching the bottom of the reactor vessel. This is supported by the observation that during the experiment, the bottom flange of the reactor would reach but never exceed 100°C, suggesting that liquid water was present in large amounts on the flange and was boiling as it was heated. Some conversion of $CuCl_2$ to Cu_2OCl_2 occurred as demonstrated by the acidity of the recovered liquids, but as evidenced by the XRD profiles, the conversion rate was still lower than expected. This is likely caused by the outer layers of the droplets being boiled off during the atomization process releasing very little solid $CuCl_2$ into the vessel to react with the 400°C steam environment. The inner layers of these $CuCl_2$ and water droplets are then passing through to the bottom of the reactor, where the water begins to evaporate, eventually leaving a mostly dry solid crust of $CuCl_2$, CuCl, and little Cu_2OCl_2. Given the steam-to-copper ratio during pumping of around 12, the reactor's maximum theoretical conversion rate would be 60% [32]. The lack of inert carrier gas in the reactant stream can also have contributed to poor conversion. Inert carrier gasses can be used to drive the reaction forwards and minimize reverse reactions, as found by previous studies [32] [18]. This highlights the importance of inert gases and partial pressure control for scaled-up Hydrolysis reactors. The use of inert gases must be considered for industrial reactors to ensure a high yield.

3.4 Summary

The results from the preliminary experiments performed at CERL in 2018 suggest that a simplified Hydrolysis reactor is possible, but will require significant materials science work to ensure that the reactor can operate without damage. XRD and pH analysis suggest that the reactor is currently capable of operating at 7-10% yield, which is well below the yield required for large-scale deployment of the Cu-Cl cycle. The reactor's components, constructed from 316 stainless steel, sustained extensive corrosion damage which led to reaction conditions insufficient for high conversion. Large droplets of $CuCl_2$ solution passed through the reactor without reacting, leading to low yield. Chemical equilibrium within the reactor was also hindered by the lack of any partial-pressure control systems which could have been used to shift the reaction further in the forward direction.

The design of the simplified Hydrolysis reactor suggests that a scaled-up reactor can be constructed using off-the-shelf components if we can ensure that critical components are corrosion resistant. The atomizing nozzle used to provide a fine mist of aqueous $CuCl_2$ proved to be the weak link in the Hydrolysis reactor system and is limited in its material selection by the temperatures which the nozzle must sustain. If a nozzle were constructed from a corrosion-resistant material such as PTFE, fine $CuCl_2$ powder could be made reliably for a long period of operation. Locating the atomizing nozzle within the 400°C Hydrolysis reactor precludes the use of such corrosion-resistant plastics. As such, Hydrolysis can benefit from separating the spray drying step from the Hydrolysis reaction itself, with solid $CuCl_2$ powder produced by the use of low-temperature spray drying and conveyed to the Hydrolysis reactor using screw conveyors. A gas-solid Hydrolysis reactor,

such as the fluidized bed design, would be necessary to react $CuCl_2$ with steam while keeping the solid powder from forming clumps.

Chapter 4 Design of a new Hydrolysis Reactor

As shown in Chapter 3, while the simplified Hydrolysis reactor was able to perform using largely off-the-shelf components, the conversion was very low, and most components suffered considerable damage from continuous exposure to $CuCl_2$ and HCl. The low yield appears to be due in large part to poor contact between the $CuCl_2$ solution droplets and steam in the reactor vessel, causing the $CuCl_2$ solution droplets to pass through the steam without drying or reacting. This was demonstrated by the buildup of a crystalline crust at the bottom of the reactor, suggesting that water was present at the bottom of the reactor that then evaporated, leaving crystals behind. Further evidence of this can be found from temperature data from thermocouples located at the bottom of the reactor that showed a steady temperature of 100°C, suggesting the presence of boiling water caused by incomplete heat transfer between the steam environment and the droplets of $CuCl_2$ solution.

To increase the contact area between the $CuCl_2$ and steam in the reactor vessel, a very fine mist of $CuCl_2$ solution is needed. This fine mist increases the contact area between the droplets and the steam, allowing for better heat transfer. Sufficiently fine mists can be achieved using atomizing nozzles, however, these nozzles are very sensitive to the chemical and thermal environment present in the reactor chamber. Conversations with industrial suppliers of these nozzles suggested that a nozzle would likely not survive more than an hour in the high-temperature HCl and steam environment while in direct contact with $CuCl_2$. Without serious changes to the materials used in the ultrasonic nozzle to a non-reactive or corrosion-resistant material, it is unlikely that an ultrasonic nozzle can be used directly with a scaled-up Hydrolysis reactor.

To allow for fine particles of $CuCl_2$ to be used in the Hydrolysis reactor while also minimizing damage to the atomizing nozzle the spray drying step should be separated from the Hydrolysis step. This allows for $CuCl_2$ powder to be created at low temperatures around 100°C, meaning that chemically non-reactive materials such as PTFE can be used. The resulting powder can then be reacted with steam in a dedicated Hydrolysis reactor without integrating a spray nozzle, effectively keeping the nozzle out of harm's way. Thus, a two-phase gas-solid Hydrolysis reactor can be used, such as a fluidized bed. The fluidized bed allows for simple integration with up-and-down-stream processes while providing high contact area between $CuCl_2$ and steam.

A new concept for the Hydrolysis reactor was initiated in early 2020, involving a recirculating steam sub-system that could be used to recycle unused steam from a Hydrolysis reactor. This newly designed reactor allows for a lower amount of steam to be used during the overall operation while increasing the concentration of HCl in the condenser. This new reactor design was proposed during the Covid-19 pandemic and was modeled theoretically without proof of concept experiments at this time.

4.1 The Recirculating Steam Fluidized Bed

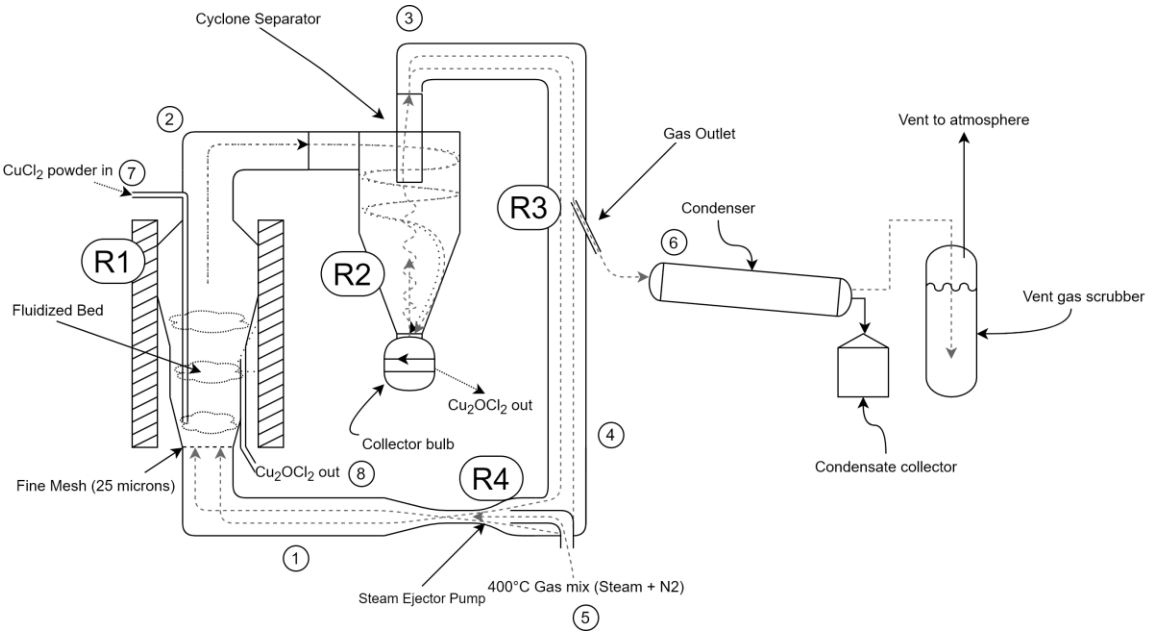

Figure 4-1: Diagram of a Recirculating Steam Fluidized Bed reactor

To address some of the challenges discussed regarding previous Hydrolysis reactors, a novel design for a new concept Hydrolysis reactor is presented and discussed. By modifying a traditional fluidized bed with a recirculating steam flow, the Recirculating Steam Fluidized Bed reactor allows for a portion of the unreacted excess steam leaving the reactor to be captured and recirculated through the reactor chamber. To do this, three major components are included in a traditional fluidized bed design shown in Figure 4-1:

- A cyclone separator (R2), which allows for the removal of small particles entrained in the steam flow

- A Steam removal port (R3), which allows for some of the exhaust gas to be removed; and

- A Steam injector (R4), which injects high-pressure make-up input steam and provides motive power to the stream to counter the pressure drop caused by the fluidized bed and the cyclone separator.

The streams and components of the Recirculating Steam Fluidized Bed reactor are tabulated in Tables 4-1 and 4-2. The component labels correspond to the labels shown in Figure 4-1.

Stream	Composition	Description
1	H2O + HCl	Gas reactant input stream to the fluidized bed
2	H2O + HCl + $CuCl_2$ + Cu_2OCl_2	Gas stream from fluidized bed, containing some small amount of entrained solids
3	H2O + HCl	Gas output stream having been filtered of solids
4	H2O + HCl	Recirculating stream
5	H2O	Primary steam input stream for the system, to be mixed with recirculating stream 4
6	H2O + HCl	Primary gas product output stream, a portion of stream 3
7	$CuCl_2$	Primary CuCl2 input stream for system
8	Cu_2OCl_2	Cu_2OCl_2 product outlet stream

Table 4-1: Streams for the RSFB concept

Component	Description
R1	Fluidized bed reaction vessel.
R2	Cyclone separator used to clean the fluidized bed outlet of any entrained solids
R3	Fractional splitter, which divers some of the flow to be output in stream 6, the remainder flowing through stream 4
R4	Steam ejector pump which provides makeup H_2O and pressure to drive system.

Table 4-2: Components for the RSFB concept

The goal of recirculation is to lower the steam excess requirements by re-using unreacted steam from each pass through the fluidized bed. $CuCl_2$ powder is introduced using either a side port in the reactor or through inlet pipes which allow particles to be introduced directly into the reactor. Steam is introduced through the steam injector. Cu_2OCl_2 is removed through a port or pipe on the opposite side of the reactor (Stream 8), or through particle ablation. As the reaction progresses, collisions between the particles can cause particles to fracture and ablate, resulting in solid transport through the top of the reactor as

the fine fragments of Cu_2OCl_2 are entrained in the flow of steam and removed through a cyclone separator.

Heat is provided through heat exchanger coils around the fluidized bed, and via the introduction of superheated dry steam through the steam injector. Heat requirement is reduced by re-circulating steam and not condensing all of its exhaust after a single pass through the reactor.

4.2 Methodology

4.2.1 Mathematical background

To model the RSFB reactor, a system of equations is used, forming the basis of components and streams. The components together with the equations which are used to model their performance are presented here. These equations, which describe the various systems, are linked together by mass and energy balance equations in Engineering Equation Solver (EES) to form a model which can be evaluated by changing any number of variables. This model takes advantage of the NIST REFPROP libraries built into EES for thermophysical properties of the various components. The equations used in EES represent the system mathematically and are linked by mathematical equivalence.

Each component in EES is modeled according to a common set of mole balance equations for the inputs and outputs, with various component-specific equations which determine the performance of the specific component. Assuming all the HCl produced can be captured in the condenser, and converted into H_2 in the Electrolysis step, then the HCl molar balances are as follows.

$$\dot{N}_{H2} = 2 * \dot{N}_{HCl(6)} \quad (4\text{-}1)$$

Molar balance in the outlet (Figure 4-1 component R3):

$$\dot{N}_{HCl(6)} = \dot{N}_{HCl(3)} * OutletRatio \quad (4\text{-}2)$$

The coefficient $OutletRatio$ is the fraction of steam and HCl which leaves the outlet towards the condensers to the steam which recirculates.

Molar balance in the fluidized bed and the cyclone separator: (Figure 4-1 components R1 & R2)

$$\dot{N}_{HCl(1)} + \dot{N}_{HCl(produced)} = \dot{N}_{HCl(2)} = \dot{N}_{HCl(3)} \quad (4\text{-}3)$$

Molar balance in the jet pump and outlet (Figure 4-1 components R3 & R4):

$$\dot{N}_{HCl(1)} = \dot{N}_{HCl(4)} = \dot{N}_{HCl(3)} - \dot{N}_{HCl(6)} \quad (4\text{-}4)$$

The other major component of the flow in the Recirculating Steam Fluidized Bed is steam, which has the following set of molar balances.

Molar balance in the fluidized bed (Figure 4-1 component R1):

$$\dot{N}_{Steam(1)} - \dot{N}_{Steam(consumed)} = \dot{N}_{Steam(2)} \quad (4\text{-}5)$$

Molar balance in the cyclone separator (Figure 4-1 component R2):

$$\dot{N}_{Steam(2)} = \dot{N}_{Steam(3)} \quad (4\text{-}6)$$

Molar balance in the outlet (Figure 4-1 component R3):

$$\dot{N}_{Steam(3)} = \dot{N}_{Steam(4)} + \dot{N}_{Steam(6)} \quad (4\text{-}7)$$

$$\dot{N}_{Steam(6)} = \dot{N}_{Steam(3)} * OutletRatio \quad (4\text{-}8)$$

Molar balance in the jet pump (Figure 4-1 component R4):

$$\dot{N}_{Steam(4)} + \dot{N}_{Steam(5)} = \dot{N}_{Steam(1)} \quad (4\text{-}9)$$

These molar balance equations will be the foundation of the mathematical model of the RSFB reactor concept. It should be noted that the RSFB has two steam-to-copper ratios. The "System-wide" steam-to-copper ratio is defined as the ratio of input steam at point 5 to the copper entering the fluidized bed at point 7, $SCR = \dot{N}_{H_2O\,(5)}/\dot{N}_{CuCl_2\,(7)}$. The second steam-to-copper ratio is the *effective* steam to copper ratio, SCR_{eff}, and is the ratio of steam-to-copper in the *fluidized bed itself*, $SCR_{eff} = \dot{N}_{H_2O\,(1)}/\dot{N}_{CuCl_2\,(7)}$. The goal of the RSFB reactor concept is to allow the effective steam-to-copper ratio SCR_{eff} to be significantly higher than the system-wide steam-to-copper ratio SCR. The EES code used in this section can be found in Appendix B: EES code. Results and parametric tables are available in Appendices 3 and 4.

4.2.1.1 Component: Fluidized Bed

The Fluidized bed (Figure 4-1 component R1) consists of a chamber containing a flow of steam that suspends a bed of fine $CuCl_2$ powder (Figure 4-2). This chamber must be sized to provide a sufficient superficial velocity of steam, which fluidizes the particles. A particle bed that is just above the minimum fluidization velocity will smoothly fluidize with gas permeating the solid powder bed homogenously. As the superficial velocity increases well above the minimum fluidization velocity, bubbles form and travel through the bed causing the bed height to grow and provide greater mixing [37]. Increasing the superficial velocity past this point can result in the transport of particles elutriating up and out of the bed

through the gas flow. Particle entrainment and transport can result in premature particle removal, and thus incomplete conversion of the $CuCl_2$ particles. For this reason, the fluidized bed should be in the bubbling regime, but avoid the turbulent or transport regime, with the superficial velocity $U < U_{mf} \times 20$ [37].

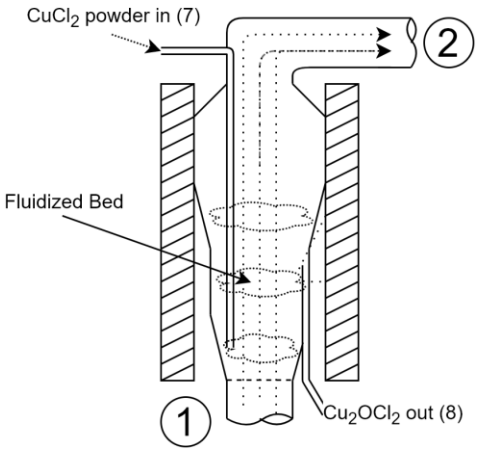

Figure 4-2: Fluidized bed with circulating steam flows (numbers correspond to Figure 4-1)

4.2.1.1.1 Fluidizing velocity

Fluidization of the bed of particles is dependent on the velocity (and therefore, the volumetric flow rate) of the fluidizing gases. The bed of particles will experience a pressure drop as the particles drag on the fluidizing gas. When the minimum fluidization point is reached, the bed begins to be fluidized and gas begins to rise through the bed in bubbles or voids between the particles. As pressure increases, the turbulence increases, and smaller particles will become more easily entrained and transported through the gas flow.

Using the Archimedes number to determine the Reynold's number [38] [37], the minimum fluidization velocity can be estimated:

$$Ar = \frac{\rho_g d_p^3 (\rho_p - \rho_g) g}{\mu^2} \tag{4-10}$$

$$Ar = 1{,}650Re_{p,mf} + 24.5Re_{p,mf}^2 \quad (4\text{-}11)$$

$$Re_{p,mf} = \frac{\rho_g u_{mf} d_p}{\mu} \quad (4\text{-}12)$$

Where:

Ar is the Archimedes Number

d_p is the mean particle diameter

μ is the fluid viscosity

$Re_{p,mf}$ is the Reynold's Number determined at the minimum fluidization velocity

ρ_g is the gas density

u_{mf} is the minimum fluidization velocity

Solving Equation 4-12 for u_{mf} gives the minimum fluidization velocity at which the bed becomes fluidized. Superficial velocity can be found by multiplying the minimum fluidization velocity by some amount, in this case, assumed to be no more than 20 times the minimum fluidization velocity [37].

4.2.1.1.2 Pressure drop in the bed

As the fluidizing gas flows through the bed of particles, the pressure decreases. The pressure drop across the bed is a function of the bed density and height.

$$\Delta P_{bed} = H_{bed} \frac{g}{g_c} \left(\rho_p (1 - \varepsilon) - \rho_g\right) = H_{bed} \frac{g}{g_c} \rho_{\text{bulk}} \quad (4\text{-}13)$$

Where:

ΔP_{bed} is the pressure drop across the bed

H_{bed} is the height of the bed when fluidized

g is the acceleration due to gravity

g_c is the force-weight conversion factor

ρ_p is the particle density

ρ_g is the gas density

ρ_{bulk} is the bulk density

4.2.1.2 Component: Cyclone Separator

The cyclone separator (Figure 4-1 component R2) is used to remove the majority of particles that can be transported out of the fluidized bed. Collisions between the particles can cause the particles to fracture, resulting in fragments too small to remain fluidized which would be pneumatically transported up and out of the reactor. The negative thermal expansion of Cu_2OCl_2 will cause further issues with elutriation, as the reacted particles of Cu_2OCl_2 are only 66% of their original size [21]. Loss of these particles would be detrimental, and their inclusion in the hydrochloric acid output would introduce contamination to the downstream processes. As such, a mechanism to remove these particles from the recirculating stream is needed. A cyclone separator, or series of successive cyclone separators, can be used to remove the particles from the recirculating steam flow through the use of centrifugal force generated by a cyclone. As the input stream enters the cyclone separator, it is directed to flow along the wall of the separator, resulting in a downward cyclone of gas. Centrifugal force acts on the particle, propelling it against the wall where it is slowed by friction causing the particle to eventually lose enough energy; fall out of the stream and into a collection basin. This stream can then exit through the top of the separator, having been cleaned of most of the entrained solids. The efficiency of the cyclone to remove solid particles is dependent on the size of the particles with larger particles being more effectively removed [39]. Since the rate of particle collisions in the

fluidized bed will need to be determined experimentally, it is assumed for this investigation that no particles leave the reactor through pneumatic transport. The cyclone separator as modeled in this investigation only influences the pressure of the stream.

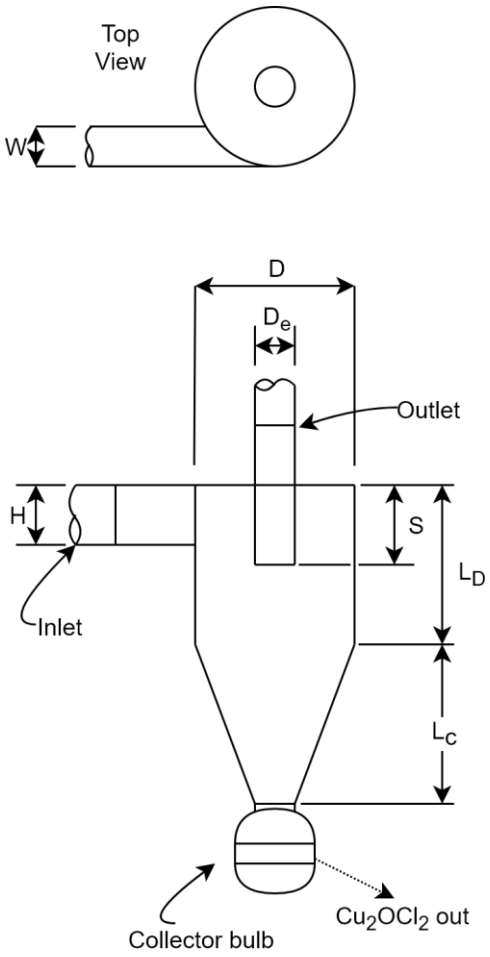

Figure 4-3: Cyclone separator schematic

The cyclone separator is defined by ratios of each of its features, as shown in Figure 4-3. These ratios, along with the conditions of the fluid and particles entering the separator, define the performance. Different groups of ratios exhibit different capabilities, such as high-throughput, high collection efficiency, etc. The selected ratios used for this design specification are:

Height of the inlet: H/D = 0.5

Width of the inlet: W/D = 0.2

Diameter of the exit: $D_e/D = 0.5$

Vortex finder length: S/D = 0.5

Length of body: $L_b/D = 1.5$

Length of the cone: $L_c/D = 2.5$

Diameter of collector: $D_d/D = 0.375$

The design of the cyclone separator used in the Recirculating Steam Fluidized Bed is based on industry-standard sizes for high-efficiency collection cyclones [39]. These ratios provide for the collection of small particles needed to ensure that such particles are removed from the stream before entering the condenser.

4.2.1.2.1 Fractional collection efficiency

The percent chance of a particle being collected is measured by the fractional collection efficiency. The percent efficiency of the cyclone separator to collect a particle of a given diameter is given by the following equation [39].

$$\eta_j = \frac{1}{1+\left(d_{pc}/d_{pj}\right)^2} \tag{4-14}$$

Where η_j is the efficiency of the separator at collecting a particle j of diameter d_{pj}, and d_{pc} is the particle cut-point diameter.

For example, a cyclone separator with a volumetric flow of steam of 0.3099 m^3/s and a gas input velocity of 1.717 m/s, with a body diameter of 42.2 cm with ratios defined above has the following fractional efficiency curve. The cut-point diameter can be seen at 9.108 μm, where a particle of this size would have a 50% chance of being captured. For particles

larger than 29 µm, particles have a 90% chance of being captured. The example cyclone separator used here is sized for compatibility with the recirculating steam reactor to capture particles that exit fluidization due to the fracturing of the particles during conversion, or by wear as particles are abraded by friction with other particles. The fractional collection efficiency of this example cyclone is shown in Figure 4-4.

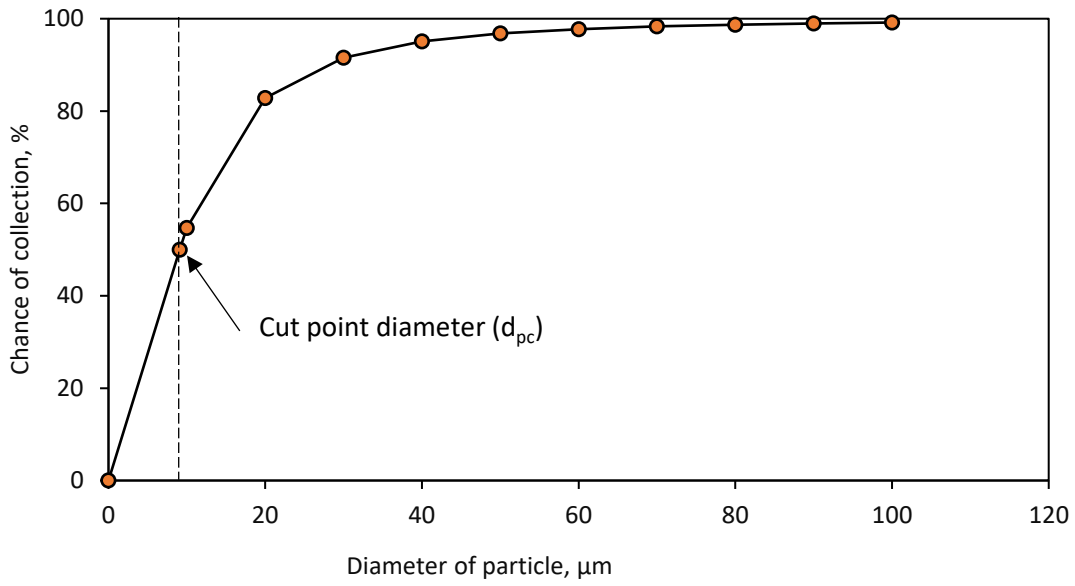

Figure 4-4: Fractional collection efficiency of a cyclone separator

The cut-point diameter can be seen at 9.1×10^{-6} m, where a particle of this size would have a 50% chance of being captured. The cyclone separator demonstrated in Figure 4-4 is an example of the cyclone separator used in the Recirculating Steam Fluidized Bed concept.

4.2.1.2.2 Pressure drop in the cyclone

The cyclone separator has an associated pressure drop as well, which can be determined with the following equation [39].

$$\Delta P = \frac{1}{2}\rho_g V_i^2 K \left(\frac{HW}{D_e^2}\right) \quad (4\text{-}15)$$

Where:

ρ_g is the gas density

V_i is the gas inlet velocity

K is a cyclone constant (Between 12 and 18)

H is the height of the cyclone inlet

W is the width of the cyclone inlet

D_e is the diameter of the gas outlet

4.2.1.3 Component: Outlet Splitter

The outlet splitter (Figure 4-1 component R3) is the simplest component of the RSFB system. It consists of a stream being divided into two streams; one stream (stream 4) contains the recirculating steam, while the other (stream 6) carries steam and the product HCl to the condensers and downstream components of the Cu-Cl cycle. One control is present on the outlet splitter, which is the split fraction, determining the fraction by volume which gets exhausted. A higher split fraction results in less recirculation, and thus more steam required by the steam ejector pump.

4.2.1.3.1 Outlet split fraction

$$\dot{N}_{HCl(3)} * Split\ Fraction = \dot{N}_{HCl(6)} \quad (4\text{-}16)$$

$$\dot{N}_{Steam(3)} * Split\ Fraction = \dot{N}_{Steam(6)} \quad (4\text{-}17)$$

If any particles of Cu_2OCl_2 pass through the cyclone separator, they will be exhausted through the outlet splitter in the same manner as the gasses:

$$\dot{N}_{CuOCuCl2(3)} * Split\ Fraction = \dot{N}_{CuOCuCl2(6)} \quad (4\text{-}18)$$

4.2.1.4 Component: Steam Ejector Pump

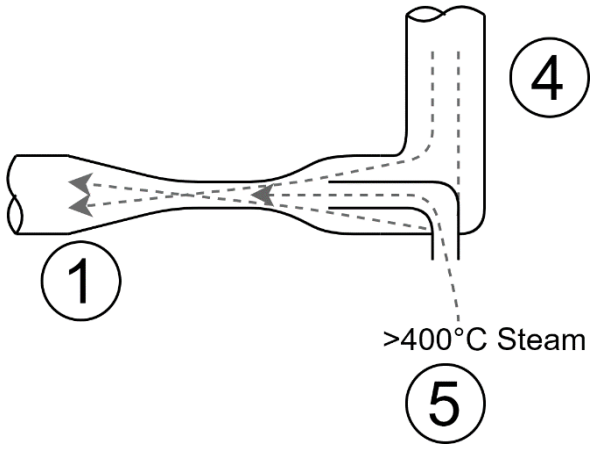

Figure 4-5: Steam ejector pump (numbers correspond to Figure 4-1)

To maintain recirculation, a pump or compressor is needed. This pump or compressor must be able to take the recirculating flow and the make-up flow and propel them through the RSFB components. To do this, compressor blades could be installed in the system with a mechanically driven shaft, although this option presents issues by requiring corrosion-resistant blades, shafts, and bearings. Instead, a steam ejector pump is used. The steam ejector pump (Figure 4-1 component R4) is the last component of the RSFB reactor, consisting of a jet of high-pressure steam which is directed through the center of the flow, causing the flow to be pulled along. This pump has no moving parts; only a jet nozzle for steam in the center and a mixing tube. The lack of moving parts makes this component more resistant to corrosion by the HCl present in the recirculating steam and can withstand most temperatures without binding or losing performance. The mass transfer of the steam ejector pump is modeled in EES as a mixing point between flow 4 and flow 5, mixing to

form flow 1. The pressure effects caused by the high velocity of flow 5 at the nozzle are modeled separately from the mass transfer, with the pump acting simply as a pressure increase. The pressure increase across the pump is matched to counterbalance the pressure drops across the rest of the system, keeping the flow in motion.

4.2.1.4.1 Jet pump equations

There are several variations for the equations that describe a jet pump operation which are differentiated by the states of the fluids involved. If the fluids are both in the liquid or gas phase but with a small pressure difference, a simple form of the equations can be used [40]. If the pressure ratio is above 1.8, a different system of equations must be used which tends to be more complicated due to compressive effects and in some cases, jets reaching the speed of sound in the fluid. It has been shown that, as long as the ratio **P(5)/P(4)** is below 1.8, liquid-liquid equations can be used even in gas-gas-type pumps.

The mass flow ratio μ_m of the ejector pump is given by:

$$\mu_m = \dot{M}_4/\dot{M}_5 \tag{4-19}$$

The characteristic jet pump equation relates the pressure ratio (π_m) and the mass flow ratio (μ_m) and as reported by Wilman [41]. Inputting μ_m based on the molar flow entering the pump (Equation 4-20), and using coefficients that describe a well-designed jet pump, the value of π_m can be found. For high-performance jet pumps, the mathematical characteristic values in the model, K_s, K_t, K_m, K_d , are assumed to be 0.05, 0.05, 0.06 and 0.14, respectively. The diameter ratio δ is defined as the ratio of the diameter of nozzle divided by the diameter of the mixing tube, $\delta = \frac{d_s}{d_m}$. This ratio is usually assumed at the beginning and can be further refined to find the ratio which yields the highest efficiency.

$$\pi_m = \frac{(1+K_s)-(1+K_t)\mu_m^2\frac{\delta^4}{(1-\delta^2)^2}}{2\delta^2+2\mu_m^2\frac{\delta^4}{(1-\delta^2)^2}-(1+K_m+K_d)(1+\mu_m)^2\delta^4} \quad (4\text{-}20)$$

With the value of π_m found, we can now estimate the value of P_5 by solving the pressure ratio, with P_1 and P_4 known.

$$\pi_m = \frac{P_1-P_4}{P_5-P_1} \quad (4\text{-}21)$$

P_5 is the pressure of the gas input which is required to size the steam super-heater and generator needed to feed the reactor. With the pressure ratio π estimated, the diameter of the nozzle required to produce sufficient pressure can be now determined. First, the flow coefficient φ must be calculated.

$$\varphi = (1+K_s) - (1+K_t)\mu_m^2\frac{\delta^4}{(1-\delta^2)^2} \quad (4\text{-}22)$$

$$d_s = 1.13\sqrt{\dot{M}_5}^4\sqrt{\frac{\varphi}{2\rho\pi(P_1-P_4)}} \quad (4\text{-}23)$$

With the diameter ratio δ known, the diameter of the mixing tube can be calculated.

$$d_m = \frac{d_s}{\delta} \quad (4\text{-}24)$$

The other dimensions can be determined by using known, experimentally proven ratios for well-functioning steam ejector pumps. The length of the nozzle can be calculated with $l_n = 6 * d_s$. The length of the mixing tube by $l_m = 8 * d_m$, the length of the diffuser by $l_d = 0.6 * d_m$, and the radius of the internal blends just ahead of the nozzle by $r = 0.5 * d_m$. With this, complete information for the sizing of a jet pump is available.

4.2.2 Aspen Plus modeling

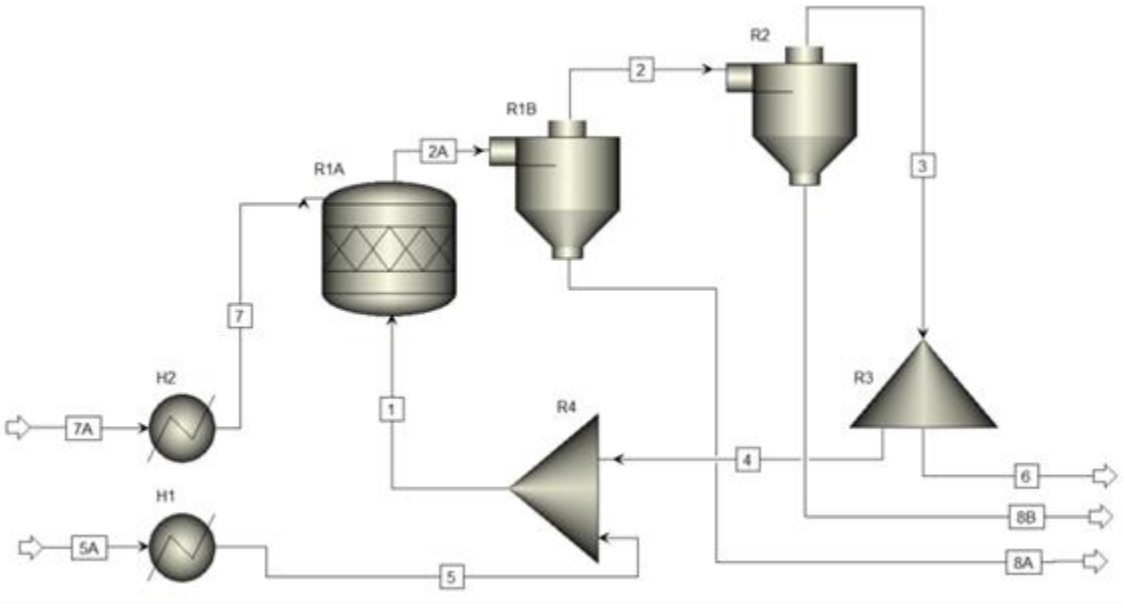

Figure 4-6: Aspen Plus Output: model flowsheet

The Aspen Plus model was used to replicate the conditions of the RSFB reactor concept and validate the results calculated using EES. The Aspen Plus model is composed of components and streams which link together, with flow rates that can be computed once starting conditions are given. The flowsheet of the reactor in Aspen Plus (Figure 4-6) can also be updated in the future to model the reaction kinetics of fluidized beds. With a complete Aspen Plus model of the RSFB reactor, parametric studies are conducted focusing on key parameters such as the flow of steam and HCl in various streams. The heat requirements are also available for a range of steam-to-copper ratios. However, the Aspen Plus model does not include detailed modeling of the cyclone separator or steam ejector pump. For these components, only the mathematical model in EES is used to determine the reactor's performance.

Stream	Composition	Description
1	H2O + HCl	Gas reactant input stream to the fluidized bed
2	H2O + HCl + CuCl2 + Cu_2OCl_2	Gas stream from fluidized bed, containing some small amount of entrained solids
2A	H2O + HCl + CuCl2 + Cu_2OCl_2	An imaginary stream containing entrained solids being transported to R1B phase separation within the fluidized bed
3	H2O + HCl	Gas output stream having been filtered of solids
4	H2O + HCl	Recirculating stream
5	H2O	Primary steam input stream for the system, to be mixed with recirculating stream 4
5A	H2O	Unheated water stream, input to the system at room temperature
6	H2O + HCl	Primary gas product output stream, a portion of stream 3
7	CuCl2	Primary CuCl2 input stream for system
7A	CuCl2	Unheated CuCl2 stream, input to the system at room temperature
8A	CuCl2 + Cu_2OCl_2	Primary Cu_2OCl_2 output stream, from the fluidized bed
8B	CuCl2 + Cu_2OCl_2	Secondary Cu_2OCl_2 output stream, from cyclone separator

Table 4-3: Streams for RSFB simulation in Aspen Plus

Component	Description
R1A	Half-component of the fluidized bed, modeling the chemical reaction
R1B	Half-component of the fluidized bed, modeling the phase separation effect of fluidized bed solids outlets
R2	Cyclone separator used to clean the fluidized bed outlet of any entrained solids
R3	Fractional splitter, which divers some of the flow to be output in stream 6, the remainder flowing through stream 4
R4	Mixer, modeling the steam ejector pump which mixes fresh H2O and recirculated H2O and HCl
H1	Superheated steam generator
H2	CuCl2 input heater

Table 4-4: Components for RSFB simulation in Aspen Plus

It is worth noting that, with the Aspen model, the fluidized bed in the non-kinetic model is split into two components, R1A and R1B. R1A is the reactor itself, with a single vapor phase output entrained with Cu_2OCl_2, while R1B represents the phase separation that occurs within the fluidized bed itself. In practical terms, these two components are one in the final fluidized bed design, with component R2 representing the cyclone separator needed to remove any entrained particles that escape the fluidized bed.

Streams 5A and 7A represent the H_2O and $CuCl_2$ input flows at room temperature, respectively, while flows 5 and 7 represent these flows heated to 400°C. R4 represents two

flows merging to form stream 1, modeling the steam introduction through the Jet Pump. R3 represents a flow splitter that uses a split-fraction determined mathematically to remove a portion of the flow and recirculate the remainder. By adjusting the split fraction of R3, the steam-to-copper ratio (SCR_{eff}) in the fluidized bed can be controlled while maintaining a constant system SCR of 7. This allows the design to quickly adjust to preferred operating conditions. The stream summary of results from Aspen Plus can be found in Appendix E.

4.3 Results and Discussion

4.3.1 Relationship between steam-to-copper ratio and split fraction

With the EES and Aspen models complete, the results could be presented and discussed using a parametric study to determine the performance of the newly developed RSFB under different operating conditions. The results focus specifically on the thermal and flow conditions within the RSFB reactor. All studies were conducted using a reactor operating under the following conditions unless otherwise stated:

H2 production	100 g/hr
HCl production	100 mol/hr
SCR	7
SCR_{eff}	18
Reaction Temperature	400°C
Reaction Pressure	1 atm
$CuCl_2$ particle size	100 µm

Table 4-5: Standard RSFB operation conditions

For the RSFB reactor to function, recirculation needs to be possible while maintaining a desired effective steam-to-copper ratio. This is done by adjusting the outlet split fraction.

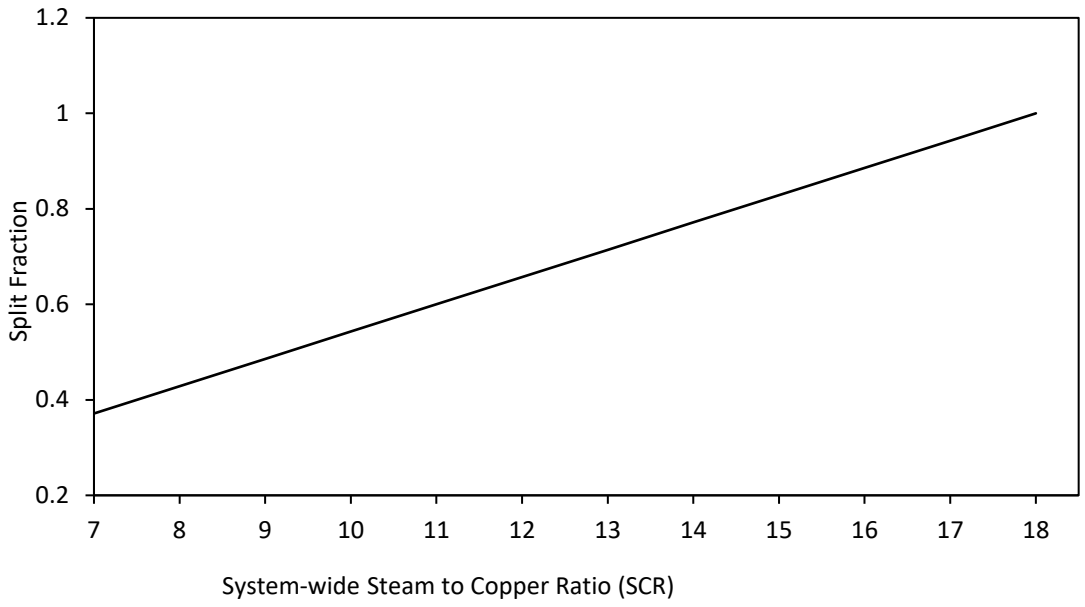

Figure 4-7: Effect of changing SCR on the split fraction

Figure 4-7 demonstrates the relationship between the system-wide SCR and the split fraction required to maintain a constant SCR_{eff} in the bed. As the system-wide SCR of the RSFB reaction is modified, the split fraction used in the outlet can be adjusted to maintain a sufficient SCR_{eff} in the reaction chamber. By changing the split fraction, operators can adjust the amount of steam to be recirculated allowing the reactor to be reconfigured for a different system-wide SCR while still maintaining the desired SCR_{eff} of 18. This confirms that the system-wide SCR can be reduced to 7 without affecting the operating conditions necessary for complete reaction with the Hydrolysis reactor.

4.3.2 Effect of steam-to-copper ratio on thermal energy

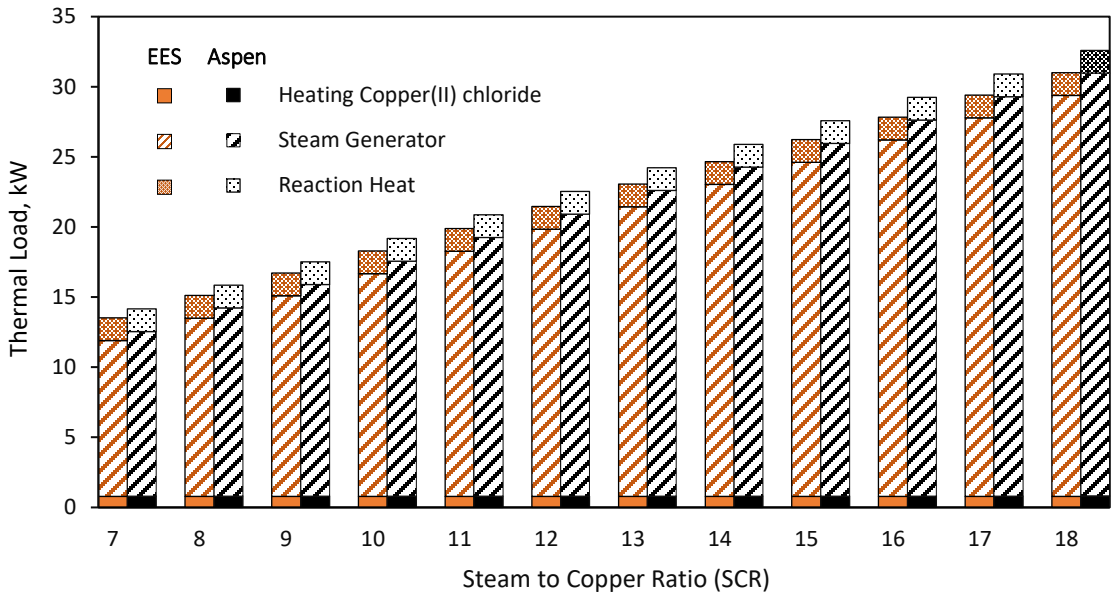

Figure 4-8: Thermal loads of reactors with various SCRs, using EES and Aspen Plus

As clearly seen in Figure 4-8 the thermal input requirement of the Hydrolysis step can be significantly reduced by recirculating some portion of the steam left unconsumed during the reaction. This can be done while maintaining a constant SCR_{eff} of 18 in the fluidized bed. As discussed earlier, this is accomplished by setting the steam supply in stream 5 to a desired system-wide SCR and adjusting the outlet split fraction to ensure recirculated steam is sufficient for the desired SCR_{eff}.

The results in Figure 4-8 for the thermal requirements plotted against the system-wide SCR are shown for both EES and Aspen Plus models. The bulk of the energy required for the reaction is provided via steam generation (hatched orange bars for EES and hatched black bars for Aspen+). The energy required to heat CuCl2 to reaction temperature (solid orange and black bars), and the heat of reaction (dotted orange and black bars) are fixed values

and constitute a small amount in comparison to the energy from steam generation. It is worth noting that the small discrepancy between the results from Aspen Plus and EES (6.7% on average) is likely due to differences in the thermophysical properties of H_2O in the libraries of the programs used in each model.

As can be seen, the thermal load is reduced when SCR is reduced from 18 to 7. The result is significant since it effectively translates to major savings in energy input. This is evident when we compare a reactor operating without recirculation at SCR 18 to a reactor operating with recirculation at SCR 7. Consider the Aspen Plus results. At SCR 18, the thermal requirement for a reactor producing 100 mol of HCl per hour is 32.6 kW, while at SCR 7, a reactor sized for the same production requires only 14.2 kW. This translates to a saving of approximately 56% in the thermal energy input.

4.3.3 Ejector pump nozzle velocity

Lowering the system-wide SCR also requires adjusting the flow through the steam ejector pump nozzle. As recirculation increases, the amount of new steam supplied is lowered, requiring less steam but at a much higher velocity. To avoid the damaging effects of sonic shockwaves, the steam flow is kept well below the speed of sound. The SCR used in this study is 7, which corresponds to a nozzle velocity of 200 m/s; well below the speed of sound in steam. As SCR is reduced, the nozzle velocity becomes increasingly high, as demonstrated in Figure 4-9. A steam-to-copper ratio lower than 7 increases the velocity significantly and could produce undesired effects from sonic shocks that can damage the reactor's equipment.

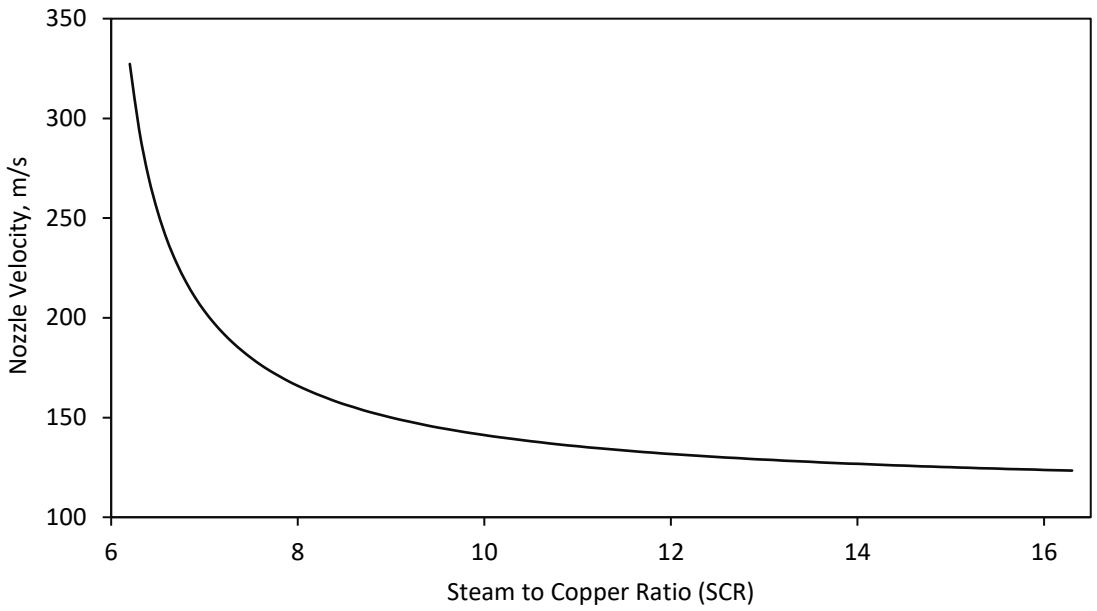

Figure 4-9: Nozzle velocity vs. SCR

4.3.4 HCl recirculation and acid concentration

Another advantage of this system is its ability to adjust the outlet split fraction. In doing so, the SCR_{eff} also changes yielding an increase in the concentration of HCl in the steam recirculating flow. The effect of the outlet split fraction on the SCR_{eff} and the concentration of HCl in the recirculating flow is shown in Figure 4-10. Using the outlet split fraction to control steam recirculation and SCR allows for the RSFB Hydrolysis reactor to be tuned and adjusted during operation to achieve a preferred SCR in the bed while leaving the rest of the operation unaffected. This is an important consideration as a higher concentration of HCl in the steam flow, if not handled properly, can result in reverse reactions.

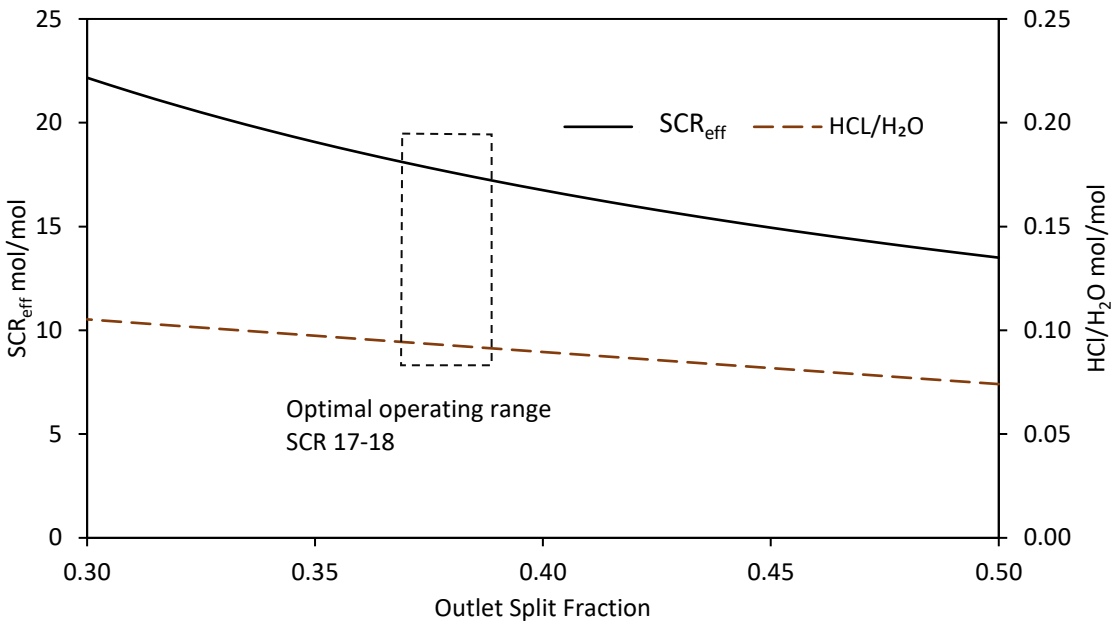

Figure 4-10: Effect of split ratio on SCR and HCl concentration in recirculated steam

As shown in Figure 4-10, the concentration of recirculated HCl reaches a maximum of 0.105 mol HCl/mol H_2O at the lowest split fraction of 30%. During the normal operation for a reactor at SCR_{eff} of 18, and a system-wide SCR of 7, the outlet split fraction is calculated to be 0.3714, resulting in 0.047011 mol/s of HCl and 0.500018 mol/s of H_2O to be present in the fluidized bed's inlet. In this case, HCl represents 9.4% of the flow by mole. The amount of HCl in the recirculating flow is an important factor for determining the extent of reverse reactions, as will be discussed in Section 4.3.5. Results reported by Wang *et al.* have shown that 11 Molar HCl solution is required to produce Hydrogen [7] [31]. Since available designs for Hydrolysis reactors involve large amounts of excess steam, the concentration of HCl produced in them is limited by the ratio of HCl and the unreacted excess steam producing a concentration ~3.16 M. This requires an intermediate step of pressure-swing distillation to raise the HCl concentration from 3.16 M to 11 M [35]. A major benefit to the RSFB over other open-loop reactors is process integration. It is

understood that using a fluidized bed without recirculation produces a very dilute acid not suitable for immediate use downstream in the Electrolysis cell. However, by altering the balance of water and $CuCl_2$ (i.e., the system-wide steam-to-copper ratio, SCR), the concentration of the resulting acid in the condenser can be controlled. This relationship between SCR and the molarity of the HCl products is shown in Figure 4-11.

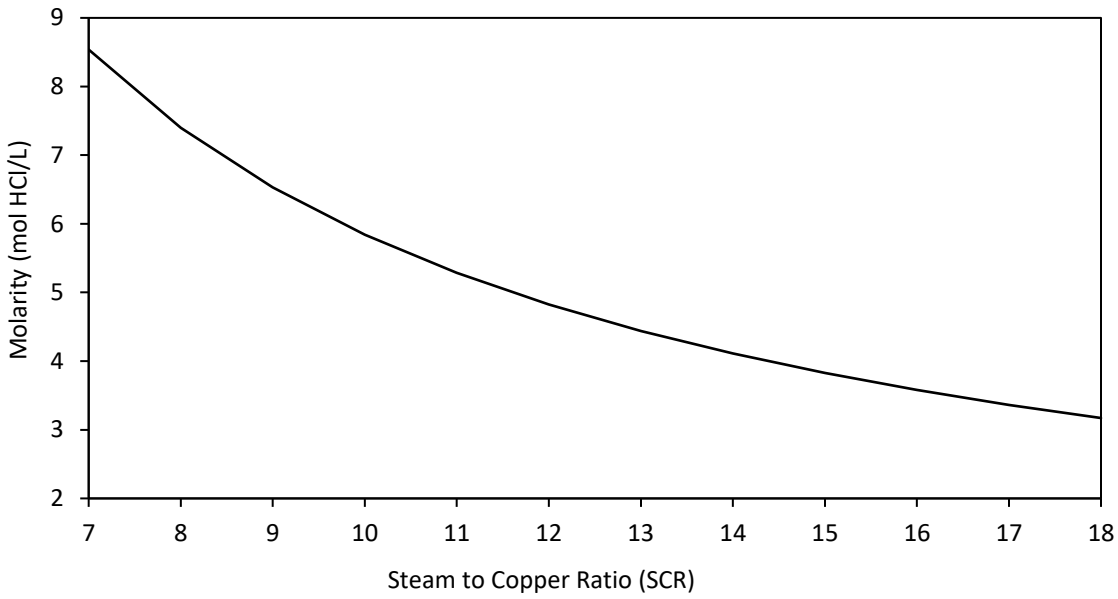

Figure 4-11: Molarity of product HCl vs. SCR

By running the reactor at a lower system-wide SCR, the molarity of the output acid is significantly increased from 3.17 mol/L to 8.54 mol/L. This is much closer to the molarity of HCl required for completing the Electrolysis step. By producing a stronger product acid, further savings can be made by requiring less distillation of the HCl acid. This also reduces the complexity of the intermediate steps required to integrate the Hydrolysis reactor into a fully operational CuCl Hydrogen production cycle.

4.3.5 Reaction kinetics

In the Recirculating Steam Fluidized Bed, the concentration of HCl in the input stream increases as the concentration of H_2O increases, due to the nature of recirculation. Figure 4-10 shows that for a steam-to-copper ratio of 18, the mole fraction of HCl to H_2O in the input stream is 0.9, and rises as the steam-to-copper ratio is increased. This concentration of HCl in the input stream has been found in previous studies by Daggupati *et al.* to increase the steam required, with even low concentrations of HCl causing the reaction to effectively stop. To fully investigate the effect of HCl recirculation, the chemical equilibrium of the RSFB reactor must be investigated.

The chemical equilibrium equations presented by Pope *et al.* in 2012 and 2013 provide an equation to determine the limit of HCl in the Hydrolysis reaction at equilibrium. Exceeding this limit would result in the reaction halting or reversing. Using Equations 2-1, 2-4, and 2-7 from Chapter 2, we can determine the Equilibrium constant, and compare it against the reaction quotient for the range of system-wide Steam-to-copper ratios. Equations 2-1, 2-4, and 2-7 are repeated here for convenience.

$$K_e = \mathrm{e}^{\left(-\frac{\Delta G_R^\circ}{RT}\right)}$$

$$Q_R = \frac{N_{HCl}^2}{N_{H_2O}}\left(\frac{p_T}{N_{HCl}+N_{H_2O}+N_i}\right)$$

$$X_{HCl} = \sqrt{\left(\frac{e^{-\left(\frac{\Delta G_R^\circ}{RT}\right)}}{2\left(\frac{p_T}{P_0}\right)}\right)^2 + \frac{e^{-\left(\frac{\Delta G_R^\circ}{RT}\right)}}{\left(\frac{p_T}{P_0}\right)}} - \frac{e^{-\left(\frac{\Delta G_R^\circ}{RT}\right)}}{2\left(\frac{p_T}{P_0}\right)}$$

Evaluating K_e, Q_R, and X_{HCl} (at equilibrium, referred to as X_{HClmax}) across steam-to-copper ratios 7 through 18, we can see that even with recirculation, the reaction quotient Q_R doesn't reach K_e. At an SCR of 7 and an SCR_{eff} of 18, the RSFB reactor was found to have an equilibrium constant of 0.05786, and a reaction quotient of 0.02051. The reaction quotient being lower than the equilibrium constant suggests that reactions will continue in the forward direction.

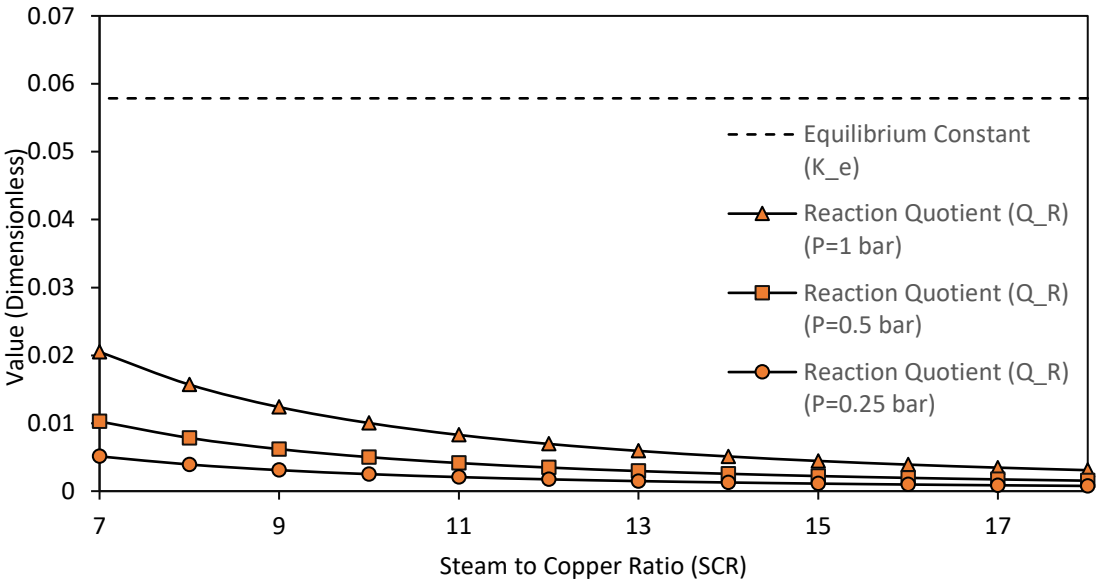

Figure 4-12: Reaction quotient vs. SCR and Pressure

The mole fraction of HCl X_{HCl} similarly does not exceed the maximum mole fraction of HCl at equilibrium X_{HClmax}. This suggests that across this range of steam-to-copper ratios, despite the HCl buildup due to recirculation, the reaction doesn't meet or exceed equilibrium. It can therefore be assumed that the reaction will be still progressing in the forward direction, without the complete halt of conversion that Daggupati *et al.* [24] predicted. The reaction quotient can be further shifted downward – and the maximum mole fraction of HCl can be shifted upward – by changing the pressure of the reaction (Shown

in Figure 4-13). A similar effect can be found by adjusting the content of nitrogen in the system and is displayed in Figure 4-14. The mole fraction of Nitrogen is defined by Equation 4-25.

$$X_{N_2} = \frac{\dot{N}_{N_2}}{\dot{N}_{H2O}+\dot{N}_{HCl}+\dot{N}_{N_2}} \tag{4-25}$$

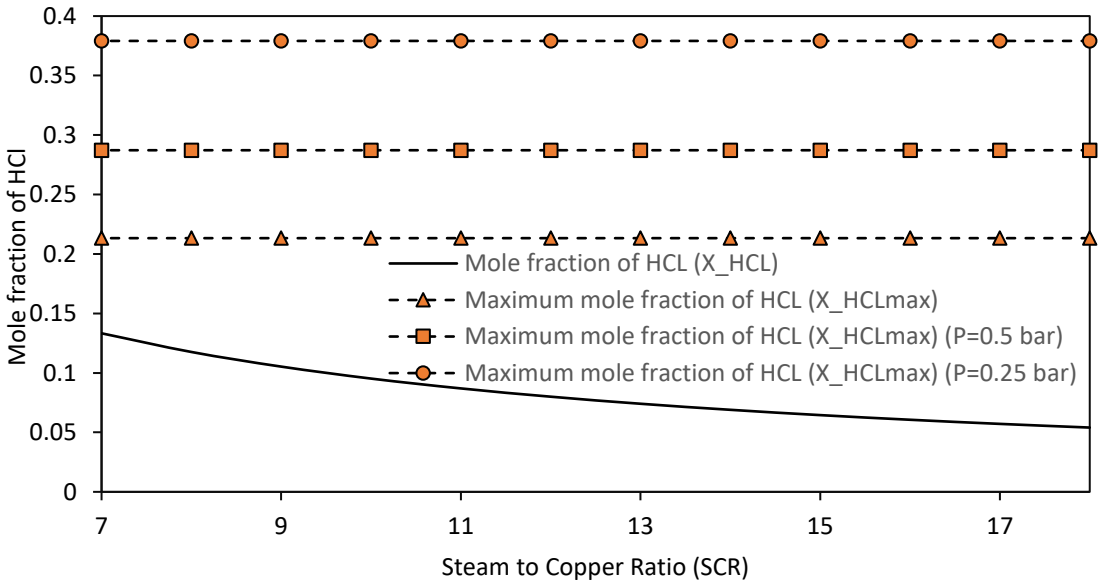

Figure 4-13: Maximum mole fraction of HCl vs. SCR and Pressure

By increasing the amount of inert Nitrogen carrier gas, the reaction quotient is lowered, indicating a further shift towards forward reactions and further away from stopping the reaction. The equilibrium data calculated in this thesis suggests that the reaction is capable of being sustained despite the high concentration of HCl in the recirculating steam flow. Any negative effects of HCl recirculation can be mitigated by the addition of inert carrier gasses such as Nitrogen, or by reducing the pressure in the reactor vessel. To determine the true effect of HCl recirculation and the effect of these mitigation methods, experimental studies are required. The higher reaction quotient seen under normal operating conditions

can lead to an increase in required residence time, or a decrease in yield, and requires experimental data to verify the feasibility of the RSFB Hydrolysis reactor concept.

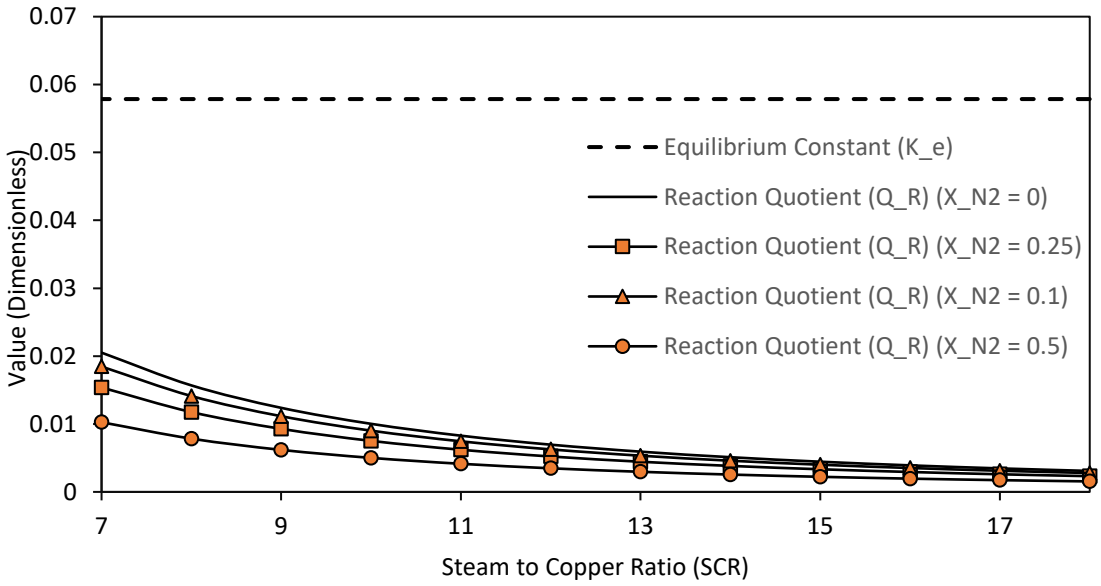

Figure 4-14: Reaction quotient vs. SCR and Nitrogen mole fraction

4.4 Summary

Investigating the Recirculating Steam Fluidized Bed reactor concept has yielded a few key insights for the future of the Cu-Cl cycle. Using a system of outlet splitters and a steam ejector pump, the Recirculating Steam Fluidized Bed can maintain a high effective steam-to-copper ratio while keeping the system-wide steam-to-copper ratio low. The RSFB concept is thermodynamically sound and can be achieved using well-understood components. The RSFB was found to produce stronger HCl acid in the condenser while lowering the energy demand of the system. Through the course of operation, HCl was found to accumulate in the recirculating steam flow at a steady 9% (mole fraction 0.13) for standard operation. Previous research by Daggupati *et al.* [24] found that concentrations of

HCl exceeding 3% in the steam input flow to Hydrolysis would result in a complete halt of the Hydrolysis reaction. However, using a method to predict the maximum concentration of HCl at equilibrium presented by Pope *et al.* [18], the RSFB reactor was found to be well below the maximum concentration of HCl. Using reaction equilibrium data for the system across a range of Steam-to-copper ratios it was found that no SCR between 7 and 18 would lead to the concentration of HCl surpassing the maximum. The reaction quotient (Q_R) was compared to the equilibrium constant (K_e) across steam-to-copper ratios 7 through 18 and indicates that the reaction is well below equilibrium and is progressing in the forwards direction, despite the concentration of HCl present in the recirculating steam. To further drive the reaction forwards, the partial pressures of gaseous components can be lowered. This can be accomplished by either lowering the reactor pressure or introducing inert carrier gasses. These methods were found to dramatically reduce the reaction quotient and increase the maximum concentration of HCl.

The data presented in this chapter provide a clear image of the RSFB reactor concept and the implications of recirculating steam. By recirculating un-used steam, the RSFB reactor is capable of operating using less steam than any other Hydrolysis reactor while maintaining reaction kinetics favorable to complete conversion of $CuCl_2$. The RSFB reactor concept yields an HCl acid solution of much higher concentration than is commonly available, reducing the load on the pressure-swing-distillation system required to concentrate HCl and integrate with Electrolysis.

Chapter 5 Conclusions and Future Work

5.1 Conclusions

In the interest of advancing the Cu-Cl cycle towards full-scale deployment, several Hydrolysis reactors were investigated in this thesis. An initial concept for a simplified Hydrolysis reactor was proposed and constructed using simplified components, and tested through a series of experiments. The simplified reactor was of a conventional spray type but used solely liquid inputs to transport $CuCl_2$ and water into the reaction chamber. The solid products of these reactions were evaluated using X-ray diffraction to determine the prominent chemical components, while gaseous products were condensed into a liquid that was tested to determine the pH, indicating the presence of HCl in water.

Corrosion issues were encountered during the experiments with the simplified reactor, caused by contact between the $CuCl_2$ solution and the stainless steel atomizing nozzles which were required to generate sufficiently small particles of $CuCl_2$. These issues led to the destruction of the nozzle's internal working components, which resulted in large droplets of $CuCl_2$ solution being introduced into the reactor. In experiments 1 through 4, a low conversion of $CuCl_2$ of 7-10% was found when analyzing the products. This was attributed to poor contact between solid $CuCl_2$ and steam; only reacting on the outer portion of a large droplet of aqueous $CuCl_2$ solution. Thermal data from the reactor indicated the presence of liquid H_2O at the bottom of the reaction chamber despite surface heating to stop condensation from forming, confirming that liquid $CuCl_2$ was passing through the reactor largely unreacted. However, some conversion was still found, suggesting that given sufficient drying of $CuCl_2$ particles, the reactor can be capable of performing Hydrolysis.

Following the completion of work on the simplified Hydrolysis reactor, further experiments were halted due to lab shut-down during the COVID-19 pandemic. Instead, the theoretical design and analysis of a new Hydrolysis reactor were selected to support potential adoption in future cycles. This led to the proposal of a Hydrolysis reactor that uses a recirculating steam flow which would reduce the overall steam demands of the Hydrolysis system. A lower steam demand allows for less energy to be consumed by the Hydrolysis reactor. This new design was referred to as the "Recirculating Steam Fluidized Bed" or RSFB. The Recirculating Steam Fluidized Bed concept linked a conventional fluidized bed with a loop of components to allow for the recirculation of a portion of the steam flow, kept circulating by a steam ejector pump. This design was evaluated using EES and Aspen Plus thermodynamic simulation packages.

The RSFB reactor was found to be capable of providing a wide range of steam-to-copper ratios while maintaining a single system-wide steam-to-copper ratio which was lower than most other Hydrolysis reactors. The range of steam-to-copper ratios was found to be limited by the input pressure of steam available, and the velocity of steam that was ejected from the nozzle; however, consistent recirculation of steam was found to be feasible. The RSFB reactor design was found to decrease the energy required to perform Hydrolysis by 50% and produce HCl acid at a higher concentration of 8.54 mol/L, allowing for easier integration with Electrolysis downstream and reducing the need for pressure-swing distillation. Recirculating the unused steam from Hydrolysis has the effect of concentrating HCl in the reactor, up to a mole fraction of 0.13 HCl for an RSFB reactor running at an effective steam-to-copper ratio of 18 and a system-wide steam-to-copper ratio of 7. This concentration has been found to cause the Hydrolysis reaction to completely halt in

previous literature. However, more recent investigations into the chemical reaction equilibrium indicate a maximum concentration of HCl in the steam flow of 21%. Under standard conditions (P = 1 bar, T = 400°C) the equilibrium constant was found to be 0.05786. At a system-wide steam-to-copper ratio of 7 and a mole fraction of HCl of 0.13, the reaction quotient was found to be 0.02051. The reaction quotient being significantly below the equilibrium constant indicates that the reaction is progressing in the forward direction, despite the concentration of HCl. To further accommodate the complete conversion of $CuCl_2$ the partial pressures of gaseous components can be lowered by either lowering the reaction pressure or by introducing inert gases such as nitrogen. The results displayed in this thesis demonstrate the Recirculating Steam Fluidized Bed's utility in the Cu-Cl cycle, which allows for simplified integration with downstream processes while providing conditions conducive to high yield of Cu_2OCl_2. The reaction equilibrium information provided suggests that more work should be undertaken to further develop the Recirculating Steam Fluidized Bed concept.

5.2 Future Work

To design a Hydrolysis reactor suitable for industrial deployment, many challenges must still be overcome. Corrosion damage to the atomizing nozzle required to provide fine particles in a spray reactor makes the spray reactor design difficult to scale up, suggesting that spray drying and Hydrolysis should be unlinked with an intermediate low-temperature spray drying step. Particles formed by spray drying can be further reduced in size by ball-milling. A gas-solid reactor could then be used to perform Hydrolysis. Fluidized beds have a unique role in the Cu-Cl cycle as they can provide the long reaction times required for larger particles of Cu-Cl, and use solid $CuCl_2$ as an input. Future work into the Cu-Cl cycle

should focus on gas-solid reactors such as the fluidized bed with an intermediate low-temperature spray drying step.

If materials science can identify a corrosion-resistant material to construct a spray-type Hydrolysis reactor nozzle, spray reactors can become preferable. The nozzle design will likely require an ultrasonic atomizing system to provide particles small enough to react within a spray reactor's limited residence time. A spray reactor using liquid and gaseous inputs would have the benefit of mechanical simplicity over a fluidized bed which requires a separate spray drying step and solids handling processes to link with upstream Electrolysis.

The Recirculating Steam Fluidized Bed concept presented in this thesis suggests a promising route forward for Cu-Cl cycle scale-up. A Proof-of-Concept is required for the reactor design. This will require experimental investigations to verify efficient conversion given the concentration of HCl. As an example, an experimental fluidized bed reactor could be constructed to operate using conventional Hydrolysis parameters, and then modified to feed in HCl at a mole fraction of 0.13. The conversion of $CuCl_2$ could then be compared to determine if HCl in the feed stream will cause negative impacts on the Hydrolysis reactor.

References

[1] Natural Resources Canada, "Hydrogen Strategy For Canada," Government of Canada, Ottawa, 2020.

[2] Y. Haseli, G. F. Naterer and I. Dincer, "Comparative Assessment of Greenhouse Gas Mitigation of Hydrogen Passenger Trains," *International Journal of Hydrogen Energy*, vol. 33, pp. 1788-1796, 2008.

[3] M. Granovsky, I. Dincer and M. A. Rosen, "Economic and Environmental Comparison of Conventional, Hybrid, Electric and Hydrogen Fuel Cell Vehicles," *Journal of Power Sources,* vol. 159, pp. 1186-1193, 2006.

[4] B. W. McQuillan, L. C. Brown, G. E. Besenbruch, R. Tolman, T. Cramer, B. E. Russ, B. A. Vermillion, B. Earl, H. T. Hsieh, Y. Chen, K. Kwan, R. Diver, N. Siegal, A. Weimer, C. Perkins and A. Lewandowski, "High Efficiency Generation of Hydrogen Fuels Using Solar Thermochemical Splitting of Water," Annual Report, GA-A24972, General Atomics, San Diego, CA.

[5] M. Lewis and A. Taylor, "High Temperature Thermochemical Processes," DOE Hydrogen Program, Annual Progress Report, pp. 182 – 185, Washington, DC, 2006.

[6] A. Terada, J. Iwatsuki, S. Ishikura, H. Noguchi, S. Kubo, H. Okuda, S. Kasahara, N. Tanaka and e. al., "Development of Hydrogen Production Technology by

Thermochemical Water Splitting IS Process Pilot Test Plan," *Journal of Nuclear Science and Technology,* vol. 44, no. 3, pp. 477-482, 2007.

[7] G. F. Naterer, S. Suppiah, L. Stolberg, M. Lewis, M. Ferrandon, W. Wang, I. Dincer, K. Gabriel, M. A. Rosen, E. Secnik, E. B. Easton, L. Trevani, I. Pioro, P. Tremaine, S. Lvov, J. Jiang, G. Rizvi, B. M. Ikeda, L. Lu, M. Kaye and S. W., "Clean Hydrogen Production with the Cu-Cl Cycle – Progress of International Consortium," *Part I: Experimental Unit Operations (pp. 15472 – 15485), and Part II: Simulations, Thermochemical Data and Materials (pp. 15486 – 15501), International Journal of Hydrogen Energy,* vol. 36, 2011.

[8] G. F. Naterer, S. Suppiah, M. A. Rosen, K. Gabriel, I. Dincer, O. A. Jianu, Z. Wang, E. B. Easton, B. Ikeda, G. Rizvi, I. Pioro, K. Pope, J. Mostaghimi and S. Lvov, "Advances in Unit Operations and Materials for the Cu-Cl Cycle of Hydrogen Production," *International Journal of Hydrogen Energy,* vol. 42, pp. 15708-15723, 2017.

[9] V. N. Balashov, R. S. Schatz, E. Chalkova, N. N. Akinfiev, M. V. Fedkin and S. Lvov, "CuCl Electrolysis for Hydrogen Production in the Cu–Cl Thermochemical Cycle," *Journal of The Electrochemical Society,* vol. 158, no. 3, pp. B266-B275, 2011.

[10] M. A. Lewis, S. Ahmed, S. Lvov and C. Fan, "Membrane/Electrolyzer Development in the Cu-Cl Thermochemical Cycle," FY 2012 annual report, DOE Hydrogen and Fuel Cells Program, 2012.

[11] L. Stolberg, "Electrolysis Cell for the Conversion of Cuprous Chloride in Hydrochloric Acid to Cupric Chloride and Hydrogen Gas". U.S. Patent 0051469, 2010.

[12] M. A. Lewis and C. Sink, "High Temperature Thermochemical Processes," *DOE Hydrogen Program FY 2007 Annual Progress Report,* pp. 216-219, 2007.

[13] M. S. Ferrandon, M. A. Lewis, D. F. Tatterson, R. V. Nankani, M. Kumar, L. E. Wedgewood and L. C. Nitsche, "The Hybrid Cu-Cl Thermochemical Cycle. I. Conceptual process desing and H2A cost analysis. II Limiting the formation of CuCl during hydrolysis.," in *American Institute of Chemical Engineers Annual Meeting*, Philadelphia, 2008.

[14] G. Marin, Z. Wang, G. Naterer and K. Gabriel, "Byproducts and reaction pathwats for integration of the Cu-Cl cycle of hydrogen production," *International Journal of Hydrogen Energy,* no. 36, pp. 13414-13424, 2011.

[15] Z. Wang, V. N. Daggupati, G. Marin, K. Pope, Y. Xiong, E. Secnik, G. F. Naterer and K. S. Gabriel, "Towards integration of hydrolysis, decomposition and electrolysis processes of the Cu-Cl thermochemical water splitting cycle," *International Journal of Hydrogen Energy,* no. 37, pp. 16557-16569, 2012.

[16] A. Farsi, C. Zamfirescu, I. Dincer and G. F. Naterer, "Thermodynamic assessment of a lab-scale experimental copper-chlorine cycle for sustainable hydrogen production," *International Journal of Hydrogen Energy,* no. 44, pp. 17595-17610, 2019.

[17] K. Pope, Z. L. Wang, G. F. Naterer and E. Secnik, "Interfacial thermodynamics and X-ray diffraction of hydrolysis products in multiphase reacting flow of the Cu-Cl cycle," *International Journal of Hydrogen Energy,* no. 37, pp. 15011-15019, 2012.

[18] K. Pope, G. F. Naterer and Z. L. Wang, "Nitrogen carrier gas flow for reduced steam requirements of water splitting in a packed bed hydrolysis reactor," *Experimental Thermal and Fluid Science,* no. 44, pp. 815-824, 2013.

[19] L. Fedunik-Hofman, A. Bayon and S. W. Donne, "Kinetics of Solid-Gas Reactions and Their Application to Carbonate Looping Systems," *Energies 2019,* 2019.

[20] V. N. Daggupati, G. F. Naterer, K. S. Gabriel, R. J. Gravelsins and Z. L. Wang, "Solid particle decomposition and hydrolysis reaction kinetics in Cu-Cl thermochemical hydrogen production," *International Journal of Hydrogen Energy,* no. 35, pp. 4877-4882, 2010.

[21] V. N. Daggupati, G. F. Naterer and I. Dincer, "Convective heat transfer and solid conversion of reacting particles in a copper(II) chloride fluidized bed," *Chemical Engineering Science,* no. 66, pp. 460-468, 2011.

[22] K. Pope, G. F. Naterer and Z. L. Wang, "Steam flow effects on hydrolysis reaction kinetics in the Cu-Cl cycle," *International Journal of Hydrogen Energy,* no. 37, pp. 17701-17708, 2012.

[23] K. Pope, G. F. Daggupati, G. F. Naterer and K. S. Gabriel, "Experimental study of gaseous effluent and solid conversion in a fluidized bed hydrolysis reactor for

hydrogen production," *International Journal of Hydrogen Energy,* no. 37, pp. 16397-16401, 2012.

[24] V. N. Daggupati, G. F. Naterer and K. S. Gabriel, "Diffusion of gaseous products through a particle surface layer in a fluidized bed reactor," *International Journal of Heat and Mass Transfer,* no. 53, pp. 2449-2458, 2010.

[25] M. S. Ferrandon, M. A. Lewis, D. F. Tatterson, A. Gross, D. Doizi, L. Croize, V. Dauvois, J. L. Roujou, Y. Zanella and P. Carles, "Hydrogen production by the Cu-Cl thermochemical cycle: Investigation of the key step of hydrolysing CuCl2 to Cu2OCl2 and HCl using a spray reactor," *International Journal of Hydrogen Energy,* no. 35, pp. 992-1000, 2010.

[26] M. Ferrandon, V. Daggupati, Z. Wang, G. Naterer and L. Trevani, "Using XANES to obtain mechanistic information for the hydrolysis of CuCl2 and the decomposition of Cu2OCl2 in the thermochemical Cu-Cl cycle for H2 production," *Journal of Thermal Analysis and Calorimetry,* pp. 975-982, 2014.

[27] A. Nixon, M. Ferrandon, M. H. Kaye and L. Trevani, "Thermochemical Production of Hydrogen: Synthesis, characterization, and decomposition of copper oxychloride," *Journal of Thermal Analysis and Calorimetry,* no. 110, pp. 1095-1105, 2012.

[28] D. Thomas, N. A. Baveja, K. T. Shenoy and J. B. Joshi, "Experimental Study on the Mechanism and Kinetics of CuCl2 Hydrolysis Reaction of the Cu−Cl Thermochemical Cycle in a Fluidized Bed Reactor," *Industrial and Engineering Chemistry Research,* no. 59, pp. 12028-12037, 2020.

[29] R. V. Singh, M. R. Pai, A. M. Banerjee, G. R. Patkare, R. V. Pai, A. Kumar, A. K. Yadav, S. Phaphale and A. K. Tripathi, "Investigations on the hydrolysis step of copper-chlorine thermochemical cycle for hydrogen production," *International Journal of Energy Research,* no. 44, pp. 2845-2863, 2019.

[30] Z. Wang, G. Naterer, K. Gabriel, R. Gravelsins and V. Daggupati, "Comparison of sulfur-iodine and copper-chlorine thermochemical hydrogen production cycles," *International Journal of Hydrogen Energy,* no. 35, pp. 4820-4830, 2010.

[31] G. Naterer, S. Suppiah, L. Stolberg, M. Lewis, Z. Wang, V. Daggupati, K. Gabriel, I. Dincer, M. Rosen, P. Spekkens, S. Lvov, M. Fowler, P. Tremaine, J. Mostaghimi, E. Easton, L. Trevani, G. Rizvi, B. Ikeda, M. Kaye, L. Lu, I. Pioro, W. R. Smith, E. Secnik, J. Jiang and J. Avsec, "Canada's progress on nuclear hydrogen production and the thermochemical Cu-Cl cycle," *International Journal of Hydrogen Energy,* no. 35, pp. 10905-10926, 2010.

[32] M. S. Ferrandon, M. A. Lewis, F. Alvarez and E. Shafirovich, "Hydrolysis of CuCl2 in the Cu-Cl thermochemical cycle for hydrogen production: Experimental studies using a spray reactor with an ultrasonic atomizer," *International Journal of Hydrogen Energy,* no. 35, pp. 1895-1904, 2010.

[33] A. Farsi, I. Dincer and G. F. Naterer, "Particle formation and heat transfer in a gas-solid hydrolysis reactor with cupric chloride conversion to copper oxychloride," *International Journal of Heat and Mass Transfer,* no. 161, 2020.

[34] M. Lescisin, O. A. Jianu, K. Pope and M. A. Rosen, "Investigating azeotropic separation of hydrochloric acid for optimizing the copper-chlorine thermochemical cycle," *International Journal of Hydrogen Energy*, no. 45, pp. 26080-26089, 2020.

[35] A. Farsi, O. Kayhan, C. Zamfirescu, I. Dincer and G. F. Naterer, "Azeotropic pressure swing distillation of hydrochloric-water for hydrogen production in the Cu-Cl cycle: Thermodynamics and design methods," *International Journal of Hydrogen Energy*, no. 44, pp. 7969-7982, 2019.

[36] "Eriochalcite: Mineral information, data, and localities," Hudson Institute of Mineralogy, [Online]. Available: https://www.mindat.org/min-1398.html. [Accessed 18 03 20201].

[37] D. W. Green and R. H. Perry, "Fluidized Bed Systems," in *Perry's Chemical Engineer's Handbook, 8th edition*, New York City, McGraw-Hill, 2008, pp. 17-5 - 17-6.

[38] R. Cocco, S. B. Reddy Karri and T. Knowlton, "Introduction to Fluidization," *American Institute of Chemical Engineers CEP*, pp. 21-29, November 2014.

[39] K. Bashir, "Design and fabrication of cyclone separator," China University of Petroleum, Beijing, China, 2015.

[40] A. J. Green, "Jet Pumps and Ejectors," 2 February 2011. [Online]. Available: http://thermopedia.com/content/902/. [Accessed 10 August 2020].

[41] J. Wilman, Jet Pumps (EUR 3253.e), Brussels: European Atomic Energy Community & Reactor Centrum Nederland, 1966.

[42] K. Gabriel, L. Finney and P. Dolloso, "Preliminary Results of the Integrated Hydrolysis Reactor in the Cu-Cl Hydrogen Production Cycle," *International Journal of Hydrogen Energy*, vol. 44, pp. 9743-9752, 2019.

Appendix A: Copyright permission letters

Copyright permission letters are included here from the International Journal of Energy Research and the International Journal of Hydrogen Energy for figures 2-2, 2-3, 2-4, 3-9, and 3-10. These letters were obtained when the title of the thesis was “A study of a novel design for an efficient hydrolysis reactor for the Cu-Cl thermochemical hydrogen production cycle”.

Marketplace™

Elsevier Science & Technology Journals - License Terms and Conditions

This is a License Agreement between Leonard Finney ("You") and Elsevier Science & Technology Journals ("Publisher") provided by Copyright Clearance Center ("CCC"). The license consists of your order details, the terms and conditions provided by Elsevier Science & Technology Journals, and the CCC terms and conditions.

All payments must be made in full to CCC.

Order Date	01-Apr-2021	**Type of Use**	Republish in a thesis/dissertation
Order license ID	1108841-1		
ISSN	0360-3199	**Publisher**	PERGAMON
		Portion	Image/photo/illustration

LICENSED CONTENT

Publication Title	International journal of hydrogen energy	**Rightsholder**	Elsevier Science & Technology Journals
Article Title	Hydrolysis of CuCl2 in the Cu-Cl thermochemical cycle for hydrogen production: Experimental studies using a spray reactor with an ultrasonic atomizer	**Publication Type**	Journal
		Start Page	1895
		End Page	1904
		Issue	5
		Volume	35
Author/Editor	INTERNATIONAL ASSOCIATION FOR HYDROGEN ENERGY.		
Date	01/01/1976		
Language	English		
Country	United Kingdom of Great Britain and Northern Ireland		

REQUEST DETAILS

Portion Type	Image/photo/illustration	**Distribution**	Worldwide
Number of images / photos / illustrations	2	**Translation**	Original language of publication
Format (select all that apply)	Print, Electronic	**Copies for the disabled?**	No
		Minor editing privileges?	No
Who will republish the content?	Academic institution	**Incidental promotional use?**	No
Duration of Use	Life of current edition	**Currency**	CAD
Lifetime Unit Quantity	Up to 499		
Rights Requested	Main product		

NEW WORK DETAILS

Copyright Clearance Center Marketplace™

Elsevier Science & Technology Journals - License Terms and Conditions

This is a License Agreement between Leonard Finney ("You") and Elsevier Science & Technology Journals ("Publisher") provided by Copyright Clearance Center ("CCC"). The license consists of your order details, the terms and conditions provided by Elsevier Science & Technology Journals, and the CCC terms and conditions.

All payments must be made in full to CCC.

Order Date	29-Mar-2021	**Type of Use**	Republish in a thesis/dissertation
Order license ID	1108048-1		
ISSN	0360-3199	**Publisher**	PERGAMON
		Portion	Image/photo/illustration

LICENSED CONTENT

Publication Title	International journal of hydrogen energy	**Rightsholder**	Elsevier Science & Technology Journals
Article Title	Hydrogen production by the Cu–Cl thermochemical cycle: Investigation of the key step of hydrolysing CuCl 2 to Cu 2OCl 2 and HCl using a spray reactor	**Publication Type**	Journal
		Start Page	1000
		End Page	1000
		Issue	3
		Volume	35
Author/Editor	INTERNATIONAL ASSOCIATION FOR HYDROGEN ENERGY.		
Date	01/01/1976		
Language	English		
Country	United Kingdom of Great Britain and Northern Ireland		

REQUEST DETAILS

Portion Type	Image/photo/illustration	**Distribution**	Worldwide
Number of images / photos / illustrations	1	**Translation**	Original language of publication
Format (select all that apply)	Print, Electronic	**Copies for the disabled?**	No
		Minor editing privileges?	No
Who will republish the content?	Academic institution	**Incidental promotional use?**	No
Duration of Use	Life of current edition	**Currency**	CAD
Lifetime Unit Quantity	Up to 499		
Rights Requested	Main product		

NEW WORK DETAILS

Copyright Clearance Center Marketplace

John Wiley & Sons - Books - License Terms and Conditions

This is a License Agreement between Leonard Finney ("You") and John Wiley & Sons - Books ("Publisher") provided by Copyright Clearance Center ("CCC"). The license consists of your order details, the terms and conditions provided by John Wiley & Sons - Books, and the CCC terms and conditions.

All payments must be made in full to CCC.

Order Date	26-Mar-2021	**Type of Use**	Republish in a thesis/dissertation
Order license ID	1107450-1		
ISSN	1099-114X	**Publisher**	JOHN WILEY & SONS LTD.
		Portion	Image/photo/illustration

LICENSED CONTENT

Publication Title	International journal of energy research	**Publication Type**	e-Journal
		Start Page	2845
Article Title	Investigations on the hydrolysis step of copper-chlorine thermochemical cycle for hydrogen production	**End Page**	2863
		Issue	4
		Volume	44
		URL	http://onlinelibrary.wiley.com/journal/10.1002/(ISSN)1099-114X
Date	01/01/1977		
Language	English		
Country	United States of America		
Rightsholder	John Wiley & Sons - Books		

REQUEST DETAILS

Portion Type	Image/photo/illustration	**Distribution**	Worldwide
Number of images / photos / illustrations	1	**Translation**	Original language of publication
Format (select all that apply)	Print, Electronic	**Copies for the disabled?**	No
		Minor editing privileges?	No
Who will republish the content?	Academic institution	**Incidental promotional use?**	No
Duration of Use	Life of current edition	**Currency**	CAD
Lifetime Unit Quantity	Up to 499		
Rights Requested	Main product		

NEW WORK DETAILS

Title	A study of a novel design for an efficient hydrolysis reactor for the Cu-Cl thermochemical hydrogen production cycle	**Institution name**	Ontario Tech University (UOIT)
		Expected presentation date	2021-04-10
Instructor name	Dr. Kamiel Gabriel		

Appendix B: EES code

```
//**********************************************************************
//   Viscosity Procedure
//**********************************************************************
PROCEDURE VISCOMIX(A,B,T,P:mu,nu,rho,cp)

x[1..2]=[(A/(B+A)),(B/(B+A))]

rho_HCl = 1.49[kg/m^3]
mu_HCl = 0.0000156 [kg/m-s]

MW_HCl = MOLARMASS(HCl)
MW_Steam = MOLARMASS(Steam)

rho_steam = DENSITY(Steam, T=T, P=P)
mu_steam = VISCOSITY(Steam, T=T, P=P)

cp_HCl = SPECHEAT(HCl, T=T)
cp_Steam = SPECHEAT(Steam, T=T, P=P)

mu = (mu_HCl*x[1]*sqrt(MW_HCl) + mu_steam*x[2]*sqrt(MW_Steam)) / (x[1]*sqrt(MW_HCl) +
x[2]*sqrt(MW_Steam))

rho = (x[1]*MW_HCl+x[2]*MW_steam)*1/(0.08205736608096*(273.16+400))

nu = mu/rho

cp =
(cp_HCl*A*MW_HCl)/(A*MW_HCl+B*MW_Steam)+(cp_Steam*B*MW_Steam)/(A*MW_HCl+B*M
W_Steam)

END

//**********************************************************************
//   Properties
//**********************************************************************

MM_Steam = 18.02 [kg/kmol]
MM_HCl = 36.46 [kg/kmol]
MM_H2 = 2 [kg/kmol]
MM_CuCl2 = 134.45 [kg/kmol]

rho_CuCl2 = 3386[kg/m^3]

DELTAh_vap_steam = 2256 [kJ/kg]
cp_water = 4.2
cp_steam = CP(steam, T=373[K], P=101[kPa])


T[0] = 298.15[K]                                    "Ambient Temperature"
P[0] = 101325 [Pa]                                  "Ambient Pressure"

//**********************************************************************
//   Operating conditions
//**********************************************************************
```

```
SCR_eff = 18                                    "Effective Steam-to-copper ratio"
SCR=7                                           "System-wide steam-to-copper ratio"
d_CuCl2 = 100E-6                                "Diameter of CuCl2 particles"


//   "Used to specify daily production"
//M_dot_H2_goal = 1[kg/day]


//   "Used to specify amount of inert gas, if applicable"
//N_dot_N2[1] = 0 [mol/s]


//**********************************************************************
//   Temperatures and pressures
//**********************************************************************
//Assuming temperature losses are minimal and sufficient heat is provided in reactor chamber to maintain T[2] = T[1]
T[1] = 400[K]+273.15[K]
T[2] = T[1]
T[3] = T[2]
T[4] = T[3]
T[5] = T[4]
T[6] = T[3]

//Assuming pressure loss due to pipe friction is negligible, pressure drop is only the result of the reactor and the separator.
P[1] = P[0]
P[2] = P[1]-DELTAP_reactor
P[3] = P[2]-DELTAP_separator
P[4] = P[3]
P[6] = P[3]

//**********************************************************************
//Production goal handling
//**********************************************************************
M_dot_H2 = M_dot_H2_goal/24[hr/day]
N_dot_H2 = M_dot_H2/MM_H2*(1000[mol/kmol]/3600[s/hr])

//**********************************************************************
//   Steam balance
//**********************************************************************
SCR = N_dot_Steam[5]/N_dot_CuCl2[7]

SCR_eff = N_dot_Steam[1]/N_dot_CuCl2[7]

N_dot_Steam[1] - N_dot_Steamconsumed = N_dot_Steam[2]

N_dot_Steam[2] = N_dot_Steam[3]

N_dot_Steam[3] * OutletRatio = N_dot_Steam[6]

N_dot_Steam[3] - N_dot_Steam[6] = N_dot_Steam[4]

N_dot_Steam[4] + N_dot_Steam[5] = N_dot_Steam[1]

//**********************************************************************
```

```
//   HCl balance
//**********************************************************************
N_dot_CuCl2[7] = 2*N_dot_Steamconsumed

N_dot_HCl[1] + N_dot_CuCl2[7] = N_dot_HCl[2]

N_dot_HCl[2] = N_dot_HCl[3]

N_dot_HCl[3] * OutletRatio = N_dot_HCl[6]
N_dot_HCl[6] = 2*N_dot_H2

N_dot_HCl[3] = N_dot_HCl[6] + N_dot_HCl[4]

N_dot_HCl[4] = N_dot_HCl[1]

//**********************************************************************
//   N2 balance
//**********************************************************************
N_dot_N2[1] = N_dot_N2[2]

N_dot_N2[2] = N_dot_N2[3]

N_dot_N2[3] * OutletRatio = N_dot_N2[6]

N_dot_N2[3] = N_dot_N2[6] + N_dot_N2[4]

N_dot_N2[4] + N_dot_N2[5] = N_dot_N2[1]

//**********************************************************************
//   Mass flows
//**********************************************************************
//Based on the established mole balance

M_dot[1] = N_dot_HCl[1]*MM_HCl + N_dot_Steam[1]*MM_Steam
M_dot[2] = N_dot_HCl[2]*MM_HCl + N_dot_Steam[2]*MM_Steam
M_dot[3] = N_dot_HCl[3]*MM_HCl + N_dot_Steam[3]*MM_Steam
M_dot[4] = N_dot_HCl[4]*MM_HCl + N_dot_Steam[4]*MM_Steam
M_dot[5] = N_dot_HCl[5]*MM_HCl + N_dot_Steam[5]*MM_Steam
M_dot[6] = N_dot_HCl[6]*MM_HCl + N_dot_Steam[6]*MM_Steam


//**********************************************************************
//   Viscosity of mixed gas streams
//**********************************************************************


//Find Mu, Nu, Rho, and Cp of all mixed streams containing H2O and HCl
//Only valid for mixes of H2O and HCl, does not consider the content of inert gases used to adjust
kinetics
CALL VISCOMIX(N_dot_HCl[1], N_dot_Steam[1], T[1], P[1]:mu[1],nu[1],rho[1],cp[1])
CALL VISCOMIX(N_dot_HCl[2], N_dot_Steam[2], T[2], P[2]:mu[2],nu[2],rho[2],cp[2])
CALL VISCOMIX(N_dot_HCl[3], N_dot_Steam[3], T[3], P[3]:mu[3],nu[3],rho[3],cp[3])
CALL VISCOMIX(N_dot_HCl[4], N_dot_Steam[4], T[4], P[4]:mu[4],nu[4],rho[4],cp[4])
CALL VISCOMIX(N_dot_HCl[6], N_dot_Steam[6], T[6], P[6]:mu[6],nu[6],rho[6],cp[6])
N_dot_HCl[5] = 0
CALL VISCOMIX(N_dot_HCl[5], N_dot_Steam[5], T[5], P[5]:mu[5],nu[5],rho[5],cp[5])
```

```
//*********************************************************************
//Steam ejector flow calculations
//*********************************************************************
//Based on Wilman 1966

G_2 = M_dot[4]/1000[g/kg]                                   "Suction Mass Flow Rate"
G_1 = M_dot[5]/1000[g/kg]                                   "Pressure Mass Flow Rate"
mu = G_2/G_1                                                "Mass flow ratio"
delta = d_s/d_m                                             "Diameter of nozzle/Diameter of mixing
tube"
delta = 0.43                                                "From Figure 20 of Wilman 1966"

pi_m = ((1+K_s) - (1+K_t)*mu^2*(delta^4/((1-delta^2)^2))) / (2*delta^2+2*mu^2*((delta^4)/(1-
delta^2))-(1+K_t)*mu^2*((delta^4)/((1-delta^2)^2))-(1+K_m+K_d)*(1+mu)^2*delta^4)

pi_m =  (P[1]-P[4])/(P[5]-P[1])

//pi = 16                                                   "Based on Wilman 1966 Figure 20, mass
flow ratio 4.3"


//Sizing constants
K_s = 0.05
K_t = K_s
K_m = 0.06
K_d = 0.14

phi = (1+K_s) - (1+K_t)*mu^2*(delta^4/((1-delta^2)^2))

DELTAP=(P[1]-P[4])*1[N/M^2/Pa]                              "Total delta P for system"

d_s = 1.13*(G_1^(1/2))*(phi/(2*rho[5]*pi_m*(DELTAP)))^(1/4)

V_dot[5] = (G_1)/(rho[5])
v[5] = V_dot[5]/(pi*(d_s/2)^2)

a_s = pi*(d_s/2)^2

a_m = pi*(d_m/2)^2

V_dot[4] = (G_2)/(rho[4])
v[4] = V_dot[4]/a_m

l_n = 6*d_s
l_e = 0.7*d_m
l_m=8*d_m
l_d=10*d_m
r=0.5*d_m

//*********************************************************************
//   Fluidized bed calculations
//*********************************************************************
//Based on Perry's handbook

Re_mf = ((1135.7+0.0408*Ar)^0.5) - 33.7
Re_mf = rho[1]*u_mf*d_CuCl2/mu[1]
```

```
Ar = d_CuCl2^3*rho[1]*(rho_CuCl2-rho[1])*9.81/(mu[1]^2)
v[1] = 20*u_mf                                          "Because of bubbling bed condition with external vortex"

V_dot[1] = v[1]*A_reactor
V_dot[1] = M_dot[1]/rho[1]/1000[g/kg]

M_dot_CuCl2[7] = N_dot_CuCl2[7]*MM_CuCl2

M_dot_CuCl2[7]*3600[s/hr] = bedmass*1000[g/kg]

bedvolume = bedmass/rho_CuCl2

bedheight = bedvolume/A_reactor

A_reactor = pi*(d_reactor/2)^2

bedmass*9.81[N/kg] = W_CuCl2

DELTAP_reactor =W_CuCl2/A_reactor

//**********************************************************************
//   Cyclone Separator
//**********************************************************************

V_dot[2] = M_dot[2]/rho[2]/1000

VelocityRatio = 0.1

v[1] = v[2]*VelocityRatio

H/D = 0.5
W/D = 0.2
D_e/D = 0.5
S/D = 0.5
L_b/D = 1.5
L_c/D = 2.5
D_d/D = 0.375
N_e = (L_b+L_c/2)/H
v[2] = V_dot[2]/(H*W)

d_pc = ((9*mu[2]*W)/(2*3.14159*N_e*v[2]*(rho_CuCl2-rho[2])))^(1/2)

V_dot[3] = M_dot[3]/rho[3]/1000

H_v = 16*(H*W)/(D_e^2)

DELTAP_separator = 1/2*rho[2]*v[2]^2*H_v


//**********************************************************************
//   Thermal Energy
//**********************************************************************
//Find energy to heat CuCl2 and react. These do not depend on the SCR.

//Fixed heat inputs for heating CuCl2 and Reaction
cp_CuCl2 = 78.74[J/mol-K] "Assume that CuCl2 is at temp before entering"
```

```
Q_CuCl2 = N_dot_CuCl2[7]*cp_CuCl2*(T[1]-T[0])
DELTAh_reaction = 116.6 [kj/mol] "Per mol H2. React to form CU2OCL2"
Q_reaction = (DELTAh_reaction)/2*N_dot_CuCl2[7]
Q_reactionTotal = Q_CuCl2/1000[J/kJ] + Q_reaction


//Energy for steam generation with recirculation
Q_waterHeat = M_dot[5]/1000[g/kg]*cp_water*(373[K]-T[0])
Q_evap = M_dot[5]/1000[g/kg]*DELTAh_vap_steam
Q_steamHeat = M_dot[5]/1000[g/kg]*cp[5]*(T[1]-T[0])

Q_steamGenerator = Q_waterHeat+Q_evap+Q_steamHeat


//Energy for steam generation without recirculation
QPRIME_waterHeat = N_dot_Steam[1]*MM_Steam/1000[g/kg]*cp_water*(373[K]-T[0])
QPRIME_evap = N_dot_Steam[1]*MM_Steam/1000[g/kg]*DELTAh_vap_steam
QPRIME_steamHeat = N_dot_Steam[1]*MM_Steam/1000[g/kg]*cp[5]*(T[1]-T[0])

QPRIME_steamGenerator = QPRIME_waterHeat+QPRIME_evap+QPRIME_steamHeat


//Compare total heat for both cases.
Q_total = Q_reactionTotal+Q_steamGenerator
QPRIME_total = Q_reactionTotal+QPRIME_steamGenerator

Q_savings = Q_steamGenerator-QPRIME_steamGenerator

//                                                    Energy Per Mole
Energypermole = Q_total * 1000[J/kJ] / N_dot_H2
Energypermoleprime = QPRIME_total * 1000[J/kJ] / N_dot_H2

//*********************************************************************
//   Reaction Kinetics
//*********************************************************************
//Gibbs free energies of reactants and products
gibbsfree_Cu2OCl2 = -369.7 [kJ/mol]
gibbsfree_CuCl2 = -173.82 [kJ/mol]
gibbsfree_HCl = -95.30 [kJ/mol]
gibbsfree_H2O = -228.61 [kJ/mol]

//Change in Gibbs free energy
DELTAgibbsfree_reaction =
(2*gibbsfree_CuCl2+gibbsfree_H2O)+(gibbsfree_Cu2OCl2+2*gibbsfree_HCL)


R1= 8.314462175 [J/mol*K]

//Equilibrium constant
K_e = exp(-DELTAgibbsfree_reaction/(R1 /1000 [J/kJ]*T[1]))

//Pressure based on bar, not kPa
P_T = P[1]/101325 [kPa/bar]
P_0 = P[0]/101325 [kPa/bar]

//HCl mole fraction at equilibrium
X_Hcl_max = sqrt((K_e/(2*(P_T/P_0)))^2+(K_e/((P_T/P_0))))-(K_e/(2*(P_T/P_0)))
```

```
//HCl under current conditions
X_HCl = N_dot_Hcl[2]/(N_dot_steam[2]+N_dot_HCl[2])
X_Hcl_max = N_Hcl_max/(N_dot_steam[2]+N_HCl_max)

//Total mole flow including inert gas
N_dot_T[1] = N_dot_HCl[1]+N_dot_Steam[1]+N_dot_N2[1]
N_dot_T[2] = N_dot_HCl[2]+N_dot_Steam[2]+N_dot_N2[2]

//Mole fraction of Nitrogen
X_N2 = N_dot_N2[1]/(N_dot_T[2])
X_N2 = 0

//Reaction quotient at current conditions
Q_R = (N_dot_HCl[2]^2/N_dot_Steam[2])*(P[1]/101325/(N_dot_T[2]))

//*********************************************************************
//    Miscelaneous calculations
//*********************************************************************

NdotCuCl2Kmol = N_dot_CuCl2[7]*3600[s/hr]/1000[mol/kmol]
NdotCuCl2Kmol = 0.1 [kmol/hr]

M_dot_HCl_condenser = N_dot_HCl[6]  * MM_HCl /1000[mol/kmol]
V_dot_H2O_condenser = N_dot_Steam[6] /1000[mol/kmol] * MM_Steam / 1 [kg/L]
M_dot_H2O_condenser = N_dot_Steam[6] /1000[mol/kmol] * MM_Steam

//HCl concentration
Molarity = N_dot_HCl[6] / V_dot_H2O_condenser
Mass_Fraction = M_dot_HCl_condenser/M_dot_H2O_condenser
pH_acid = -LOG10(Molarity)
//Mole Fraction for condensate
Mole_fraction = N_dot_HCl[6] / N_dot_Steam[6]
//Mole fraciton for recirculating stream
Molefraction = N_dot_HCl[1] / N_dot_Steam[1]

Steammolefraction = N_dot_Steam[1]/(N_dot_Steam[1]+N_dot_N2[1])
```

Appendix C: Parametric tables

Parametric tables used to generate results discussed in chapter 4 are presented here.

SCR	Split Fraction
7	0.3714
8	0.4286
9	0.4857
10	0.5429
11	0.6
12	0.6571
13	0.7143
14	0.7714
15	0.8286
16	0.8857
17	0.9429
18	1

Table C-1: Parametric Table from Figure 26

Table C-2: Parametric Table from Figure 27

SCR	Q_steamGenerator [kW]	Q_reactionTotal [kW]	Q_total [kW]	Q_savings [kW]
7	11.73	2.44	14.17	-18.43
8	13.4	2.44	15.84	-16.75
9	15.08	2.44	17.52	-15.08
10	16.75	2.44	19.19	-13.4
11	18.43	2.44	20.87	-11.73
12	20.1	2.44	22.54	-10.05
13	21.78	2.44	24.22	-8.376
14	23.45	2.44	25.89	-6.701
15	25.13	2.44	27.57	-5.026
16	26.8	2.44	29.24	-3.35

SCR	Nozzle Velocity [m/s]	SCR	Nozzle Velocity [m/s]	SCR	Nozzle Velocity [m/s]
6.2	327.3	10	141.2	13.8	127.1
6.3	294.3	10.1	140.5	13.9	126.9
6.4	270.7	10.2	139.9	14	126.8
6.5	253	10.3	139.3	14.1	126.6
6.6	238.9	10.4	138.7	14.2	126.4
6.7	227.6	10.5	138.1	14.3	126.2
6.8	218.2	10.6	137.6	14.4	126
6.9	210.2	10.7	137	14.5	125.9
7	203.4	10.8	136.5	14.6	125.7
7.1	197.5	10.9	136	14.7	125.5
7.2	192.3	11	135.6	14.8	125.4
7.3	187.7	11.1	135.1	14.9	125.2
7.4	183.6	11.2	134.7	15	125.1
7.5	179.9	11.3	134.3	15.1	124.9
7.6	176.5	11.4	133.9	15.2	124.8
7.7	173.5	11.5	133.5	15.3	124.6
7.8	170.8	11.6	133.1	15.4	124.5
7.9	168.2	11.7	132.7	15.5	124.4
8	165.9	11.8	132.4	15.6	124.2
8.1	163.8	11.9	132	15.7	124.1
8.2	161.8	12	131.7	15.8	124
8.3	160	12.1	131.4	15.9	123.9
8.4	158.2	12.2	131.1	16	123.7
8.5	156.6	12.3	130.8	16.1	123.6
8.6	155.2	12.4	130.5	16.2	123.5
8.7	153.7	12.5	130.2	16.3	123.4
8.8	152.4	12.6	129.9		
8.9	151.2	12.7	129.7		
9	150	12.8	129.4		
9.1	148.9	12.9	129.1		
9.2	147.9	13	128.9		
9.3	146.9	13.1	128.7		
9.4	145.9	13.2	128.4		
9.5	145	13.3	128.2		
9.6	144.2	13.4	128		
9.7	143.4	13.5	127.8		
9.8	142.6	13.6	127.5		
9.9	141.9	13.7	127.3		

Table C-3: Parametric Table from Figure 28

Split Fraction	SCR	N_dot_HCl [mol/s]	N_dot_H2O [mol/s]
0.5	13.5	0.02778	0.375
0.49	13.77	0.02891	0.3824
0.48	14.04	0.03009	0.39
0.47	14.33	0.03132	0.398
0.46	14.63	0.03261	0.4064
0.45	14.94	0.03395	0.4151
0.44	15.27	0.03535	0.4242
0.43	15.62	0.03682	0.4338
0.42	15.98	0.03836	0.4438
0.41	16.35	0.03997	0.4543
0.4	16.75	0.04167	0.4653
0.39	17.17	0.04345	0.4769
0.38	17.61	0.04532	0.489
0.37	18.07	0.0473	0.5019
0.36	18.56	0.04938	0.5154
0.35	19.07	0.05159	0.5298
0.34	19.62	0.05392	0.5449
0.33	20.2	0.0564	0.561
0.32	20.81	0.05903	0.5781
0.31	21.47	0.06183	0.5963
0.3	22.17	0.06481	0.6157

Table C-4: Parametric Table from Figure 29

SCR	Molarity [mol HCl/L]
7	8.538
8	7.399
9	6.529
10	5.841
11	5.285
12	4.826
13	4.44
14	4.111
15	3.827
16	3.58
17	3.363
18	3.171

Table C-5: Parametric Table from Figure 30

P=1 bar				
SCR	**Equilibrium Constant (K_e)**	**Reaction Quotient (Q_R) (P=1 bar)**	**Mole fraction of HCL (X_HCL)**	**Maximum mole fraction of HCL (X_HCLmax)**
18	0.05786	0.003089	0.05405	0.2133
17	0.05786	0.003463	0.05714	0.2133
16	0.05786	0.00391	0.06061	0.2133
15	0.05786	0.004449	0.06452	0.2133
14	0.05786	0.005109	0.06897	0.2133
13	0.05786	0.005926	0.07407	0.2133
12	0.05786	0.006957	0.08	0.2133
11	0.05786	0.008282	0.08696	0.2133
10	0.05786	0.01003	0.09524	0.2133
9	0.05786	0.01238	0.1053	0.2133
8	0.05786	0.01569	0.1176	0.2133
7	0.05786	0.02051	0.1333	0.2133
P=0.5 bar				
SCR	**Equilibrium Constant (K_e)**	**Reaction Quotient (Q_R) (P=0.5 bar)**	**Mole fraction of HCL (X_HCL)**	**Maximum mole fraction of HCL (X_HCLmax) (P=0.5 bar)**
18	0.05786	0.001544	0.05405	0.2872
17	0.05786	0.001732	0.05714	0.2872
16	0.05786	0.001955	0.06061	0.2872
15	0.05786	0.002225	0.06452	0.2872
14	0.05786	0.002554	0.06897	0.2872
13	0.05786	0.002963	0.07407	0.2872
12	0.05786	0.003478	0.08	0.2872
11	0.05786	0.004141	0.08696	0.2872
10	0.05786	0.005013	0.09524	0.2872
9	0.05786	0.006192	0.1053	0.2872
8	0.05786	0.007843	0.1176	0.2872
7	0.05786	0.01026	0.1333	0.2872

Table C-6: Parametric Tables from Figures 31, 32, 33

P=0.25 bar				
SCR		**Reaction Quotient (Q_R) (P=0.25 bar)**		**Maximum mole fraction of HCL (X_HCLmax) (P=0.25 bar)**
18	0.05786	0.0007722	0.05405	0.3791
17	0.05786	0.0008658	0.05714	0.3791
16	0.05786	0.0009775	0.06061	0.3791
15	0.05786	0.001112	0.06452	0.3791
14	0.05786	0.001277	0.06897	0.3791
13	0.05786	0.001481	0.07407	0.3791
12	0.05786	0.001739	0.08	0.3791
11	0.05786	0.00207	0.08696	0.3791
10	0.05786	0.002506	0.09524	0.3791
9	0.05786	0.003096	0.1053	0.3791
8	0.05786	0.003922	0.1176	0.3791
7	0.05786	0.005128	0.1333	0.3791
Vary SCR by mole fraction of N2	**X_N2**	**Reaction Quotient (Q_R) (X_N2 = 0.1)**	**Equilibrium Constant (K_e)**	
18	0.1	0.00278	0.05786	
17	0.1	0.003117	0.05786	
16	0.1	0.003519	0.05786	
15	0.1	0.004004	0.05786	
14	0.1	0.004598	0.05786	
13	0.1	0.005333	0.05786	
12	0.1	0.006261	0.05786	
11	0.1	0.007453	0.05786	
10	0.1	0.009023	0.05786	
9	0.1	0.01115	0.05786	
8	0.1	0.01412	0.05786	
7	0.1	0.01846	0.05786	

Table C-7: Parametric Tables from Figures 31, 32, 33 continued

Vary SCR by mole fraction of N2	X_N2	Reaction Quotient (Q_R) (X_N2 = 0.25)	Equilibrium Constant (K_e)	
18	0.25	0.002317	0.05786	
17	0.25	0.002597	0.05786	
16	0.25	0.002933	0.05786	
15	0.25	0.003337	0.05786	
14	0.25	0.003831	0.05786	
13	0.25	0.004444	0.05786	
12	0.25	0.005217	0.05786	
11	0.25	0.006211	0.05786	
10	0.25	0.007519	0.05786	
9	0.25	0.009288	0.05786	
8	0.25	0.01176	0.05786	
7	0.25	0.01538	0.05786	
Vary SCR by mole fraction of N2	**X_N2**	**Reaction Quotient (Q_R) (X_N2 = 0.5)**	**Equilibrium Constant (K_e)**	
18	0.5	0.001544	0.05786	
17	0.5	0.001732	0.05786	
16	0.5	0.001955	0.05786	
15	0.5	0.002225	0.05786	
14	0.5	0.002554	0.05786	
13	0.5	0.002963	0.05786	
12	0.5	0.003478	0.05786	
11	0.5	0.004141	0.05786	
10	0.5	0.005013	0.05786	
9	0.5	0.006192	0.05786	
8	0.5	0.007843	0.05786	
7	0.5	0.01026	0.05786	

Table C-8: Parametric Tables from Figures 31, 32, 33 continued

Appendix D: EES results

EES results are presented on the following page. All variables are the result of calculating using the EES code from Appendix B.

Ar=21.51 [kg^2-1/m^3]	Energypermole=1.020E+06 [J/mol]	MM_Steam=18.02 [kg/kmol]
a_m=0.0002857 [m^2]	Energypermoleprime=2.347E+06 [J/mol]	Molarity=8.538 [mol/L]
A_reactor=0.174 [m^2]	gibbsfree_CuCl2=-173.8 [kJ/mol]	Molefraction=0.09402
a_s=0.00005282 [m^2]	gibbsfree_Cu_2OCl_2=-369.7 [kJ/mol]	Mole_fraction=0.1538
bedheight=0.02282 [m]	gibbsfree_H2O=-228.6 [kJ/mol]	mu=2.061
bedmass=13.45 [kg/hr]	gibbsfree_HCl=-95.3 [kJ/mol]	M_dot_H2=0.1 [kg/hr]
bedvolume=0.003971 [m^3/hr]	G_1=0.003504 [kg/s]	M_dot_H2O_condenser=0.003254 [kg/s]
cp_CuCl2=78.74 [J/mol-K]	G_2=0.00722 [kg/s]	M_dot_H2_goal=2.4 [kg/day]
cp_steam=1.89	H=0.2112 [m]	M_dot_HCl_condenser=0.001013 [kg/s]
cp_water=4.2 [kJ/kg-K]	H_v=6.4	NdotCuCl2Kmol=0.1 [kmol/hr]
D=0.4224 [m]	K_d=0.14	N_dot_H2=0.01389 [mol/s]
delta=0.43	K_e=0.05786	N_dot_Steamconsumed=0.01389 [mol/s]
DELTAgibbsfree_reaction=15.95 [kJ/mol]	K_m=0.06	N_e=5.5
DELTAh_reaction=116.6 [kj/mol]	K_s=0.05	N_Hcl_max=0.1318 [mol/s]
DELTAh_vap_steam=2256 [kJ/kg]	K_t=0.05	OutletRatio=0.3714
DELTAP=761.7 [N/m^2]	L_b=0.6335 [m]	phi=0.8206
DELTAP_reactor=758.2 [kPa]	L_c=1.056 [m]	pH_acid=-0.9313
DELTAP_separator=3.58 [kPa]	l_d=0.1907 [m]	pi_m=7.309
d_CuCl2=0.0001 [m]	l_e=0.01335 [m]	P_0=1 [bar]
D_d=0.1584 [m]	l_m=0.1526 [m]	P_T=1 [bar]
D_e=0.2112 [m]	l_n=0.04921 [m]	QPRIME_evap=20.33 [mol-kg-kJ/s-kmol-g]
d_m=0.01907 [m]	Mass_Fraction=0.3113	QPRIME_steamGenerator=30.15 [mol-kg-kJ/s-kmol-g]
d_pc=0.000009247 [m]	MM_CuCl2=134.5 [kg/kmol]	QPRIME_steamHeat=6.995 [mol-kg-kJ/s-kmol-g]
d_reactor=0.4706 [m]	MM_H2=2 [kg/kmol]	QPRIME_total=32.59 [kJ/s]
d_s=0.008201 [m]	MM_HCl=36.46 [kg/kmol]	QPRIME_waterHeat=2.832 [mol-kg-kJ/s-kmol-g]

Table D-1: EES Results

Q_CuCl2=820.2 [J/s]
Q_evap=7.905 [kJ/s]
Q_R=0.02051 [Pa]
Q_reaction=1.619 [kj/mol]
Q_reactionTotal=2.44 [kJ/s]
Q_savings=-18.43 [kJ/s]
Q_steamGenerator=11.73 [kJ/s]
Q_steamHeat=2.72 [kJ/s]
Q_total=14.17 [kj/s]
Q_waterHeat=1.102 [kJ/s]
r=0.009536 [m]
R1=8.314 [J/mol*K]
Re_mf=0.01317 [kg/m-s]
rho_CuCl2=3386 [kg/m^3]
S=0.2112 [m]
SCR=7
SCR_eff=18 [-]
Steammolefraction=1
u_mf=0.008686 [m/s]
VelocityRatio=0.1
V_dot_H2O_condenser=0.003254 [L/s]
W=0.08447 [m]
W_CuCl2=131.9 [N/hr]
X_HCl=0.1333
X_Hcl_max=0.2133 [s/mol]
X_N2=0

Table D-2: EES Results continued

State point	cp [kJ/kg*K]	mu [kg/m-s]	M_dot [g/s]	M_dot_CuCl2 [g/s]	nu [1/s]	N_dot_CuCl2 [mol/s]	N_dot_HCl [mol/s]	N_dot_steam [mol/s]
1								
2	1.87	0.00002341	10.72		0.00006596		0.04701	0.5
3	1.773	0.00002286	11.49		0.00006167		0.07479	0.4861
4	1.773	0.00002286	11.49		0.00006167		0.07479	0.4861
5	1.773	0.00002286	7.22		0.00006167		0.04701	0.3056
6	2.07	0.00002445	3.504		0.00007497		0	0.1944
7	1.773	0.00002286	4.266		0.00006167		0.02778	0.1806
8				3.735		0.02778		
State point	**P [Pa]**	**rho [kg/m3]**	**T [K]**	**v [m/s]**	**V_dot [m3/s]**	**N_dot_T [mol/s]**	**N_dot_N2 [mol/s]**	
1	101325		298.2					
2	101325	0.3548	673.2	0.1737	0.03022	0.547	0	
3	100567	0.3707	673.2	1.737	0.03099	0.5609	0	
4	100563	0.3707	673.2		0.03099		0	
5	100563	0.3707	673.2	68.18	0.01948		0	
6	101429	0.3261	673.2	203.4	0.01074		0	
7	100563	0.3707	673.2				0	

Table D-3: EES State points array

Appendix E: Aspen Plus stream summary

Stream number	**Units**	**1**	**3**	**4**	**5**	**6**	**7**	**8A**	**7A**	**2A**	**5A**
Description											
From		R4	R2	R3	H1	R3	H2	R1B		R1A	
To		R1A	R3	R4	R4		R1A		H2	R1B	H1
Stream Class		MIXCIPSD	MIXCIPSD	MIXCIPSD	MIXCIPSD	MIXCIPSD	MIXCIPSD	MIXCIPSD	MIXCIPSD	MIXCIPSD	MIXCIPSD
Maximum Relative Error											
Cost Flow	$/sec										
Total Stream											
Temperature	K	673.15	673.15	673.15	673.15	673.15	673.15	673.15	298.15	673.15	298.15
Pressure	N/sqm	100000	100000	100000	100000	100000	100000	100000	100000	100000	100000
Molar Vapor Fraction		1	1	1	1	1	0	0	0	0.975837	0
Molar Liquid Fraction		0	0	0	0	0	0	0	0	0	1
Molar Solid Fraction		0	0	0	0	0	1	1	1	0.024163	0
Mass Vapor Fraction		1	1	1	1	1	0	0	0	0.794409	0
Mass Liquid Fraction		0	0	0	0	0	0	0	0	0	1
Mass Solid Fraction		0	0	0	0	0	1	1	1	0.205591	0
Molar Enthalpy	J/kmol	-215968334.4	-208985953.2	-2.1E+08	-2.3E+08	-2.1E+08	-1.8E+08	-3.6E+08	-2.1E+08	-2.1E+08	-2.9E+08
Mass Enthalpy	J/kg	-11018533.47	-10207052.99	-1E+07	-1.3E+07	-1E+07	-1318267	-1681536	-1531036	-8454287	-1.6E+07

Table E-1: Aspen Plus stream summary

Stream number	Units	1	3	4	5	6	7	8A	7A	2A	5A
Molar Entropy	J/kmol-K	-9153.790691	-5961.226419	-5961.23	-15877.2	-5961.23	-86356.8	-1227206	-148080	-35469.8	-163139
Mass Entropy	J/kg-K	-467.0191556	-291.1514051	-291.151	-881.317	-291.151	-642.29	-5734.69	-1101.36	-1410.29	-9055.61
Molar Density	kmol/cum	0.017867381	0.017867381	0.017867	0.017867	0.017867	25.585	37.01647	25.585	0.01831	55.173
Mass Density	kg/cum	0.350208897	0.36582857	0.365829	0.321886	0.365829	3439.939	7921.407	3439.939	0.460498	993.957
Enthalpy Flow	Watt	-118140.9508	-117223.9682	-73685.2	-44455.7	-43538.7	-4923.41	-4997.82	-5718.06	-122222	-55572.3
Average MW		19.60046088	20.47466134	20.47466	18.01528	20.47466	134.4514	213.9968	134.4514	25.15068	18.01528
Mole Flows	mol/sec	0.547029041	0.56091793	0.352585	0.194444	0.208333	0.027778	0.013889	0.027778	0.574807	0.194444
CU_2OCL_2	mol/sec	0	0	0	0	0	0	0.013889	0	0.013889	0
CUCL	mol/sec	0	0	0	0	0	0	0	0	0	0
HCL	mol/sec	0.04701128	0.074789058	0.047011	0	0.027778	0	0	0	0.074789	0
CUCL2	mol/sec	0	0	0	0	0	0.027778	0	0.027778	0	0
CL2	mol/sec	0	0	0	0	0	0	0	0	0	0
H2O	mol/sec	0.500017761	0.486128872	0.305573	0.194444	0.180556	0	0	0	0.486129	0.194444
CU	mol/sec	0	0	0	0	0	0	0	0	0	0
Volume Flow	cum/sec	0.030616073	0.031393406	0.019733	0.010883	0.01166	1.09E-06	3.75E-07	1.09E-06	0.031394	3.52E-06
MIXED Substream											

Table E-1: Aspen Plus stream summary (continued)

Stream number	Units	1	3	4	5	6	7	8A	7A	2A	5A
Phase		Vapor Phase	Vapor Phase	Vapor Phase	Vapor Phase	Vapor Phase				Vapor Phase	Liquid Phase
Temperature	K	673.15	673.15	673.15	673.15	673.15				673.15	298.15
Pressure	N/sqm	100000	100000	100000	100000	100000	100000		100000	100000	100000
Molar Vapor Fraction		1	1	1	1	1				1	0
Molar Liquid Fraction		0	0	0	0	0				0	1
Molar Solid Fraction		0	0	0	0	0				0	0
Mass Vapor Fraction		1	1	1	1	1				1	0
Mass Liquid Fraction		0	0	0	0	0				0	1
Mass Solid Fraction		0	0	0	0	0				0	0
Molar Enthalpy	J/kmol	-215968334.4	-208985953.2	-2.1E+08	-2.3E+08	-2.1E+08				-2.1E+08	-2.9E+08
Mass Enthalpy	J/kg	-11018533.47	-10207052.99	-1E+07	-1.3E+07	-1E+07				-1E+07	-1.6E+07
Molar Entropy	J/kmol-K	-9153.790691	-5961.226419	-5961.23	-15877.2	-5961.23				-5961.23	-163139
Mass Entropy	J/kg-K	-467.0191556	-291.1514051	-291.151	-881.317	-291.151				-291.151	-9055.61
Molar Density	kmol/cum	0.017867381	0.017867381	0.017867	0.017867	0.017867				0.017867	55.173
Mass Density	kg/cum	0.350208897	0.36582857	0.365829	0.321886	0.365829				0.365829	993.957
Enthalpy Flow	Watt	-118140.9508	-117223.9682	-73685.2	-44455.7	-43538.7				-117224	-55572.3
Average MW		19.60046088	20.47466134	20.47466	18.01528	20.47466				20.47466	18.01528
Mole Flows	mol/sec	0.547029041	0.56091793	0.352585	0.194444	0.208333	0	0	0	0.560918	0.194444

Table E-1: Aspen Plus stream summary (continued)